ENERGY EFFICIENT THERMAL MANAGEMENT OF DATA CENTERS VIA OPEN MULTI-SCALE DESIGN

A Dissertation
Presented to
The Academic Faculty

by

Emad Samadiani

In Partial Fulfillment
of the Requirements for the Degree
Doctor of Philosophy in the
G.W. Woodruff School of Mechanical Engineering

Georgia Institute of Technology
December 2009

ENERGY EFFICIENT THERMAL MANAGEMENT OF DATA CENTERS VIA OPEN MULTI-SCALE DESIGN

Approved by:

Dr. Yogendra Joshi, Co-Advisor
School of Mechanical Engineering
Georgia Institute of Technology

Dr. Farrokh Mistree, Co-Advisor
School of Mechanical Engineering
Georgia Institute of Technology

Dr. Janet K. Allen
School of Mechanical Engineering
Georgia Institute of Technology

Dr. Karsten Schwan
College of Computing
Georgia Institute of Technology

Dr. Thorsten Stoesser,
School of Civil and Environmental Engineering
Georgia Institute of Technology

Dr. Hendrik F. Hamann
Photonics & Thermal Physics
IBM Watson Research Center

Dr. Madhusudan K. Iyengar
Advanced Thermal Laboratory
IBM Systems & Technology Group

Date Approved: August 19, 2009

ACKNOWLEDGEMENTS

First of all, I express my sincere thanks to Dr. Yogendra Joshi, for his support and guidance during my doctoral studies. I also greatly appreciate the support and encouragement of Dr. Farrokh Mistree. They have shaped me as a researcher and influenced me as a thinker. I am grateful for their insight and particularly their confidence in me.

I express my appreciation to my committee members for their valuable suggestions and commitment to this dissertation. Also, I am thankful for all my current and former colleagues for the valuable discussions we have had concerning this and many other research topics. My special gratitude goes to Nathan Rolander, Dr. Jeff Rambo, and Dr. Qihong Nie, my previous colleagues who helped me in understanding POD based reduced order modeling.

My sincere gratitude goes to Dr. Janet K. Allen for her suggestions and help in applying the robust design principles for the data center design problem in Chapter 5.

I am sincerely grateful to Dr. Hendrik Hamann and Dr. Madhusudan K. Iyengar for their help and continuous valuable suggestions during my doctoral research. Also, I appreciate their support in doing a joint research on experimental validation of the developed reduced order modeling in an IBM data center facility. The experimental data used in Chapter 8 have been obtained completely by the staff in IBM. In this regard, I would thank the IBM Corporation and especially Dr. Hendrik Hamann, Dr. Madhusudan

Iyengar, Steven Kamalsy, and James Lacey. Also, I acknowledge Milton Bonilla and Michael Schappert in IBM.

I appreciate Hrishikesh Amur and Bhavani Krishnan and Dr. Karsten Schwan in the College of Computing at Georgia Tech for the collaborative work in coordinated IT and thermal management design in data centers. Hrishi and Bhavani have done the power profiling of the used servers in Chapter 6. Also, I thank their help and suggestions in developing the design method and obtaining the presented results in Chapter 7.

I acknowledge the support of the Consortium for Energy Efficient Thermal Management (CEETHERM) at Georgia Institute of Technology.

Last but not least, I express my deepest gratitude to my parents for their unconditional love and support.

TABLE OF CONTENTS

LIST OF TABLES

LIST OF FIGURES

NOMENCLATURE

List of Symbols

a_i, b_i	modal weight coefficient
c_P	specific heat, J/kg K
d_i^+, d_i^-	deviation variables
$g_i(\vec{x})$	inequality constraint function
$h_i(\vec{x})$	equality constraint function
k_{eff}	effective thermal conductivity, W/mK
k_{th}	thermal conductivity, W/mK
n	number of observations
m	number of retained modes
$\dot{m}$	mass flow rate
q	volumetric heat generation, W/m^3
s	number of algebraic equations
u	velocity field, m/s

x_i	design variables
$x_{i,L,U}$	lower/upper bound of design variable x_i
$A(\vec{x})$	achievement function
G_i	design goal target
P	Pressure, Pa
Q	heat generation rate, W
R,R'	covariance matrix
T	temperature, k
V	average velocity on a surface, m/s
W_i	goal weighing factor
Z	Archimedian objective function
β	air recirculation parameter
λ	eigenvalue
ρ	density, kg/m^3
ψ	POD mode
υ_{eff}	effective viscosity, m^2 /s

$k-\varepsilon$	turbulent kinetic energy-turbulent dissipation

Subscripts

obs	observation
cond	conduction

Superscripts

*	transpose
+	psuedo-inverse

List of Abbreviations

CRAC	Computer Room Air Conditioner
cDSP	Compromise Decision Support Problem
CFM	Cubic Feet per Minute
CFD	Computational Fluid Dynamics
DOF	Degree of Freedom
DOE	Design of Experiments
HT	Heat Transfer
LPM	Liters per Minute

POD	Proper Orthogonal Decomposition
RANS	Reynolds Average Navier Stokes
TIM	Thermal Interface Material

SUMMARY

Data centers are computing infrastructure facilities that house arrays of electronic racks containing high power dissipation data processing and storage equipment whose temperature must be maintained within allowable limits. The heat generated by the electronic equipment and the costs of powering the cooling systems in data centers are increasing continually. This requires the typical air cooling system in data centers to be designed more intelligently or augmented by other techniques. Having concluded that typical designs of air-cooling systems are not efficient and even adequate anymore for current and upcoming data centers, a research question is raised to identify and satisfy the needed design specifications and framework of new energy efficient thermal solutions, considering the design environment of the next generation data centers.

In this research, the sustainable and reliable operations of the electronic equipment in data centers are shown to be possible through the Open Engineering Systems paradigm. After the open design requirements of current air cooling and future multi-scale cooling systems in data centers are identified, a design approach is developed to bring adaptability and robustness, two main features of open systems, in multi-scale convective systems such as data centers. The presented approach is centered on the integration of three constructs: a) a Proper Orthogonal Decomposition (POD) based multi-scale modeling approach, b) compromise Decision Support Problem (cDSP), and c) robust design to overcome the challenges in thermal-fluid modeling, having multiple objectives, and inherent variability management, respectively. The method is verified to

achieve an adaptable, robust, and energy efficient thermal design of an air-cooled data center cell with an annual increase in the power consumption for the next 10 years. The results show a 12-46% reduction in the energy consumption of the center in addition to being adjustable to the newer IT equipment and higher heat loads compared with a traditional design. Compared with an optimal solution, a robust solution can reduce the variability in the thermal response by 73.8% with only 7.8% increase in the center energy consumption.

Also, a design approach based on POD based modeling and power profiling of IT equipment is presented and used to bring adaptability and concurrency for coordinated minimization of cooling and IT power consumption in future open data centers. The results for a test case show the design approach results in 12-70% saving in the total energy consumption of the data center cell in different scenarios, compared with traditional design of data centers.

Two new POD based reduced order thermal modeling methods are presented to simulate multi-parameter dependent temperature field in multi-scale thermal/fluid systems such as data centers. The methods are discussed and compared with each other through application to similar data center cells. The method results in average error norm of ~ 6% for different sets of design parameters, while it can be up to ~250 times faster than CFD/HT simulation in an iterative optimization technique. Also, a simpler reduced order modeling approach centered on POD technique with modal coefficient interpolation is validated against experimental measurements in an operational data center facility. It is

found that the average error in POD re-construction is 0.68 ^{o}C or 3.2%, compared with the experimentally measured data for two different values of CRAC flow rates.

CHAPTER 1

INTRODUCTION

The principal goal in this dissertation is to:

Principal Research Objective: Identify and satisfy required design specifications of new energy efficient thermal management solutions for next generation data centers.

The hypothesis in achieving this objective is centered on design of an energy efficient "open" cooling system using multi-scale nature of data centers:

First Research Hypothesis: The sustainable and reliable operation of the future data centers are possible through design of an energy efficient "open" cooling system using multi-scale nature of data centers.

Satisfying the design requirements of an energy efficient open cooling system in today's and future air-cooled data centers is challenged by thermal modeling, inherent variability management, and having multiple objectives. These challenges are solved through a Proper Orthogonal Decomposition (POD) based reduced order thermal modeling, robust design principles, and the compromise Decision Support Problem (cDSP) construct:

Second Research Hypothesis: Open design of air-cooled data centers can be done through a POD based reduced order thermal model, robust design principles, and cDSP to achieve significant gains in energy efficiency.

In this chapter an introduction to the work undertaken in this dissertation is presented. In Section 1.1 the background and motivation for the work presented in this dissertation is derived and explained. Then, in Section 1.2 a review of the dissertation organization is presented.

1.1 Background and Motivation

1.1.1 Data Centers and Thermal Management

Data centers, as shown in Figure 1.1, are Information Technology (IT) infrastructure facilities that house arrays of electronic racks containing high power dissipation data processing and storage equipment whose temperature must be maintained within allowable limits. These equipment are utilized by a broad range of end-users including internet service providers, banks, stock exchanges, corporations, educational institutions, government installations, and research laboratories. Data centers have a multi-scale nature spanning several length scales from the chip level to the room level as shown in Figure 1.1. Proper operation of computing equipment imposes unique thermal management requirements. The typical approach currently used for thermal management of data centers consists of computer room air conditioning (CRAC or AC) units that deliver cold air to the racks arranged in alternate cold/hot aisles through perforated tiles placed over an under-floor plenum, see Figure 1.2. The chip level determines the rate of the heat generation in the data center, while the CRAC units at the room level are responsible to provide the cooling solution to keep the chip temperatures in a safe range. Several researchers have simulated this configuration [1-13]. Optimization [14-16] and design [17-21] of the different parameters involved in these systems have also been

performed. Several alternate air-delivery and return configurations are employed, particularly when a raised floor arrangement is un-available. Some of these are seen in Figure 1.3 [22].

Figure 1.1. Data center and its multi-scale nature

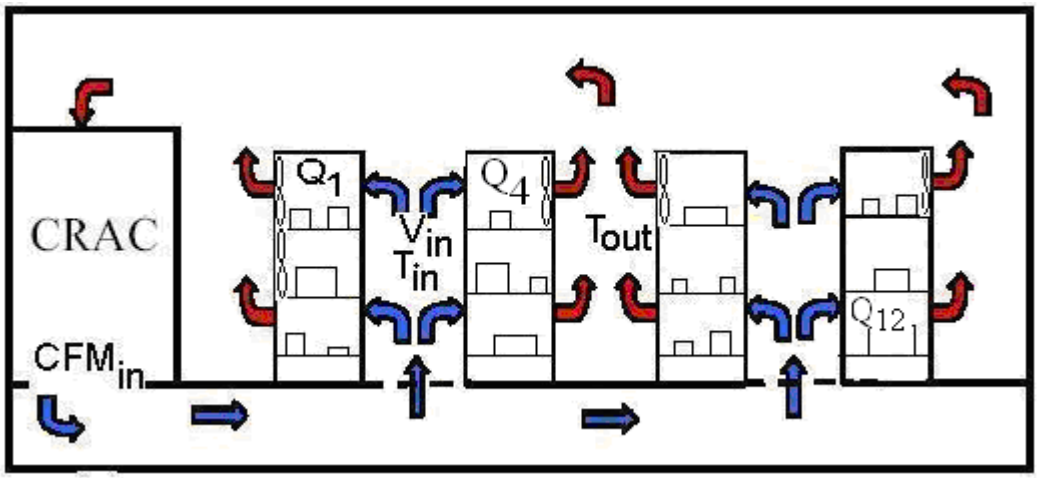

Figure 1.2. Typical air cooling system in data centers

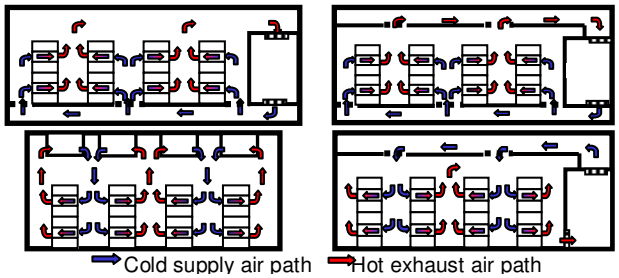

Figure 1.3. Different air-delivery and return configurations in data centers [22]

1.1.2 Data Center Energy Usage Trends

The power consumption of data center facilities is in the range of tens of MW, with an additional 30% or more needed for powering the cooling systems. Data center energy consumption is an increasingly important concern. In 2006 data centers in the United States consumed about 61 billion kWh, or 1.5 % of total U.S. electricity consumption, for a total electricity cost of about $4.5 billion [8]. This estimated level of electricity consumption is equivalent to the amount of electricity consumed by approximately 5.8 million average U.S. households and is estimated to be more than double the electricity that was consumed for this purpose in 2000. Such sharp rise in energy consumption by data centers have prompted a directive by the United States Congress, and a coordinated response by the various stake-holders, as detailed in [8]. Recent benchmarking studies by Lawrence Berkeley National Laboratories [10] show an increase in data center floor heat loads per unit area over the past few years, as seen in Figure 1.4. This is consistent with the projected trend towards denser computing architectures, such as blade servers. The American Society of Heating Refrigeration and Air-conditioning (ASHRAE) projects significant increase in rack level powers [23], as seen in Figure 1.5. Due to the relatively frequent upgrades in the computing equipment, both existing and new facilities are being subjected to these sharp increases in floor heat loading.

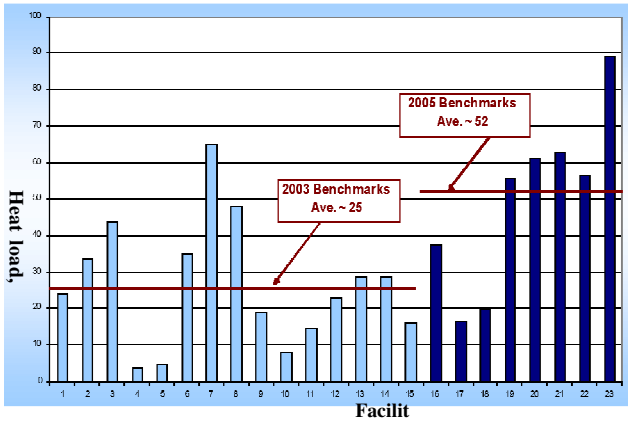

Figure 1.4. Data center floor heat load per unit area [24]

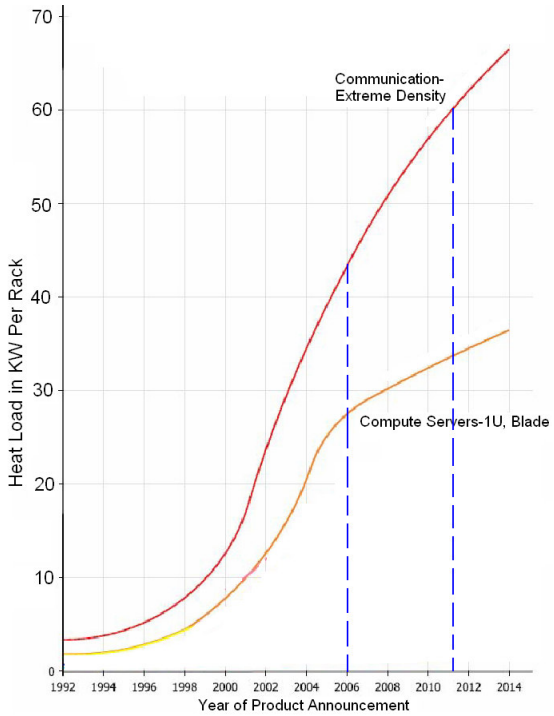

Figure 1.5. ASHRAE Heat load projections for communication and computing racks [23]

1.1.3 Challenges in Data Center Thermal Management

A significant fraction of the energy costs associated with the operation of a typical data center can be ascribed to the cooling hardware. As seen in Figure 1.6, the ratio of the total power input to data center, to the power to the information technology (IT) equipment has dropped from 1.95 to 1.63 during 2003-2005, for a number of benchmarked facilities [24]. Despite this, energy usage by the cooling equipment continues to be a major concern. In the recent benchmarking study of eleven existing facilities by the Lawrence Berkeley Laboratories [10] the power consumption by the heating, ventilating and air-conditioning systems ranged from 22% to 54% of the overall supply. Energy-efficient design of the cooling systems is essential for containing operating costs, and promoting sustainability. Through better design and preventing over-provisioning, it should be possible to reduce energy consumption by the cooling systems.

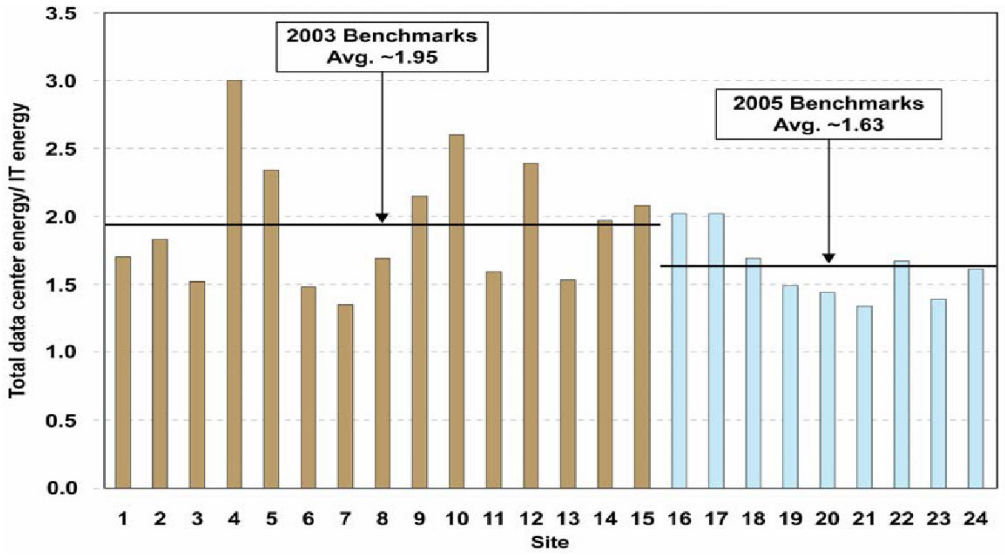

Figure 1.6. Ratio of total data center power input to the power input into the information technology (IT) equipment for benchmarked facilities [24]

In addition to the energy efficiency challenges, today air-cooled systems have practical limitations on effectively cooling the electronic equipment in data centers. Because of the low thermal capacity of air, high flow rates are needed to satisfy the cooling needs of the high power density racks. These large flow rates and their accompanied high noise make the data center environment unpleasant for the people working there. Also, the flow rate provided by the CRAC units has an upper practical limit. Typical data centers with air-cooling systems have an average design cooling capacity of 3 kW per rack, with a maximum of 10–15 kW per rack while the typical practical air flow supplied by the CRAC units to a single rack is approximately 0.094-0.24 m^3/s (200-500 CFM), with 0.47 m^3/s (1,000 CFM) being an absolute upper bound [25], based on constraints such as blower acoustic noise.

In the future, increase in the computational performance will lead electronic racks to house high performance chips with heat fluxes approaching 100 W/cm^2. This is likely to result in increased heat loads at both the rack and the facility levels, which will require higher flow rates of chilled air than the typical data center air-cooling systems of today can provide. As shown in Figure 1.5 and indicated in [23], the heat load of a compute server rack in 2002 was just around 13 KW while it is now around 28 KW. For instance, IBM [26] has recently developed its eServer™ BladeCentert® compact server infrastructure for installation in an industry-standard rack. The power density of such rack would be 30 kW. The effective cooling of this rack requires 0.38-0.71 m^3/s (800-1,500 CFM) of chilled air which is more than the upper limit of the typical CRAC units [25]. Inadequate air flow may cause mixing of the hot air with the chilled air before

entering the racks (recirculation), which develops hot spots and consequently may cause chips to overheat and degrade the computing performance.

With continuing increase in rack heat loads, as seen in Figure 1.5, traditional design of direct air cooling will need to be optimized and augmented by other techniques, such as single phase, or phase change liquid cooling, or refrigeration. Recent attention has also been focused on the reduction of energy usage through the utilization of ambient outside air for cooling. Depending upon geographical location and season, it may be possible to either bring in outside air directly into the data center (air economizers), or utilize an air-to-liquid heat exchanger for pre-cooling the CRAC coolant (fluid economizers). With the air economizers, there are concerns about introducing particulate or gaseous contamination into the facility. With both techniques, the return on investment is a key issue. Experimental measurements of these effects have been made [27], which suggest that it may be possible to mitigate these concerns. For the facilities studied, ~5% of energy used for the cooling equipment could be saved annually.

Also, the industry has suggested several solutions to resolve this problem [26, 28-31]. Most of these solutions consist of using macro heat exchangers with water or refrigerant as a working fluid at the rack or facility level. Also several approaches for the integration of liquid cooling, specifically using water as the working fluid, have been proposed in the literature [32-35]. These solutions should be optimized to handle the increased power densities and heat loads being projected by the manufacturers of datacom equipment [36, 37].

1.2 Research Objectives and Overview

Having concluded that the current designs of air-cooling systems are neither efficient nor sometimes adequate for current and upcoming data centers, a research question is raised to identify the needed design specifications and framework of new energy efficient thermal solutions, considering the design environment of the next generation data centers.

First Research Question: What should the design specifications of new energy efficient thermal solutions be in the next generation data centers?

In order to successfully address this research question, the requirements of the future thermal solutions must be identified and various design specifications of next generation data centers must be explored. In Chapter 2, these requirements based on vision of an ideal future design environment are identified through examining existing state-of-the-art. Then, utilizing the Open Engineering Systems concept [38], it is demonstrated that the key to the success of the future commercial data centers lies in the development and sustainment of an energy efficient open cooling system using multi-scale nature of data centers. So, the associated research hypothesis is:

First Research Hypothesis: The sustainable and reliable operation of the future data centers are possible through design of an energy efficient "open" cooling system using multi-scale nature of data centers.

The first research hypothesis is validated in Chapter 2 through comparison between an open multi-scale solution and a typical air cooling system in a data center example with different scenarios.

With the necessity of having an open cooling system in data centers, the next obvious question to answer is: how can an energy efficient open design be realized in air-cooled data centers?

Second Research Question: How can an energy efficient open air cooling system be designed and realized in data centers?

In Figure 1.7, the requirements, challenges, and tools for having an open design process and product for multi-scale convective systems such as air-cooled data centers are summarized. In Chapter 3, the challenges in developing a design method to achieve an open air cooling systems in data centers are explained and classified into three categories: multi-scale thermal modeling, inherent variability management, and presence of multiple objectives. In this research, the integration of Proper Orthogonal Decomposition (POD) based reduced order thermal modeling, robust design principles, and the compromise Decision Support Problem (cDSP) construct are proposed as a practical design method to achieve energy efficient open air cooling systems, as demonstrated in Figure 1.7:

Second Research Hypothesis: Open design of air-cooled data centers can be done through a POD based reduced order thermal model, robust design principles, and cDSP to achieve significant gains in energy efficiency.

In Chapter 3, robust design principles and compromise Decision Support Problem (cDSP) are described as the two tools used in this research to solve the challenges in inherent variability management and presence of multiple objectives. Also, the recent studies in modeling and design of data centers with the available promising tools in the literature are reviewed. It is concluded in Chapter 3 that a new reduced order thermal modeling approach is required to answer the second research question.

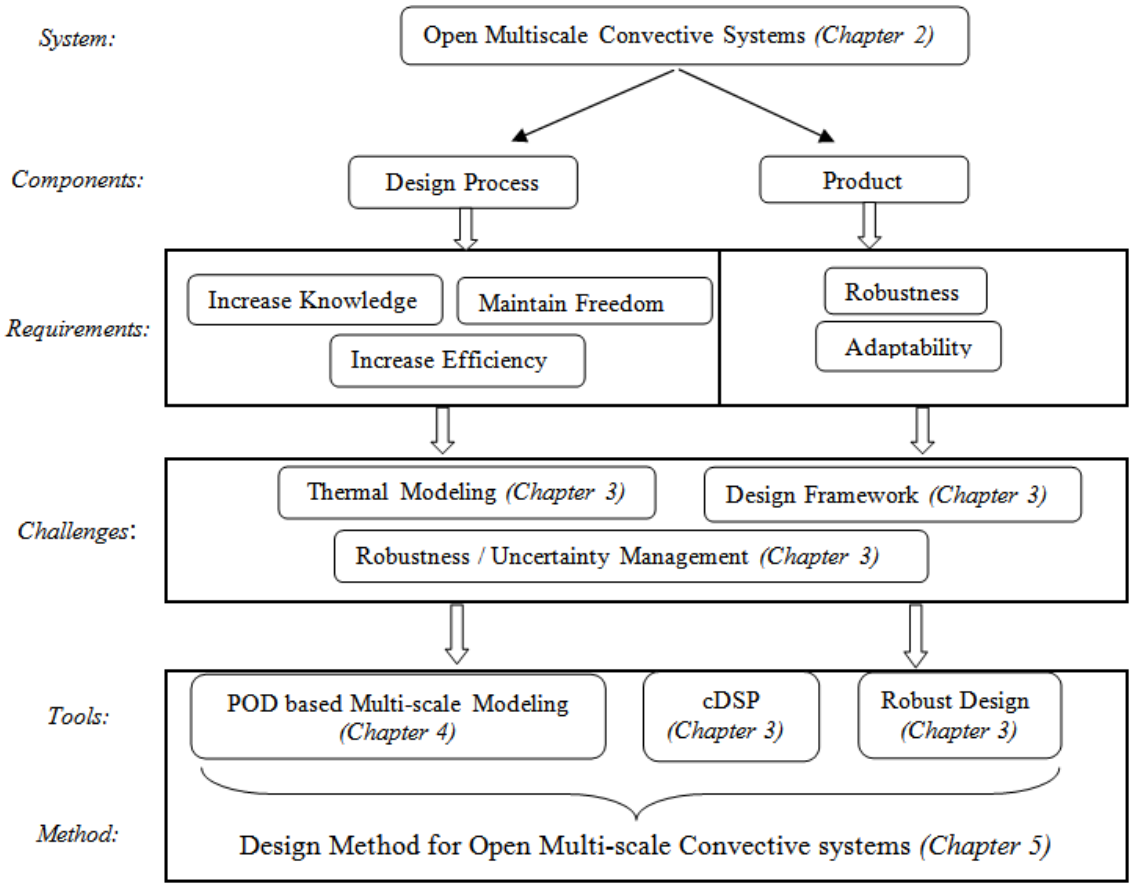

Figure 1.7. Requirements, challenges, and tools to design open multi-scale convective systems

In Chapter 4, a multi-parameter Proper Orthogonal Decomposition (POD) based reduced order thermal modeling approach is developed to resolve the challenges in accurate and computationally efficient thermal modeling of multi-scale thermal-fluid systems as shown in Figure 1.7. The method is validated through application for an air-cooled data center example and the results are presented and discussed.

In Chapter 5, the design approach based on the integration of the three constructs is presented to bring adaptability and robustness, two main features of an open system, to multi-scale convective systems. As shown in Figure 1.7, the design method is centered on the POD based reduced order thermal modeling, robust design principles, and the cDSP construct. The method and the second research hypothesis are validated through application for an adaptable robust thermal design of an energy efficient air-cooled data center cell with an annual increase in the power consumption for the next 10 years. The results are presented and discussed.

To answer the second research question completely, the realization of the presented design method in operational data centers must be considered. The realization requirements of the open design method for operational data centers have been shown in Figure 1.8. Concurrency with IT designers, and modification and validation of the POD method are required for realization the open design method in operational data centers. These requirements are addressed in Chapters 6, 7, and 8, respectively.

In Chapter 6, the concurrency and exchanging design knowledge among the thermal and IT management are studied. As mentioned in Chapter 2, this concurrency is required to realize an energy efficient open cooling system in operational data centers. In

Chapter 6, the design approach is modified to bring adaptability and concurrency for coordinated minimization of cooling and IT power consumption in data centers. The modified approach is centered on the POD based thermal modeling and power profiling of the IT equipment. The method is validated through application for a data center cell with different rack and server architectures. The results are presented and discussed.

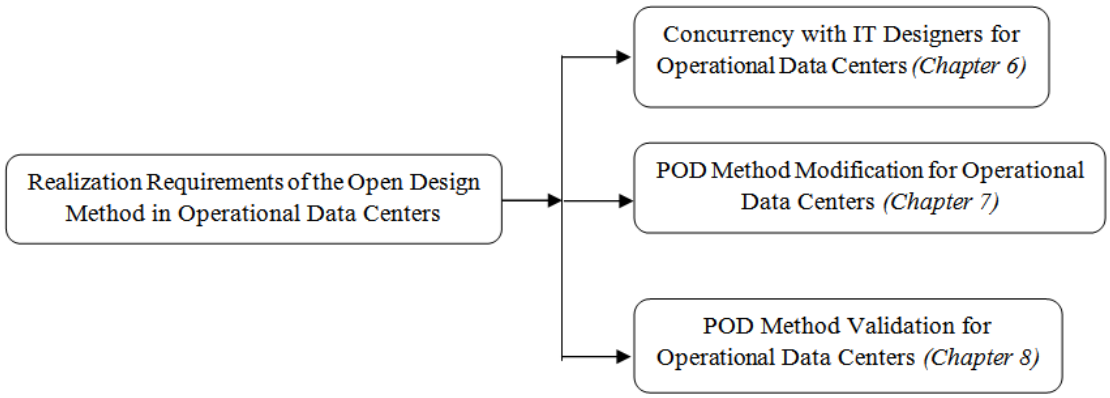

Figure 1.8. Realization requirements of the open design method in operational data centers

In Chapter 7, another POD based reduced order thermal modeling approach is presented to predict the effect of the involved parameters on the temperature field in data centers. Compared with the method developed in Chapter 4, this method is much simpler and its application is easier for reduced order thermal modeling of operational data centers, where the observation data are gathered experimentally and thermal sensors are deployed at the inlet/outlet of the servers. The effectiveness of the presented approach is studied and validated through application to an air-cooled data center cell and the results are discussed.

Although the experimental validation of the developed POD based methods in operational data centers was not possible due to the experimental limitations, the effectiveness of a simpler POD based reduced order thermal modeling for operational data centers is studied in Chapter 8. An operational data center of 102.2 m^2 (1,100 square feet) with a hot and cold aisle arrangement of racks cooled by one CRAC unit is considered. The POD based method, which utilizes selected sets of observed thermal sensor data inside the data center, is applied to predict the data center temperature field as a function of the air flow rate of the CRAC unit. The results are presented and discussed.

Finally, the dissertation is concluded in Chapter 9 and some extensions of the current work for future investigations are suggested.

CHAPTER 2

OPEN CONCEPTUAL DESIGN OF DATA CENTERS

In this chapter, the first research question is answered to identify the required design specifications for new energy efficient thermal solutions in data centers. For this purpose, the requirements of the future thermal solutions are identified and various design specifications of an ideally open thermal solution for a next generation data center are explored. In Section 2.1, these requirements based on an ideal vision of the future design environment are identified through examining existing state-of-the-art. In Section 2.2, an open thermal design is defined. As a potential approach to an open cooling system for the future data centers, the concept of a thermal solution centered on the multi-scale (multilevel) nature of the data centers is discussed in Section 2.3. The potential of this solution to be open, along with its theoretical advantages compared with the typical air cooling solutions are demonstrated through selected scenarios in Section 2.4. The realization problems and the future research needs are highlighted in Section 2.5 to achieve a practical open multi-scale thermal solution in data centers. The chapter is summarized in Section 2.6.

2.1 Requirements of an Ideal Thermal Design

To explore new thermal solutions for the next generation data centers, first the design requirements and specifications of an ideal solution should be identified. These requirements based on an ideal vision of the future design environment are identified

through examining existing state-of-the-art [11, 21, 23, 26, 28-30, 39] and classified into ten categories. In the following, each of these is introduced and divided into more detailed design requirements that should be satisfied by an ideal thermal solution and/or be considered by the designer:

1. *Quality, Sustainability, and Reliability*: Satisfy high reliability requirement of the processing equipment; Consider equipment requirements on its operating temperature and ambient conditions; Design for sustainable and stable operation of the electronics.

2. *Reduction of Cost and Time-to-market*: Effective design for reduction of cost and time-to-market; minimize product realization costs and time for current and future requirements; minimize future development costs and time; allow for development to occur more cost-effectively; facilitate quick and timely development; Consider long-term investment.

3. *Lifecycle Mismatch*: Consider the lifecycle mismatch between the equipment, the facility and cooling systems; Sustain high thermal efficiency and reliable operation, while integrating new equipment into the existing infrastructure during its lifetime; Minimize data center equipment reconfiguration and temporary halts during its lifecycle.

4. *Environmentally benign and green system*: Implement more environmentally friendly solutions; reduce data center power, cooling, and facilities operating costs; Comply with environmental directives for the entire life cycle [11].

5. *Concurrency*: Facilitate concurrency, collaboration, and exchanging information and design knowledge among thermal designers and manufacturers and equipment designers and manufacturers of different scales, facility designer, and cost management of the data center for current usage and future developments.

6. *Flexibility, adaptability, and mutability*: Incorporate flexibility and adaptability into the design; Provide additional freedom to adjust and adapt to future technology, changes in environment, changes in customer demands, performance growth of technology based on footprint, change in processing capability compared to storage capability, change in applications over time, change in asset turnover, and change in product cycle vs. building life cycle [23].

7. *Robustness*: Consider design for robustness; Keep the thermal efficiency and effectiveness with the reliability and operational stability of the equipment in spite of a large amount of uncertainty, internal and external variability and changes.

8. *Mass customization*: Improve customization and standardization; Optimize availability, increase agility, and lower costs through the use of standardized, modular architecture for data centers; Use modular, scalable components to simplify planning; Determine and predict what consumers want; Employ mass customization to satisfy different desires and needs of current and future customers.

9. *Continuous improvement and indefinite growth*: Consider and facilitate provisions, continuous improvement, and indefinite growth in the design to have a

sustained reliable and stable operation of the equipment under large continual internal and external variability and changes.

10. *Multiscale Systems*: Facilitate effective design for a multi-scale system, such as a data center; Take full advantage of designing products at multiple scales; Utilize increased design freedom of multi-scale systems; Facilitate and deal with concurrent and collaborative design and manufacture for integration of designs at different scales.

2.2 Definition of an Open Thermal Design

Comparing the design requirements of the future ideal data centers mentioned in Section 2.1 with the specifications of the Open Engineering Systems paradigm [38], we believe that the key to the success of the future commercial data centers lies in the development and sustainment of an open thermal solution to effectively and efficiently cool the equipment. Simpson et al. [38] defined open engineering systems as follows:

"*Open engineering systems are systems of industrial products, services, and/or processes that are readily adaptable to changes in their environment which enable producers to remain competitive in a global marketplace through continuous improvement and indefinite growth of an existing technological base*."

Accordingly, we describe an ideal open thermal design of future data centers as follows:

Considering design of specifications, geometries, and configurations of chips, servers, racks, and center, an Ideal Open Thermal Design of Future Data Centers is a not

rigidly specified design of specifications, geometries, and configurations of the cooling systems of chips, servers, racks, and center that can be readily adjusted, adapted, modified, and so remained robust to changes in its environments (i.e., changes in any component of the data center, the cooling system, customer demands, the environment, or anything that effects the operation of the data center and cooling systems) which enable cooling systems of the data center to meet thermal effectiveness, efficiency, sustainability, reliability, and a green system demands and so remain usable and suitable within the continual improvements of the future data processing equipments through considering mass customization, continuous improvement, and indefinite growth of an existing technological design base of the data center and its cooling systems.

As mentioned in [38] and extracted from the above definition, inherent advantages of designing an open engineering system include increased quality, reliability, and sustainability, decreased time-to-market and increased return on investment, and improved customization. Also, characteristics of an open system are robustness, modularity, adaptability, and mutability that *promote flexibility and facilitate continuous growth and improvement in the face of change* [38]. Also, the problem of lifecycle mismatch in data centers is a kind of change in its design environment that the open thermal solution would be adaptable and robust to. So, comparing with the requirements of an ideal thermal design listed in the previous section, we can see that an ideal open thermal design will directly satisfy all the requirements except Design for Concurrency and Design for Multiscale Systems. It is concluded that an ideal thermal design of a next generation data center has to be as close as possible to the design specifications of an open engineering system. In the next sections, we see that the requirement of Design for

Multiscale Systems could be considered as a potential solution to approach an open thermal solution in data centers. Also, as discussed in Section 2.1, Design for Concurrency must be considered and satisfied within all steps of the design for deployment of such solution in a data center.

2.3 Multi-scale Thermal Solution

In this section, a Multiscale Thermal Solution is introduced as a potential solution to achieve an ideal open thermal solution in the next generation data centers. A multiscale thermal solution is centered on the multiscale (multilevel) nature of the data centers. Introducing the expression of "*Advanced Thermal Architecture*", Zou [39] states that "*by understanding the different levels (scales) of thermal problems in electronic enclosures, we can select technologies to address the problems at component levels and to achieve the best overall effectiveness at the system level*". In fact, designing and connecting cooling systems at different scales (levels) of a datacenter increases design freedom and results in a greater flexibility in configuring the system to achieve desired behavior and so enables designers to achieve a high power dissipating rack that was not possible before. All of the current air-cooling solutions and the innovative future approaches can be addressed within a multi-scale framework. Also, a multi-scale solution leads designers to achieve several innovative methods to achieve the design requirements of the next generation data centers. The obtained manageable heat load through an ideal multiscale thermal solution is believed to be the maximum heat load at chip and rack levels which could be effectively cooled in the next generation data centers.

To examine the different scales and their relative thermal solutions, a typical blade server rack, shown in Figure 2.1 , in a representative data center, shown in Figure 2.2, is considered. A multi-scale thermal solution for this rack in the data center can be developed by effective design and combination of different scale thermal solutions in their relative levels. In the following, these levels with some scale solutions are explained:

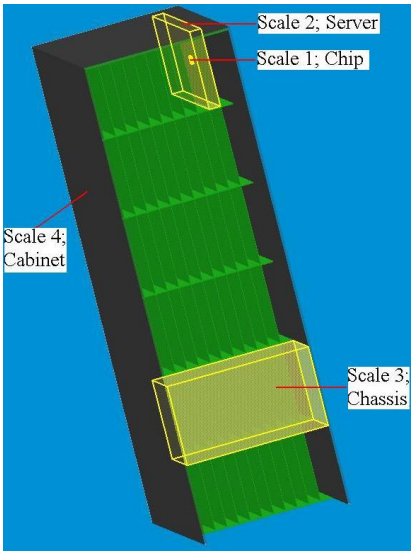

Figure 2.1. A blade server rack with involved scales

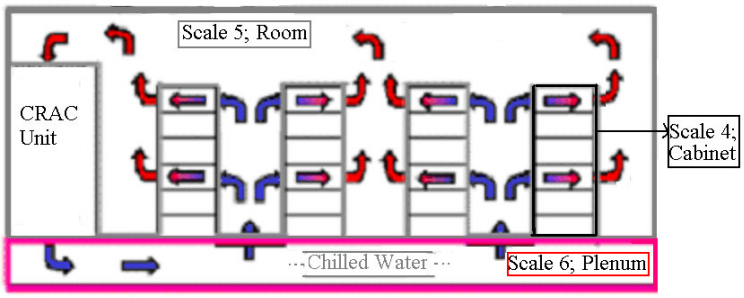

Figure 2.2. Air-cooled data center with involved scales

1. *Scale 1; Chip Level*: This scale solution includes different methods to enhance heat dissipation from the chip itself. For example, it includes the design of effective heat sinks and micro heat exchangers attached to the chip for single or two-phase heat transfer. Also, design of new high conductive thermal adhesives or innovative methods for the attachment the die to the heat spreader, including the use of solder may be considered in this scale. The theoretical limitation of the heat removal from the chip is discussed in [40] and a good review of different options and works done in this scale can be found in [41, 42].

2. *Scale 2; Server Level*: These scale solutions happen within or on the printed circuit board of the server. These solutions mostly are related to designing of different cold plates in combination with the chip scale solutions. A Liquid Cooling System (e.g. [30]) is a good example to use in this scale. Also, as suggested by Gurrum *et al.* [40], the innovative solutions in this scale should focus on effective directing of heat through a path from the chip to the board and finally to the ultimate ambient. The heat rejection through path of chip/substrate/board can be done by, for example, using additional solder balls as the thermal interconnects and heat spreaders or board-integrated liquid cooling as the board heat removal means [40]. The work done by Wiliams and Roux [43] in designing an air cooled base plate channel with implemented graphite foam or a microfibrous material as mini-heat exchangers is an innovative cooling system that can be used in the server level of the rack.

3. *Scale 3; Chassis Level*: In current air cooling systems, this scale is used to install the designed fans. This scale encompassing the space in front of each set of the

blade servers could play a great role in applying various solutions to the rack, especially in combination with two previous scales. For example, this large space can be used by one or more macro heat exchangers. These heat exchangers can transfer the heat from the chips of the servers into the cold air flowed by CRAC units in the rack scale (Scale 4). Also, installing a plate in this scale can provide a support for some components of a compact refrigeration system [44] installed within these three scales to maintain the chip operating temperature as low as -70°C, if required.

4. *Scale 4; Rack Level*: This scale is suitable for using macro heat exchanger for heat removal from the hot air exiting through the rack before entering the room (Scale 5). IBM rear door water-cooled heat exchanger [34] is an innovative solution in this scale offered by IBM [26] to cool the hot air before entering the hot aisle of a data center. Also, an air-water or air-refrigerant heat exchanger can be designed to install on the top or sides of the rack while they can directly use the chilled water flowing through the tubes in the plenum of the data center.

5. *Scale 5; Room Level*: This scale has been of interest of various researchers in the recent years working to enhance the effectiveness of the typical air-cooling systems and prevent the recirculation. The efforts to optimize the configurations of the racks and CRAC units and the dimensions of the racks and room to prevent the recirculation are some of these works [14-18, 20, 21]. Also, the heat transfer in this scale can be enhanced by using the different heat exchangers in possible connection with the rack (Scale 4) and their tubing through the room, if needed, such as the solutions offered by APC [29] and

Liebert [28]. Also, the InfraStruXure™ Hot-aisle Containment System is an innovative solution in this scale offered by APC [29].

6. *Scale 6; Plenum Level*: Some done research in this scale includes optimization of the air flow through the plenum and perforated tile considering the plenum depth, under-floor partitions, and tile specifications [19, 45]. Moreover, because the chilled water pipes pass through the plenum and below the racks, the plenum can have more roles in cooling the future data centers. The effective use of this scale combined with the previous scales can bring a lot of options in configuring the liquid-cooling systems for racks of data centers.

Finally, by properly designing and effectively combining the various solutions at each scale, an effective and efficient cooling solution for the next generation data center would be designed and deployed. In the next section, the potential of the multi-scale solution to be open, along with its theoretical advantages compared with the typical air cooling system is illustrated.

2.4 Openness of a Multiscale Thermal Solution

To show the potential of a multiscale solution to be open and its theoretical advantages compared with the typical air cooling system, a representative data center with typical CRAC units is considered. Several changes in the heat load of the data center caused by virtual continuous IT advancements are applied to the data center. The adaptability of two different cooling systems to these changes is compared: the current

air-cooling system and a simple water-cooling solution within the multi-scale framework of the data center.

The representative data center consists of 4 CRAC units and 32 racks arranged symmetrically in 4 rows with cold-hot aisle configuration. Each rack is filled by 6 7U (311.15 mm) servers. To understand the effect of the changes in the data center heat load on its performance, one-fourth of the representative data center and the plenum is simulated by commercial computational fluid dynamics/heat transfer (CFD/HT) code, Fluent v. 6.1. Turbulent flow and heat transfer are simulated assuming $k-\varepsilon$ model. The coefficients used are: $C_{1\varepsilon}=1.44$, $C_{2\varepsilon}=1.92$, $C_{\mu}=0.09$, $\sigma_k=1$, $\sigma_{\varepsilon}=1.3$, and $\mathrm{Pr}_t=0.85$. The geometry of this section of the data center is shown in Figure 2.3. The height of the racks and CRAC unit are 2 m and the plenum is 0.86 m high. Each rack is modeled as a heat generation source with 6 representative fans in its exit and a lumped pressure jump in its inlet to obtain a typical flow rate per rack. The air pressure drop through perforated tiles is modeled as a porous jump boundary condition. They are assumed to be 20% open and 0.035 m thick with the relative pressure drop coefficient obtained from Fried and Idelchik [46]. The CRAC unit has a nominal capacity of 95 KW and 4.81 m^3/s (10,200 CFM). The CRAC supply is modeled as a constant velocity inlet discharging the cooling air into the plenum at 15 ^oC and 1.78 m/s. Also, the return air to the CRAC is assumed to be at the same constant velocity, at a higher temperature calculated through overall energy balance between the racks heat loads and the cooling air. More details about the applied boundary conditions are available in [22, 47]. The final mesh contains 198,588 grid cells. A 93% refined mesh with 383,826 grid cells leads to just 2.3% and 3.1% change in maximum velocity and temperature, respectively.

The objective of the cooling systems in data centers is to maintain the chip temperatures below a typical value of 85 °C for silicon components, based on electrical performance and extended materials usability constraints. To analyze the thermal performance of the typical air-cooling systems in data centers, a corresponding criterion may be used that is to maintain the inlet cooling air temperature to the servers in a specific range. The allowable inlet temperature is considered to be between 15 °C and 32 °C, as mentioned in [34].

With a model of the representative data center and suitable performance criteria, the adaptability and possible improvement of the typical air-cooling solution, and a simple multi-scale cooling solution are demonstrated through several scenarios mentioned below:

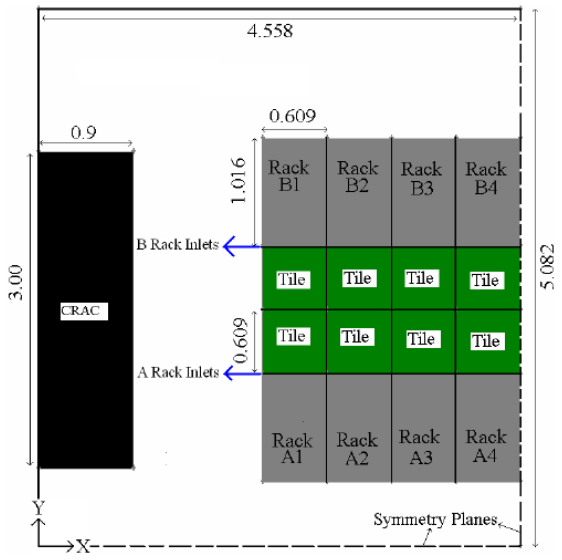

Figure 2.3. Case study data center cell top view; Dimensions in m.
Only one quarter of the cell is shown due to symmetry.

a) Each rack of the representative model of the data center shown in Figure 2.3 is loaded with 6 7U (311.15 mm) rack-mounted servers generating a heat load of 525 W. This leads to 3.15 KW at the rack level and 25.2 KW at the room level. The lumped pressure drop and representative fan specification curve are applied such that nearly 0.35 m^3/s (750 CFM) air flows through each rack, which corresponds to 0.059 m^3/s (125 CFM) per server. The needed air flow rate for 8 racks is 2.83 m^3/s (6000 CFM), which is 59% of the total air flow rate provided by CRAC, 4.81 m^3/s (10,200 CFM). The simulated temperature profile of the inlet air to the racks is shown in Figure 2.4. Also, the temperature contours at the perforated tile and rack outlets have been shown in the figure. While the air temperature at the tile exit is 15 °C, the inlet air temperatures for all racks except A4 and B4, see Figure 2.3 and Figure 2.4 for the rack designations, is not uniform and is higher than 15 °C. This increase in the inlet temperature is due to the air recirculation and mixing of the hot air with the chilled air before entering the racks. As seen in Figure 2.4, this recirculation causes the inlet temperature in the middle servers of racks A1 and B1 to reach 25 °C. The effect of the recirculation reduces with going farther than the CRAC unit such that the Racks A4 and B4 almost are not affected by the recirculation and the inlet temperature throughout these racks is almost 15 °C. Since the maximum rack inlet temperature in the data center is 25 °C and so is less than the maximum allowable temperature of 32 °C, the servers will operate safely within this data center, provided there is no change in their heat loads and the operation of the CRAC unit.

b) Now, we assume that one rack in the data center is populated with 6 7U (311.15 mm) blade servers, as shown in Figure 2.1. This change is a result of technology

enhancement due to demand for miniaturization leading to larger numbers of chips in the same foot print area. Each server chassis of this new rack includes 10 500 W blade servers leading to 5 KW per server chassis and 30 KW per rack. Assuming there is no preference on the location of this rack in the data center, it should be replaced for A4 or B4 rack because the recirculation has the minimum effect on these racks based on the results of Case (a) shown in Figure 2.4. After the replacement with A4, the total heat load of the modeled data center is 52.05 KW. The lumped pressure drop in the model of the A4 rack is changed such that average 0.21 m^3/s (455 CFM) flow rate per server chassis and 1.29 m^3/s (2730 CFM) per rack is satisfied. These flow rates are specified by [25] and needed for the effective cooling of the blade servers. So, the total required flow rate for the racks becomes 3.77 m^3/s (7980 CFM), which is 78% of the capacity of the CRAC. The simulation results for this new configuration show that the maximum rack inlet temperature occurs in inlet of the A1's middle servers and is equal to 29.5 °C. So, the data center will be still operating safely below the maximum of 32°C. Replacement of another blade server rack with one of the spatially non-effective current racks can happen over the time. Replacement of B4 with a blade server rack having the same specifications of the previous one leads to a 78.9 KW heat load at the room level. The needed flow rate for whole racks becomes 4.7 m^3/s (9960 CFM) that is 98% of the total air flow provided by the CRAC. The temperature profile obtained by simulation for the modeled data center having 2 blade server racks is shown in Figure 2.5. The circulation now affects A4 and B4 racks in addition to other racks. Also, the maximum rack inlet air temperature occurs in front of B1 and is nearly 32 °C, the maximum allowable inlet temperature to the servers. Although the server will be safe, the data center and its air-cooling system are

being used at their full potentials and any further increase in the data center heat load must be cooled by another cooling solution, provided the CRAC unit and the air flow rate of the CRAC unit and the dimensions and configurations of the racks in the data center are all fixed.

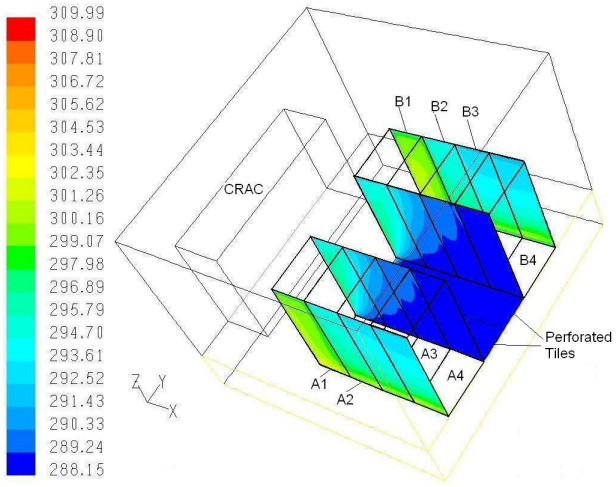

Figure 2.4. Temperature profile (in K) at perforated tiles and inlets and outlets of racks with configuration of Case a)

c) Since the current air-cooling system is not capable anymore to effectively satisfy higher cooling needs, other solutions must be explored to effectively dissipate the higher heat loads of the advanced future processors. Now, we assume, because of the need for higher processor speeds, one of the blade servers of the B4 rack is replaced with a blade server having a 3 cm*3 cm chip generating a high heat load of 900 W, that is equal to a heat flux of 100 W/cm^2. One solution to cool this new blade server is utilizing the multi-scale nature of the rack and data center through a water-cooling system. This solution is shown in Figure 2.6. The system consists of a micro heat exchanger, attached to the high heat load chip (Scale 1), with a valve, flow meter, and the needed tubing to

direct the chilled water from a pump and chiller outside of the data center through the plenum (Scale 6), the rack (Scale 4), chassis (Scale 3), and the blade server (Scale 2) to the micro heat exchanger. Also, the hot water exiting the heat exchanger is returned to the chiller to become cooled. A 3cm*3cm micro channel heat exchanger including 50 channels with dimensions of 0.3 mm*1.5 mm is designed to dissipate the high heat load of the chip. Considering the unit cell in Figure 2.7 as the computational domain with the specified boundary conditions in the figure, the performance of the heat exchanger is simulated numerically. The final mesh contains 168,000 grid cells. A 82% refined mesh with 306,000 grid cells leads to just 0.48% and 0.27% change in maximum velocity and temperature, respectively. The obtained maximum temperature of the base surface of the heat exchanger at different flow rates of the 27°C chilled water are shown in Table 2.1. Since the purpose of this section is understanding the openness of the cooling system, not the detailed design of the system, we neglect the thermal resistance of the Thermal Interface Material (TIM) between chip and the heat exchanger and assume that the temperature of the chip is equal to the temperature of the base surface of the heat exchanger. So, the intended chip will operate safely if the maximum temperature of the basement of the heat exchanger doesn't exceed over 85 °C. As seen in Table 2.1, this heat exchanger at flow rate of $1.13*10^{-5}$ m^3/s (675 mLPM) is able to keep the chip temperature below 85 °C. Using the valve and the flow meter of the system, the flow rate becomes fixed at $1.13*10^{-5}$ m^3/s (675 mLPM) to effectively cool the chip.

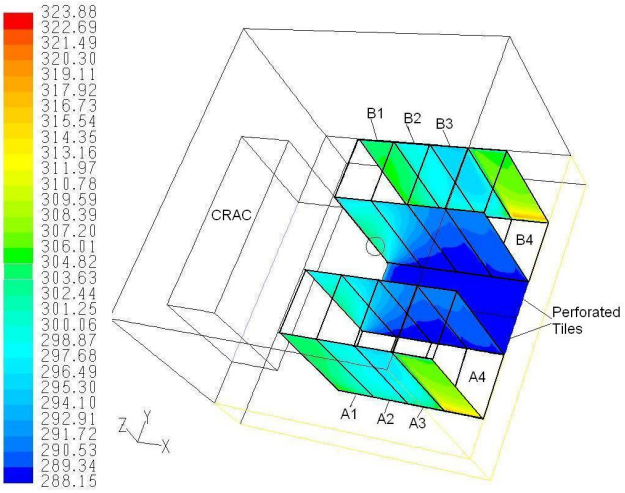

Figure 2.5. Temperature profile (in K) at perforated tiles and inlets and outlets of racks with configuration of Case b)

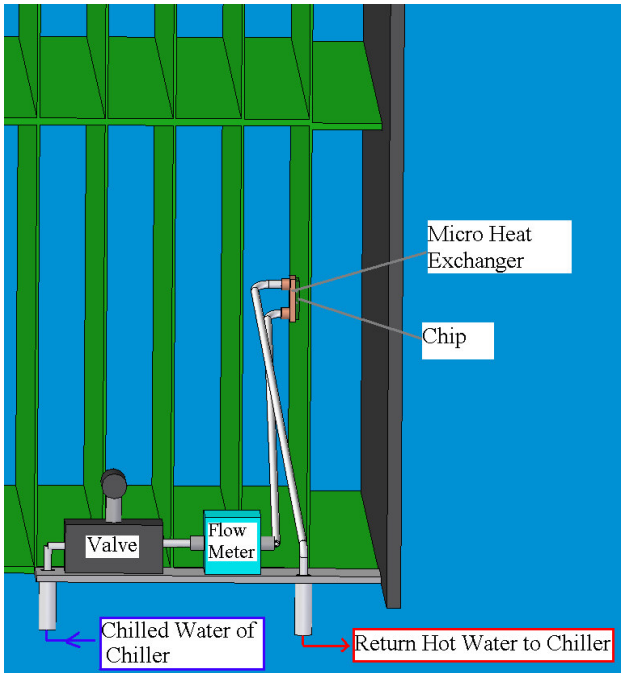

Figure 2.6. Multiscale water-cooling system

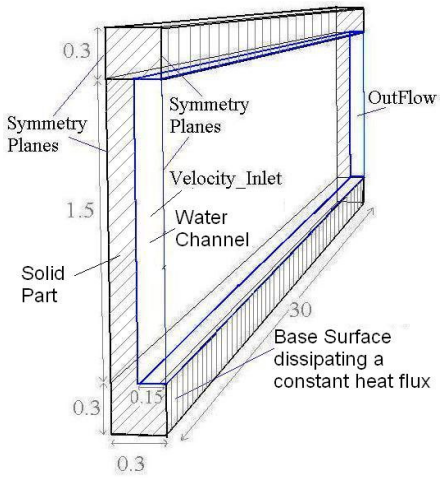

Figure 2.7. Unit cell of micro-channel heat exchanger as the computational domain (Dimensions in mm)

Table 2.1. Base surface temperature of the heat exchanger at different flow rates and heat fluxes

Water Flow rate (mLPM)	337.5	675	675	1012	1012	2025
Heat Flux (W/cm^2)	100	100	150	150	200	200
Maximum Basement Temperature (°C)	89	71	93	83	101	85

d) We assume the intended chip is replaced again with one newer chip with higher heat flux of 150 W/cm^2. The results in Table 2.1 show that the temperature of the chip reaches 93 °C at 150 W/cm^2 and 1.13*10^{-5} m^3/s (675 mLPM) so the chip cannot sustain its safe operation. Therefore, a water-cooling system must be adapted to satisfy the new thermal needs of the system. Considering Table 2.1, it is seen that if the flow rate increases to 1.69*10^{-5} m^3/s (1012 mLPM), the previous heat exchanger satisfies the changed thermal requirement. Using the valve and the flow meter, the water flow rate is

easily adapted and the performance of the data center remains sustainable in face of the change.

e) In a similar way, in Table 2.1 it is seen that this simple cooling-system can be adapted to increase the heat flux of the chip to 200 W/cm^2 by increasing the water flow rate to $3.38*10^{-5}$ m^3/s (2025 mLPM). In addition to the variable water flow rate, there are some other options that bring the possibility of the indefinite growth in this water-cooled system to adapt against higher chip heat loads. Decreasing the inlet chilled water temperature to the heat exchanger is one of these options. To increase the thermal performance of the water-cooled system, the inlet water temperature can decrease to the dew point temperature of the air without any condensation problem. Also, with suitable insulation, this temperature can decrease to yet lower temperatures. Replacing the micro heat exchanger with one having greater thermal performance is another possible adaptation to an increase the heat load. The system can be adapted by changing the specification and/or dimensions of the heat exchanger. Use of smaller micro channels in the heat exchanger, a stacked micro channel heat exchanger, or other micro heat exchangers with more complex structures developed by microfabrication methods dissipates the higher heat loads. Again, increasing the water flow rate and decreasing the inlet water temperature for each heat exchanger extend the range of the solution. The final adjustment could be focusing on two-phase water cooling system at sub-atmospheric water pressure. A boiling enhancement structure with specially designed micro heat exchangers can be used for thermal management of very high heat load chips. Focus on the optimum design of the different parameters involved in the two-phase system for higher heat loads can bring some other adaptation and flexibility. The above

discussion shows that use of a simple multiscale solution has potential of indefinite growth and sustainable operation at least for many years beyond a typical air-cooling solution.

The adaptability and possible improvement of this simple multiscale cooling solution that were explained through the different scenarios demonstrate the potential of a general multiscale solution in being adaptable, flexible, modular, and robust though continuous growth and improvement in the face of changes that are the main characteristics of an open system as mentioned in Section 2.2. In fact, a multi-scale thermal solution with the specifications of an open engineering system is believed to be the most effective and efficient thermal solution for the next generation data centers. In the next section, the problems in realization of an ideal open multiscale solution in data centers are discussed.

2.5 Realization of an Open Multiscale Solution

To understand the difficulties of design and application of an open solution for data centers, we consider more challenging changes in the system of the last section example. We assume we have one processor that needs to operate at low temperature of -70°C. One solution to this requirement is using a compact refrigeration system stated in Section 2.3 and explained in [44] as a possible solution within Scales 1, 2, and 3. Assuming having the solution available, some new questions are raised: should the previous water cooling solution be replaced with the refrigeration system or is it better to keep the liquid cooling solution for future possible applications? Is there any available space for the installation of the refrigeration system- this installation needs three empty

rack spots of the datacenter? Has the data center designer already predicted this situation? Similar questions and situations show that the open multiscale solutions have several limitations to be effectively and efficiently designed, manufactured, and used commonly in the near future data centers. The main issues in realization of an open multiscale solution in data centers are classified into three categories as explained in the following:

a) *Design of Multiscale Systems*: Due to a greater coupling in the design, the complexity in design of multiscale systems is significantly greater than in conventional systems. Interactions between components and couplings between physical phenomena at different scales and their effects on the ultimate behavior of the whole system all have to be considered, while designing products across multiple scales. For instance, the inter-scale bridging of analytical results at different scales of typical air cooled data centers, shown in Figure 2.1 and Figure 2.2, has been demonstrated in Figure 2.8. Clearly, the analysis at the chip level needs to be interfaced with the design of the package at the server level, and beyond to the CRAC units at the room level. As can be seen, a multiscale thermal solution increases the interactions and design complexity. A systematic method is required to manage this complexity, and effectively and efficiently utilize information and knowledge generated in wide range of models, advances, designs, and solutions that predict and manage system behavior at different scales in order to satisfy design objectives. More research is needed to systematically and efficiently achieve an effective design for a multiscale system through seamless selection of a combination of different scale solutions and then obtaining the involved design variables to satisfy the final objective of the whole system [48, 49].

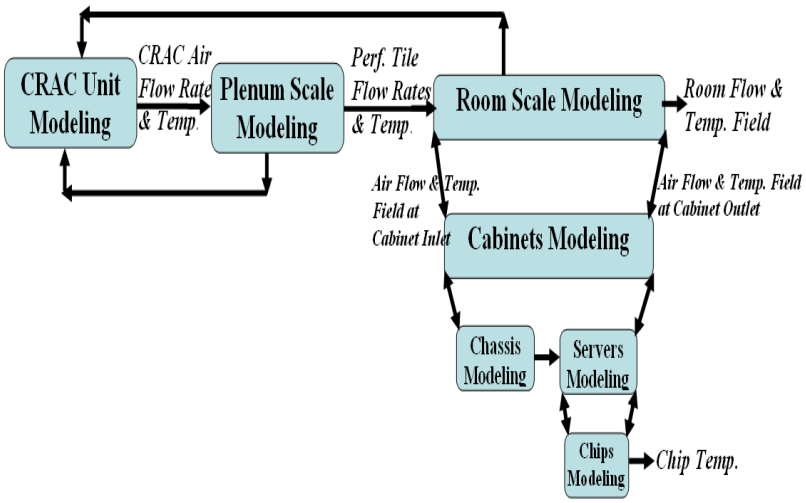

Figure 2.8. Inter-scale bridging of analytical results in a typical air-cooled data cent

b) *Design for Openness*: As explained in Section 2.2, the general concept of openness has some main characteristics that design process and implementation methods for each of them, such as design for robustness, design for modularity and mass customization have been of interest to many researchers in the last few years. However, developing specific methods for implementation of an open thermal solution in data centers is worthy of investigation. These specific methods should be in harmony and combination with the systematic multiscale method mentioned above to achieve an open multiscale thermal solution in data centers.

c) *Design for Concurrency*: As stated in Section 2.1, one of the main requirements of the ideal thermal solution for the future data centers is design for concurrency. The definition and characteristics of an open thermal system, as defined in Section 2.2, do not directly satisfy this need. However, since the open multiscale solution must be manufactured and applied in data centers, deployment of such solution in a data center needs this concurrency and this requirement must be considered and satisfied

within all steps of the design of an open multiscael solution. Collaboration, and exchanging information and design knowledge among thermal designers and manufacturers and equipment designers and manufacturers of different scales, facility designer, and cost management of the data center for current usage and future developments are needed for deployment of an open multiscale thermal solution for the next generation data centers. Currently, there is a big gap in industry between these involved groups that must be filled for realization of these thermal solutions. Concurrency between different participants has been of interest to many researchers in different fields in the recent years. However, to the best knowledge of the author, there is no systematic framework for the required concurrency in the data center design application and more research on this issue seems necessary.

As discussed above, design and deployment of an ideally open multiscale thermal solution in data centers are challenging. Considering an open system as the final goal to achieve the most effective and efficient thermal solution for the next generation data centers, design and manufacture of partly open multiscale cooling solutions are obviously possible as explained through a simple example in Section 2.4.

2.6 Chapter Closure

While the heat flux generated by the electronic equipment in data centers is increasing continually due to demands for higher processor speeds and miniaturization, their sustainable and reliable operation are believed to be possible through the Open Engineering Systems paradigm shift in the next generation data centers. In this chapter, the requirements of the future thermal solutions were identified and various design

specifications of an ideally open thermal solution for a next generation data center were explored. To approach such open cooling system, the concept of a multi-scale thermal solution centered on the multi-scale (multilevel) nature of the data centers was discussed. The potential of this solution to be open along with its theoretical advantages compared with the typical air cooling solutions were illustrated through a simple water-cooling solution within the multi-scale framework of a representative data center. In fact, the adaptability and possible improvement of this simple multiscale cooling solution that were explained through the different scenarios demonstrate the potential of a general multiscale solution in being adaptable, flexible, modular, and robust though continuous growth and improvement in the face of changes that are the main characteristics of an open system. Although a multi-scale solution with the specifications of an open engineering system is believed to be the most effective and efficient thermal solution for the next generation data centers, such solutions have several limitations to be effectively and efficiently designed, manufactured, and used commonly in the near future data centers. Accordingly, the design and deployment problems and the future research needs were highlighted to achieve an open multi-scale thermal solution for next generation data centers.

With the necessity of having an open cooling system in data centers, the design challenges and tools in addressing the second research question are studied in Chapter 3 in order to achieve an energy efficient open multi-scale design in air-cooled data centers.

CHAPTER 3

DESIGN CHALLENGES AND TOOLS FOR AN OPEN AIR COOLED DATA CENTER

In this chapter, the requirements, challenges, and available tools in addressing the second research question to develop a design method to achieve an open multi-scale convective system such as an air-cooling system in data centers are explained. In Section 3.1, the requirements and challenges are reviewed. Robust design is used in this research to solve the challenges in the inherent variability management, which is explained in Section 3.2. In Section 3.3, the compromise Decision Support Problem (cDSP) is described. The cDSP is a mathematical multi-objective design framework which is utilized in this research to overcome the challenges in having multiple design objectives. In Section 3.4, the thermal modeling challenges in multi-scale systems and particularly in air-cooled data centers are discussed through reviewing the recent studies on the Computational Fluid Dynamics/Heat Transfer (CFD/HT), meta-modeling, and reduced order modeling applications. It is concluded that new reduced order modeling approaches need to be developed for thermal-modeling of air cooled data centers. In Section 3.5, the chapter is summarized.

3.1 Requirements and Challenges

As explained in Chapter 2, to be effective in today's global market, companies, including those with thermal-fluid engineering applications, must have an intimate

knowledge of their customers' changing demands and wishes and be flexible enough to respond to them quickly. In this regard, designing open and adaptable engineering systems is needed to accomplish more with fewer resources [38]. In many engineering applications, thermal-fluid systems have inherent variability and involve multiple components, length scales, and physical phenomena interacting with each other, making their thermal-fluid modeling and systematic design very challenging. This brings the necessity to consider the variability in the system parameters and uncertainty in the modeling approach. As mentioned in Chapter 2, robustness and adaptability are characteristics of an open system that promote flexibility and facilitate continuous growth and improvement in the face of change. Accordingly, developing adaptable robust systems is vital for thermal management of multi-scale convective systems. Data centers are a representative example of a multi-scale turbulent convective system in need of adaptable robust thermal design.

The next question is: how can adaptable robust multi-scale convective systems such as a data center be designed? Generally speaking, without flexibility in both product and design process a system is limited (closed) and cannot be adapted to changes in its environment [38, 50]. The flexibility in the design process relies heavily on three requirements: increasing design knowledge, maintaining design freedom, and increasing efficiency during the design [38]. Accordingly, the requirements, challenges, and tools for having an adaptable robust simulation based design process and product for multi-scale convective systems are demonstrated in Figure 3.1. There are three main challenges:

a) Thermal modeling: Computational Fluid Dynamics/Heat Transfer (CFD/HT) is currently used to simulate the flow velocity and temperature fields inside these systems to study the effect of the parameters impacting thermal performance. Using CFD/HT for complex multi-scale systems design is time-consuming and costly and is not practical for iterative, optimization-based design methods. An adaptable and computationally efficient compact model which could run much faster than CFD/HT models, while incorporating all important scale parameters with sufficient fidelity is essential.

b) Mathematical design framework: An adaptable mathematical design framework is needed to use the thermal modeling efficiently to satisfy multiple design goals and constraints. While fulfilling some of these simultaneously may be impractical, the design method should give a designer the ability to weigh the different objectives.

c) Uncertainty management and robustness application: In complex thermal-fluid systems, there are uncertainties and variability in the system parameters and performance. Also, the trade-off between accuracy and efficiency in compact modeling generates uncertainty in the thermal model of complex systems. The design solution should be robust to these uncertainties. Also, to maintain adaptability of the system, regions of 'good' designs should be located and not a specific optimum point.

In this research compromise Decision Support Problem (cDSP) is used to overcome the challenges in solving a multi-objective design problem. The cDSP is explained in Section 3.2. In Section 3.3, it is briefly explained how uncertainty is managed in this dissertation through robust design principles. More details during the

example application in Chapter 5 are provided. Thermal modeling challenges are explained in more details in Section 3.4 through reviewing the recent studies on the full field and low dimensional thermal modeling of data centers and turbulent convective systems.

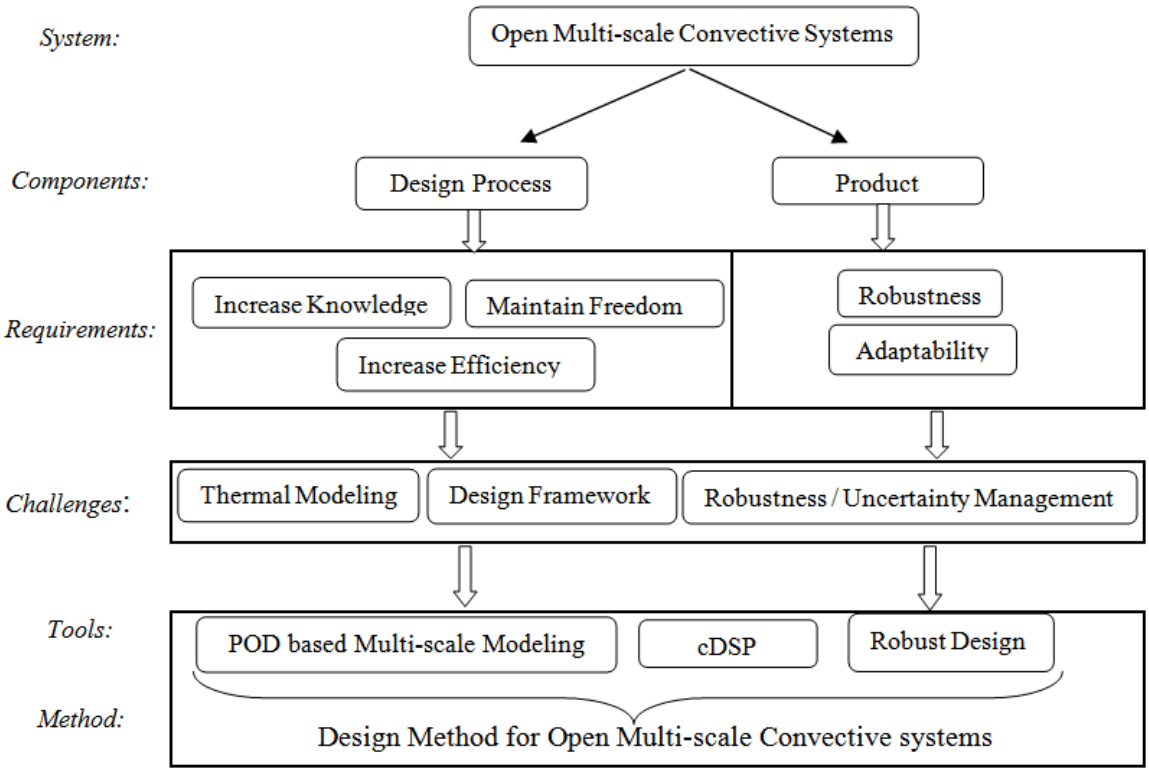

Figure 3.1. Requirements, challenges, and tools to design open multi-scale convective systems

3.2 Compromise Decision Support Problem (cDSP)

There are several methods to solve a multi-objective design problem and be used as a design framework in Figure 3.1. Generally speaking, there are two classes of design optimization methods that can be used for optimizing thermal design problems of data centers. These two classes are gradient- and non-gradient-based methods. One popular

and general class of non-gradient-based techniques for design optimization is Genetic Algorithms (GAs) [51]. Li et al. [51] presented a genetic algorithm-based multi-objective optimization framework and demonstrate applicability of this framework to thermal design of data center racks.

A mathematical construct to model and solve multi-objective, non-linear, optimization problems with some constraints is the Compromise Decision Support Problem (CDSP) technique [12] which is used in this research. The compromise Decision Support Problem, cDSP, [12] provides a modular, adaptable, and computationally efficient mathematical framework for solving design problems with multiple objectives and constraints, making the cDSP very suitable for designing adaptable robust systems. Its structure, based on the Archimedean, or weighted sum, formulation is illustrated in Figure 3.2. Mathematically, the cDSP is a hybrid formulation based on Mathematical Programming and Goal Programming [12]. It is used to determine the values of the design variables, which satisfy a set of constraints and bounds and achieve as closely as possible a set of conflicting goals. The structure of the cDSP is as follows:

Given: A feasible alternative, assumptions, parameter values and goals.

Find: Values of design and deviation variables.

Satisfy: System constraints, system goals, and bounds on variables

Minimize: Deviation variable that measures distance between goal targets and design points

Design solutions are rarely evaluated on the basis of a single objective, but rather upon how well they balance multiple objectives often associate with cost, efficiency,

robustness, and reliability. In order to solve this problem, the cDSP implements objectives based upon goal programming. The focus of goal programming is to establish goals for each objective and attain each of them to the extent possible [12]. The corresponding mathematical formulation is as follows. For each objective, an achievement function, $A_i(x)$, represents the value of the objective as a function of the set of design variables, $\vec{x}$, while the target value, G_i, is given as the goal target for each objective. Deviation variables, d_i^+ and d_i^-, represent the extent to which the achievement underachieves or overachieves its goal:

$$A_i(\vec{x}) + d_i^- - d_i^+ = G_i \tag{3.1}$$

The overall objective function is therefore expressed as a function of the deviation variables. This function can be expressed based on the Archimedean, or weighted sum, as:

$$Z = \sum_{i=1}^{No.obj} (W_i^+ d_i^+ + W_i^- d_i^-) \qquad \begin{aligned} &\sum_{i=1}^{No.obj} W_i = 1 \\ &d_i^- \bullet d_i^+ = 0 \\ &d_i^- \geq 0 \\ &d_i^+ \geq 0 \end{aligned} \tag{3.2}$$

where *No.obj* is the number of objectives. The conceptual basis of the cDSP is to minimize the difference between what is desired, the target G_i, and what can be achieved, $A_i(x)$, represented by the deviation variable, d_i. The key benefit of the cDSP is that the designer preferences over different goals can be applied by easily weighing the coefficients, W_i, of the deviation variables d_i associated with each goal. As seen in Figure 3.2, a simulation

model, $f(x_i)$, relating the objective function to control variables is needed in the cDSP framework. In this research, this model is obtained using the POD based thermal modeling developed in Chapter 4.

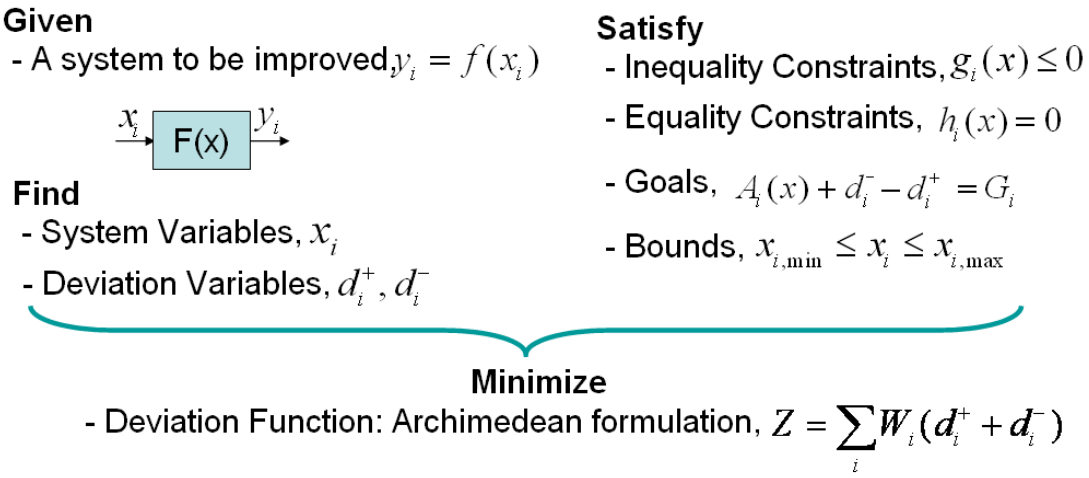

Figure 3.2. cDSP structure

3.3 Robust Design Principles

In typical optimization approaches for design, only the mean response is moved to a target while the effects of the variation in the system parameters or design variables on the performance evaluation are ignored. But, as shown in Figure 3.1 and explained in Section 3.1, uncertainty management and robustness consideration are necessary to design open systems. By accounting for variation, the results obtained by robust design techniques are effective regardless of changing noise factors, uncontrollable parameters (Type I) and/or design variables (Type II) [9]. The difference between having an optimal solution and

robust solution for design goals and constraints is illustrated in Figure 3.3. Considering the design goals, a robust solution happens in a flat region with minimal variability of the response, while an optimal solution happens at the lowest or highest value of the response regardless of the response variability. The trade-off between finding the robust or optimal solution is based on the level of variation of each design variable and the designer's preferences, which could be implemented through the cDSP. Considering the constraints, a robust solution always happens in the feasible design space despite the variable changes, while an optimal solution might fail to satisfy the constraints due to the changes in the design variables.

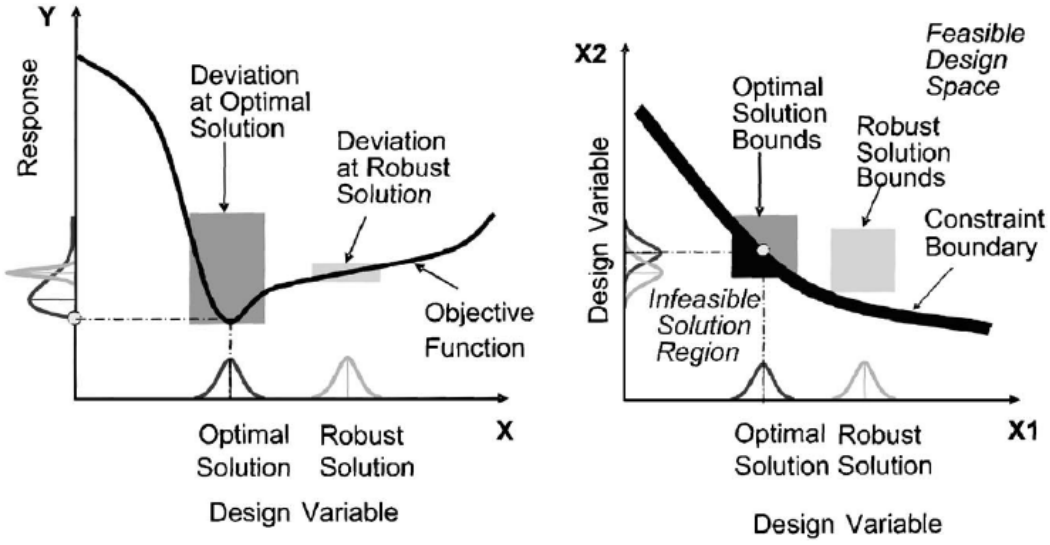

Figure 3.3. Type-II robust design *a)* goals and *b)* constraints representation [52]

3.4 Thermal Modeling Challenges

Predicting the flow and specially temperature fields inside data centers in terms of the involved design parameters is necessary for an energy efficient and open cooling system design, as shown in Figure 3.1 and explained in Section 3.1. Most of the recent

studies on simulating the air velocity and temperature fields in data centers are based on CFD/HT, which are reviewed in Section 3.4.1. Meta-modeling and reduced order modeling techniques are tools to generate accurate and quick surrogate models for a complex system response. These tools are reviewed in Section 3.4.2. The reduced order modeling techniques base on turbulence coherent structures and the Proper Orthogonal Decomposition (POD) are explained and reviewed in more details. In Section 3.4.3, the available approaches and gap in the literature for rapid thermal modeling of data centers are reviewed. It is concluded that a new reduced order modeling approach need to be developed for multi-scale convective systems such as data centers to be utilized for design purposes.

3.4.1 CFD/HT Modeling of Data Center

Generally, the air flow inside data centers is turbulent. Also, buoyancy effects can be neglected [53]. The Reynolds-averaged Navier-Stokes equations (RANS) are commonly used to simulate the turbulent mean flow in complex systems like air-cooled data centers, by modeling the effect of turbulence on the mean flow as a spatially dependent effective viscosity:

$$\nabla u = 0 \tag{3.3}$$

$$u\nabla u - \nabla(\upsilon_{eff}\nabla u) + \frac{1}{\rho}\nabla p = 0 \tag{3.4}$$

Also, the mean energy equation with effective thermal conductivity can be used to compute the temperature field. The mean energy equation, ignoring viscous dissipation, is:

$$\rho c_p u \nabla T - \nabla(k_{eff} \nabla T) = q \tag{3.5}$$

Several researchers have simulated the air flow and temperature fields in today's data centers [1-8, 10, 11, 13]. Optimization [14-16] and design [17-21] of the different parameters involved in these systems have also been performed. Computational Fluid Dynamics/Heat Transfer (CFD/HT) is usually used to predict the air velocity and temperature fields inside the data center. CFD modeling of data centers was introduced in 2001 by Patel et al. [54]. Schmidt et al. [55] have compared experimental measurements through raised floor data center perforated tiles with two-dimensional computational models. Their experimental validation shows fair overall agreement with select tile flow rates, with large individual prediction errors. Van Gilder and Schmidt [7] present a parametric study of plenum airflow for various data center footprints, tile arrangements, tile porosity and plenum depth. Previous research to numerically determine the air flow rate from the perforated tiles [6, 7, 55-57] has modeled the plenum only and does not simulate the effect of the air flow inside the computer room on the perforated tile flow distribution. Samadiani and Joshi [58] have shown that modeling the computer room, CRAC units, and/or the plenum pipes could change the tile flow distribution by up to 60% for the facility with 25% open perforated tiles and up to 135% for the facility with 56% open perforated tiles [58].

Numerical thermal modeling has been used for geometrical optimization of plenum depth, facility ceiling height and cold aisle spacing for a single set of CRAC flow rates and uniform rack flow and power dissipation [16]. A unit cell architecture of a raised floor plenum data center is formulated in [3] by considering the asymptotic flow

distribution in the cold aisles with increasing numbers of racks in a row. The results indicated that for high flow rate racks, 4 rows of 7 racks adequately models the hot-aisle cold-aisle configuration and is representative of a 'long' row of racks [3]. In [1, 5, 54, 59], researchers have either modeled the rack as a black-box with prescribed flow rate and temperature rise, or as a box with fixed flow rate and uniform heat generation. A procedure to model individual servers within each rack was developed in [2]. Rambo and Joshi [2] have used CFD/HT to develop a multi-scale model of typical air-cooled data centers using commercial finite volume software. In their work, each rack is modeled as a series of sub-models designed to mimic the behaviour of a server in a data center. Rambo and Joshi [22] have done a parametric numerical study of various supply and return schemes, coupled with various orientations between the racks and the CRAC units, identified the causes of recirculation and non-uniformity in thermal performance throughout the data center.

The multi-scale nature of data centers need to be considered in the numerical modeling of air cooled data centers. Also, as predicted in [13], the future state-of-the-art of thermal management in data centers will include a combination of cooling solutions at different scales. This increases the need to have a multi-scale model for thermal phenomena happening at all important scales. The multi-scale model of a representative data center in [2, 22] consists of ~1,500,000 grid cells and needs more than 2400 iterations to obtain a converged solution. This model took about 8 hours to converge on a 2.8 GHz Xeon with 2 GB memory [22]. Also, it should be noted that this model is still a significant departure from reality because it doesn't include finer details at the server and chip level. In light of this, a comprehensive CFD/HT multi-scale model of operational

data centers, which may contain thousands of racks, seems almost impossible due to limits on available computing. A compact or low-dimensional model which could run much faster, while involving all important scale parameters with sufficient fidelity is essential. A good literature review of data center numerical modeling with a study on the necessity of compact airflow/thermal modeling for data centers have been done in [60].

3.4.2 Low-dimensional Modeling Approaches

Meta-modeling and reduced order modeling techniques can be used to extract the dominant characteristics of a system, trading a degree of accuracy for much greater computational speed. These techniques are briefly reviewed in Section 3.4.2.1 and 3.4.2.2.

3.4.2.1 Meta-Modeling

Approaches such as simple linear response surfaces using Design of Experiments (DOE), kriging, multivariate adaptive regression splines, and other more advanced interpolation approaches offer superior approximations to generate a surrogate model of the system response in terms of the design variables [61]. A literature review and comparison of different meta-modeling techniques with recommendations for computer-based engineering design has been done in [61].

Kriging, called as Gaussian process modeling as well, is a useful method for developing meta-models from expensive computer or experimental simulations for product design optimization [62-64]. Computer models are often deterministic and there is no random error in the output. So, kriging, providing an interpolating meta-model, is

more suitable than the other common alternatives such as quadratic response surface model. For example, kriging has been used for the thermal design of wearable computers [65] and a variable thickness piezoelectric bimorph actuator [66]. Also, Guinta [67] presents an investigation into the use of kriging for the multidisciplinary design optimization of a High Speed Civil Transport aircraft. See [61] for more examples of kriging applications.

Joseph et. al. [68] proposes a modified kriging method, called blind kriging, which has an unknown mean model. The unknown mean model is identified from experimental data using a Bayesian variable selection technique. They applied the blind kriging for making a surrogate model of an engine block and head joint sealing assembly, piston slap noise, and for the flow rate through a borehole. Remarkable improvement is shown in prediction using blind kriging over ordinary kriging. Also, it is concluded that a blind kriging predictor is simpler to interpret and is more robust against the mis-specification in the correlation parameters than an ordinary kriging predictor [68].

Qian et. al. [69] present a two-step approach for building low-cost surrogate models based on data from both detailed and approximate simulations. In their method, a Gaussian process model is first fitted using only approximate simulation data. Then, the fitted model is adjusted with detailed simulation data. They demonstrated the approach with the application for an electronic cooling heat exchanger design involving linear cellular materials. The approach can be used especially when a physics-based model and an approximate model are available. For example in the flow modeling application, the approach can use an approximate model based on Euler equation along with an accurate

model based on Navier-Stokes equation. Qian and Wu [70] have extended the work in [69] to carry out location and scale adjustments more flexibly and absorb uncertainty in the model parameters in the prediction. The prediction in their approach is based on a new Bayesian hierarchical Guassian process model. They applied the method for modeling linear cellular alloys and fluidized-bed processes based on low-accuracy and high-accuracy data.

3.4.2.2 Reduced Order Modeling

The process of taking a model from a large number of degrees of freedom (DOF), either from detailed numerical simulations or full-field experimental measurements, to a model involving significantly fewer DOF is termed model reduction. A number of tools exist for reducing the number of internal states of large systems. For example, some tools can be obtained from discretizing differential equations for linear or simple non-linear systems [71].

An approach to develop reduced order modeling of turbulent flows is obtained based on the observation that many turbulent flows are characterized by characteristic recurrent forms that are collectively called coherent structures. These are energetically dominant in many flows. So, it should be possible to build a relatively realistic, low-dimensional model of the flow by keeping only the dominant coherent structures, and simulating the effect of the smaller, less energetic, apparently incoherent part of the flow in some way [72]. For this, we should first identify the dynamically active structures, classify their elementary interactions, and define an averaging procedure to construct some appropriate averaged quantities which would be the appropriate variables to

describe turbulence and then find the corresponding transport equations to compute the evolution of these new quantities [73].

Flow structure identification techniques can be used to capture the coherent structures of turbulent flows, using a time dependent data set obtained after refining some numerical or experimental velocity data. Eulerian coherent structures can be obtained from, for example, Q-criterion [74] and the swirling strength criterion [75]. These criteria are typically formulated in terms of the invariants of the velocity gradient tensor. Other Eulerian criteria have also been used for structure identification, and some of these have been compared to Lagrangian criteria in [76]. Lagrangian coherent structures can be obtained from the Okubo-Weiss criterion or finite-time Lyapunov exponents [77]. Haller [77] has examined the relevance of Lagrangian coherent structures for the true flow in two-dimensional domains. Green et. al. [78] have identified Lagrangian coherent structures for two three-dimensional flows in a plane channel, including an isolated hairpin vortex and a fully developed turbulent flow, by calculating the direct Lyapunov exponent (DLE). The Lagrangian method captures features of the flow that are familiar from flow visualization experiments, and are also described by various Eulerian criteria currently in use, but the DLE field yields greater detail than existing Eulerian criteria. This is partially because, unlike Eulerian criteria, the DLE may be evaluated on a finer grid than the original velocity data [78].

Appropriate averaging procedures and corresponding transport equations are needed to compute the evolution of the coherent structures in turbulent flows. The fundamental principle in generating low dimensional turbulence modeling based on the

coherent structures is to find a representative set of modes or bases to project the governing equations onto, reducing the solution procedure to finding the appropriate weight coefficients that combine the modes into the desired approximate solution. All classical methods in turbulence rely on the Fourier representation. While the dissipation term is optimally represented in Fourier space because Fourier modes diagonalize the Laplacian operator (for periodic boundary conditions), the nonlinear convective term is very complicated in Fourier space where it becomes a convolution, i.e., all Fourier modes are involved [73]. Also, turbulent motions are nonseparable in the Fourier representation.

Wavelet transform-based techniques are alternative tools to identify the coherent/incoherent structures, and model and compute turbulent flows. The most useful property of the wavelet transform is its ability to detect and accurately measure the strength of individual singularities in a signal. So, wavelet-based techniques can be used to separately model the coherent and incoherent flow components, something that Fourier based models cannot do. Farge et. al. [73] have done a nice review on the application of wavelet-based techniques for turbulent flows. They have shown numerous promising experiments in computing partial differential equations in wavelet space, including heat equation or Stokes equation in 2D and Navier-Stokes equations in 2D. Also, wavelet based techniques can be used to add detail to existing fluid simulations as a user-controlled post-process. Kim et. al. [79] have presented a novel wavelet method to enable large- and small-scale detail to be edited separately. Instead of solving the Navier-Stokes equations over a highly refined mesh, they used the wavelet decomposition of a low-resolution simulation to determine the location and energy characteristics of missing

high-frequency components. Then, these missing components were synthesized using a novel incompressible turbulence function [79].

In addition to the Fourier and wavelet based techniques, the Proper Orthogonal Decomposition (POD) can be also used to generate low dimensional turbulence modeling [21, 53, 72, 80]. The POD, also known as the Karhunen-Loeve decomposition, is a statistical technique and has several properties that make it well suited for turbulent flows. First, it has been shown experimentally that low-dimensional models using POD can well address the role of coherent structures in turbulence generation [72]. Secondly, it captures more of the dominant dynamics for a given number of modes than any other linear decomposition [72]. Finally, the empirical determination of the basis functions makes this method ideal for nonlinear problems. A review of the POD and its application for turbulence modeling has been done in [72].

In the POD-based model reduction technique, a set of data are expanded on empirically determined basis functions for modal decomposition. It can be used to numerically predict the temperature field more rapidly than full-field simulations. The temperature field is expanded into basis functions or POD modes:

$$T = T_0 + \sum_{i=1}^{m} b_i \psi_i \tag{3.6}$$

The general basic algorithm to generate a POD based reduced order thermal modeling in a system is illustrated in Figure 3.4 and is explained in the following:

a) Observation generation: In the first step, the design variables of the system are changed *n*-times and the temperature field for the entire domain is obtained by CFD /HT

simulations, or detailed experimental measurements for each case. These thermal fields are called observations or snapshots. An element of the reference temperature field, T_0 in Eq. (3.6), is typically considered as the average of the all observed data for a field point.

b) *POD modes, ψ_i, calculation*: The POD modes of a thermal system, ψ_i, can be calculated from observations. In Eq. (3.6), *m* is the number of retained POD modes in the decomposition which can be 1 up to *n-1*, where *n* is the number of observations. Using the method of snapshots, each POD mode can be expressed as a linear combination of the linearly independent observations [72]:

$$\psi_i = \sum_{k=1}^{n} a_k (T_{obs,k} - T_0) \tag{3.7}$$

where T_{obs} is a matrix of which each column, $T_{obs,i}$, includes a complete temperature field data from an observation. The weight coefficients, a_k , in Eq. (3.7) are obtained by solving the following *n*n* eigenvalue problem:

$$\sum_{k=1}^{n} R(i,k) a_k = \lambda a_i ; \quad i = 1,...,n \tag{3.8}$$

where $R = (T_{obs} - T_0)^* \otimes (T_{obs} - T_0)/n$ [21, 53, 72, 80] . For a given set of observations, *n* eigenvalues, λ_i, and their relevant eigenvectors are obtained from Eq. (3.8). Each eigenvector includes the weight coefficients, a_k , of the relative POD mode in Eq. (3.7), so *n* POD modes are finally calculated. The energy captured by each POD mode in the system is proportional to the relevant eigenvalue. The eigenvalues are sorted in a descending order, so the first POD modes in Eq. (3.6) capture larger energy compared with the later modes.

c) *POD coefficients, b_i , calculation for a new test case*: This key step is where the POD can be used to create a reduced order thermal/fluid model as a function of the system design variables. Generally, there are three methods to calculate the POD coefficients b_i for a new test case with a new set of design variables:

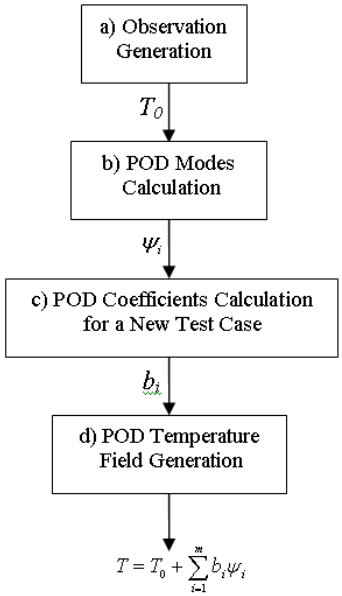

Figure 3.4. General algorithm for POD temperature field generation

- *Galerkin Projection of the system POD modes onto the governing equations:* This results in a set of coupled non-linear Ordinary Differential Equations (ODEs) in time for transient systems, or a set of algebraic equations for steady state systems, to be solved for the POD coefficients. This method has been used to create reduced order models of transient temperature fields in terms of mostly one parameter such as Reynolds/Raleigh number [81-88]. The previous investigations have been either for

prototypical flows (such as flow around a cylinder), or for simple geometries such as channel flow where inhomogeneous boundary conditions are easily homogenized by the inclusion of a source function in the decomposition.

- *Interpolation among modal coefficients*: In steady state, the POD coefficients at a new set of design variables can be obtained by an interpolation between the weight coefficients at the observed variables to match a desired new variable value [88, 89]. In this approach, the coefficients used to reconstruct an observed field $T_{obs,k}$ are found first by projecting each of the POD modes onto the observation in turn:

$$b_{i,obs} = (T_{obs,k} - T_0) \bullet \psi_i \quad i = 1,...,m \tag{3.9}$$

This can be computed for all observations within the ensemble T_{obs}. The complete coefficient matrix $B \in \Re^{m \times n}$, in which each column is the coefficient vector to reconstruct the corresponding observation from the ensemble T_{obs}, can be more efficiently computed as:

$$B = \psi^{+} \otimes (T_{obs} - T_0) \tag{3.10}$$

Where $(.)^{+}$ is the Moore-Penrose pseudo-inverse giving the least squares solution [90]. Once $b_{i,obs}$ has been found for all observations, each of which represents the solution under a specified combination of design variables, the POD coefficients b_i for a new set of design variables are calculated through the interpolation of the coefficients $b_{i,obs}$ between the corresponding observations. In other words, rather than directly interpolating between observations, interpolation is performed in the POD mode space using the

coefficients $b_{i,obs}$. For the systems with one design variable, this interpolation can be done through linear or the slightly more accurate piecewise cubic spline interpolation between coefficients. This method has been applied only for a system with one parameter and simple geometry such as cavity flow [88, 89]. However, the approach can be extended to the more complex systems with multiple design variables using higher order multi-dimensional interpolation approaches, such as kriging or multivariate adaptive regression splines (MARS) [21].

- *Flux Matching process*: In the flux matching process [53, 80], the coefficients b_i are obtained by applying Eq. (4) to some locally specified region, such as system boundaries to match the known mass or heat fluxes. Although the flux matching process has been used to develop reduced order models of the flow behavior in complex steady state systems successfully [21, 52, 53, 91], it has been applied only for thermal modeling of a simple geometry of a channel with two iso-heat flux blocks [80, 91], with no consideration of complex 3D geometry. Nie and Joshi [92] have presented a POD based reduced order modeling of steady turbulent convection in connected domains with the application for a 3D electronic rack. They developed a POD based modeling for each component separately and then subsequently combined the models together using boundary profile based flux matching. Their method is only applicable for the systems consisting of a series of nested sub-domains. Also, their method is focused on the domain complexity more for flow and pressure modeling than thermal modeling.

d) *POD temperature field generation*: With calculated T_0 , ψ_i, and b_i for a new set of design variables, the corresponding temperature field for the test case can be generated inside the entire domain from Eq. (3.6) for different numbers of used POD modes, *m*.

3.4.3 Low-dimensional Modeling of Data Centers

3.4.3.1 Heuristic Methods

Aside from CFD/HT, Simulation methods based on some heuristic approaches have also been explored [93-100] to predict the air temperature at discrete points, such as server inlets/outlets, for a new heat load distribution among the data center racks or servers. In [93-96], machine learning techniques based on the input from several deployed sensors are used to understand the relation between workload and internal and ambient temperatures. These methods require a large number of data points for interpolation and usually need a long calibration for each data center of interest before they can be used for simulation. In [100], a three-fold latent variable model, using structural-equation method (SEM) and errors-in-variables (EV) parametrization, is proposed to generate a surrogate model for maximum rack inlet temperatures in a non-raised floor data center in terms of nine design variables. The surrogate model has been used for determining practical values of the configuration variables of the data center to meet some physical and usage requirements.

In [97] , the amount of heat transferred by the airflow recirculation is described by a cross-interference coefficient matrix, which shows how much of the heat transferred by the air exiting from the outlet of each server contributes to the inlet of every other server.

Having obtained this matrix through a calibration process for a specific data center, an abstract heat flow model is developed to predict the temperatures at the server inlets/outlets versus server power consumption. In [98, 99], a coefficient matrix is made through a calibration process to provide an estimate of how sensitive each server inlet temperature is with respect to every other server heat load step change, for a given CRAC velocity. So an ambient intelligence-based load management (AILM) approach is designed to determine the maximum possible heat loads of each server to meet the corresponding thermal constraint within a given air velocity.

3.4.3.2 Gap Analysis

In Section 3.4.1, the studies on the airflow/thermal modeling of air-cooled data centers through CFD/HT were reviewed and concluded that low-dimensional models are needed in order to predict the multi-parameter dependent thermal behavior of data centers accurately and rapidly for design purposes. The available studies on rapid thermal modeling of data centers in the literature were reviewed in Section 3.4.3.1. However, the presented methods in the literature can predict the air temperatures only at some discrete points, such as server inlets/outlets. Also, the mentioned works simulate the effects of the system parameters on the temperature field in data centers based on some heuristic approaches. However, minimizing over-provisioning and designing neither overcooled or under-cooled data centers with different configurations and thermal characteristics are possible only if a deterministic and quick modeling of the data center temperature field is available in terms of the involved system parameters. So, a physics-based and rapid

modeling approach needs to be developed for design of energy efficient air cooling systems.

As explained in Section 3.4.2.2, reduced order modeling approaches based on turbulence coherent structures and POD have shown great approximation for physics-based rapid modeling of simple thermal/fluid systems. In Chapter 4, a new POD based reduced order thermal modeling approach for multi-scale systems is developed to overcome the modeling challenges in air-cooled data centers.

3.5 Chapter Closure

In this chapter, the design requirements of an open energy efficient air cooling system in data centers were explained. The challenges for such a design were outlined. Robust design principles and cDSP were explained as the two available tools to use in this research in order to overcome the challenges in inherent variability management and having multiple objectives. The main challenge in data centers is thermal modeling. The studies done in the literature on modeling of generally turbulent systems and particularly data centers were reviewed. Some potential meta-modeling techniques and reduced order modeling approaches based on coherent structures are explained and reviewed as available tools for low-dimensional turbulence modeling. While almost all of the studies in the literature on rapid thermal modeling of data centers are based on heuristic approaches, it is concluded that physics-based low-dimensional models are needed in order to predict the multi-parameter dependent thermal behavior of data centers accurately and rapidly for design purposes. This challenge is solved in this research

through development of a POD based reduced order thermal modeling approach, which is explained in Chapter 4.

CHAPTER 4

POD AND GALERKIN PROJECTION FOR THERMAL MODEL REDUCTION IN DATA CENTERS

As shown in Figure 3.1 and explained in Section 3.4.3.2, a reduced order modeling approach is needed to overcome the thermal modeling challenges in air-cooled data centers to address the second research question. In Chapter 4, a new Proper Orthogonal Decomposition (POD) based reduced order modeling of temperature field in multi-scale convective systems such as air-cooled data centers is presented to efficiently simulate the effect of the design parameters. The approach is applicable for systems where the temperature field at selected scales drives the thermal design decision. The energy equation is solved only at these dominant scales via system POD modes and Galerkin projection to obtain a more accurate zoomed prediction at these scales, instead of the entire domain. The effects of the phenomena at other scales are modeled through simple energy balance equations and known heat flux and temperature matching, as well as appropriate matching conditions at the scale interfaces.

In Section 4.1, the new POD based approach to simulate the temperature field in multi-scale thermal-fluid systems is explained. In Section 4.2, the method is applied to an air-cooled data center cell with 5 design variables. The accuracy and efficiency of the POD generated temperature field for different sets of involved design parameters are examined through comparison with CFD/HT results. The chapter is summarized in

Section 4.3. A novel feature is the use of POD modes and Galerkin projection for solving the governing turbulent convection equation in a complex multi-scale system. To the best of the author's knowledge, this work is the first attempt to develop multi-parameter reduced order thermal modeling of multi-scale convective systems.

4.1 POD Temperature Field Generation in Multi-Scale Systems

The new POD based method for the thermal modeling of multi-scale systems has been illustrated in Figure 4.1. The reduced order model is developed assuming the same POD temperature equation for the entire domain:

$$T = T_0 + \sum_{i=1}^{m} b_i \psi_i \tag{4.1}$$

So, the first and second steps in Figure 4.1 are similar to the basic POD technique, as explained in Section 3.4.2.2 and Figure 3.4. The difference is in the key step of the POD technique, where the POD coefficients, b_i , must be calculated. In the new method, after the POD thermal modes have been calculated for the entire domain, the required algebraic equations to calculate the POD coefficients, b_i , are obtained separately by focusing on different scales of the data center. The suggested algorithm is explained in the following:

a) *Observation generation*: Temperature fields in the entire domain for different combinations of input parameters are generated numerically, or experimentally. The reference field T_o in Eq. (4.1) is calculated as the average of the observations.

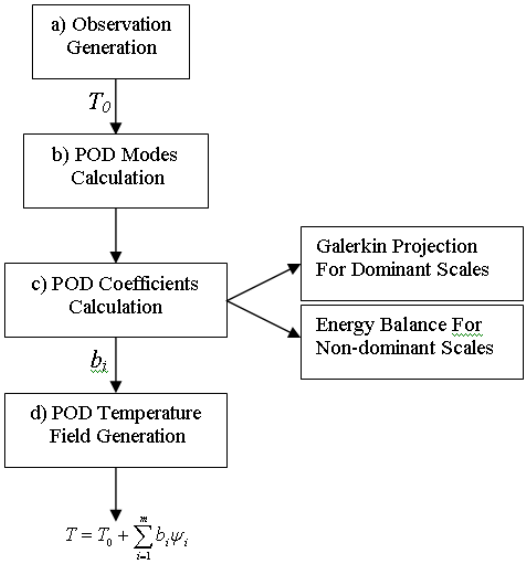

Figure 4.1. POD and Galerkin Projection based thermal modeling method to overcome the thermal modeling challenges in the design method of Figure 3.1

b) *POD modes, ψ_i, calculation*: As explained in Section 3.4.2.2, POD modes for the entire domain can be calculated through Eq. (4.2) by using the observation and solving the eigenvalue problem in Eq. (4.3):

$$\psi_i = \sum_{k=1}^{n} a_k (T_{obs,k} - T_0) \tag{4.2}$$

$$\sum_{k=1}^{n} R(i,k) a_k = \lambda a_i ; \quad i = 1,...,n \tag{4.3}$$

c) *POD coefficients, b_i, calculation*: In this step, appropriate algebraic equations are obtained to calculate the POD coefficients by focusing on the key phenomena at each scale. All equations are subsequently solved together to obtain a single set of POD coefficients, assuming the same POD temperature equation for the entire domain.

In any multi-scale thermal-fluid system, there are often one or few important length scales dominating the thermal performance of the entire system, and driving thermal design decisions. For instance, the temperature field at the rack scale usually drives the thermal decisions for designing a cooling system in a data center.

At the dominant scales, the governing energy equation is solved via POD modes and Galerkin projection to obtain a more accurate prediction at these scales compared with the entire domain. Considering each dominant scale as the computational domain as seen in Figure 4.2, the mean energy equation, ignoring viscous dissipation, is:

$$\rho c_p u \nabla T - \nabla(k_{eff} \nabla T) = q_{Domain} \tag{4.4}$$

In Eq. (4.4), q_{Domain} is the domain volumetric heat generation. In Galerkin projection, the governing equation, Eq. (4.4), is projected into the space spanned by POD modes. Using Eq. (4.1) as the temperature field, Galerkin projection results in a set of linear algebraic equations:

$$\int_{\Omega} \psi_i . (\rho c_p u . \nabla (T_0 + \sum_{l=1}^{m} b_l \psi_l) - \nabla . (k_{eff} \nabla (T_0 + \sum_{l=1}^{m} b_l \psi_l)) - q_{Domain}) \, dx \, dy \, dz = 0 \qquad i = 1,2,...,m \tag{4.5}$$

In Eq. (4.5), *m* is the number of used POD modes, which can change from 1 up to *n-1* where *n* is the number of observations. So we get m algebraic equations for each dominant scale, if m modes are retained in the linear decomposition of temperature field into POD modes. Also, the effect of phenomena at other scales on the dominant scale modeling is considered as boundary conditions at the dominant domain inlet/outlets. Since the reference temperature field, T_o ,and the POD modes are known from the previous steps at the nodes inside and outside of the dominant domain boundary, the

following equations can be used as required boundary conditions while integrating Eq. (4.5) by parts on the domain of Figure 4.2:

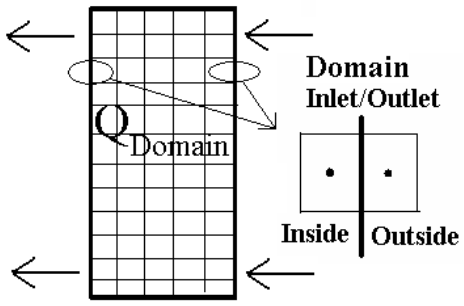

Figure 4.2. Dominant scale as the computational domain.

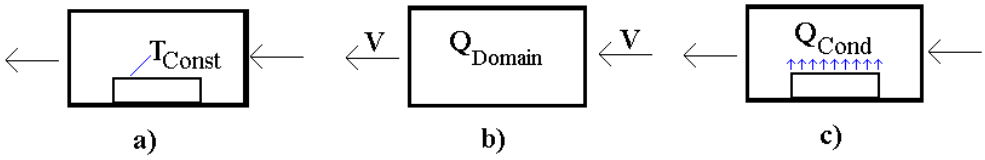

Figure 4.3. Non-dominant scale simplifications.

$$T_{B.C.} = \frac{T_{Inside} + T_{Outside}}{2} = \frac{T_{0,Inside} + \sum_i b_i \psi_{i,Inside} + T_{0,Outside} + \sum_i b_i \psi_{i,Outside}}{2} \tag{4.6}$$

$$\left(\frac{\partial T}{\partial x}\right)_{B.C.} = \frac{T_{Outside} - T_{inside}}{\Delta x} = \frac{T_{0,Outside} + \sum_i b_i \psi_{i,Outside} - T_{0,Inside} - \sum_i b_i \psi_{i,Inside}}{\Delta x} \tag{4.7}$$

On the other hand, at non-dominant scales, the algebraic equations are obtained simply through energy balance equations, heat flux matching, and/or surface temperature

matching. Although simple, heat flux matching has been used as an effective way to calculate the POD coefficients [80]. Generally, the non-dominant domains can be simplified in three ways, as illustrated in Figure 4.3. For case a) in Figure 4.3, the fluid temperature at a specific surface of the domain is kept at a known constant value of T_{Const}. From Eq. (4.1), we get

$$T_{Const} = \overline{T}_0 + \sum_{i=1}^{m} b_i \overline{\psi}_{i,Surf} \tag{4.8}$$

where $\overline{\psi}_{i,Surf}$ and $\overline{T}_0$ are the average values of the temperature POD modes and temperature reference on the surface with a constant temperature. We get one algebraic equation for each constant temperature surface of the domain.

For domains like case b) in Figure 4.3, one equation is obtained to satisfy the conservation of the energy across the domain. Applying the total energy balance across the inlet and outlet surfaces of the domain results in:

$$Q_{Domain} = \rho V A c_p \Delta T_{Domain} \tag{4.9}$$

By separating the known and unknown variables and substituting Eq. (4.1) in Eq. (4.9), we obtain:

$$\frac{Q_{Domain}}{VA\rho c_p} = \Delta T_{Domain} = \overline{T}_{0,DomianOutlet} - \overline{T}_{0,DomainInlet} + \sum_{i=1}^{m} b_i (\overline{\psi}_{i,DomainOutlet} - \overline{\psi}_{i,DomainInlet}) \tag{4.10}$$

Where $\overline{\psi}_{i,Domain\ Inlet}$ and $\overline{\psi}_{i,Domain\ Outlet}$ are the average values of the temperature POD modes on the inlet and outlet surfaces of the domain of case b) in Figure 4.3, respectively. Also,

$\overline{T}_{0,DomainInlet}$ and $\overline{T}_{0,DomainOutlet}$ are the average values of the reference temperature, T_0, on the inlet and outlet surfaces of the domain, respectively.

For domains like case c) in Figure 4.3, one equation is obtained by matching the heat flux at the surface with a constant heat flux.

$$q''_{Cond} = -k \frac{\partial T}{\partial n}|_{wall} \tag{4.11}$$

Since the flux function involves a gradient, substituting the POD temperature of Eq. (4.1) in Eq. (4.11) may produce large errors. To address this issue, a modal heat conduction function, $F_{i,ModalCond}$, is defined in the POD space. All m modal heat conduction functions can be calculated together by [80]:

$$F_{ModalCond} = Q_{CondObs} \otimes (T_{obs} - T_0)^+ \otimes \psi \tag{4.12}$$

Where $Q_{CondObs}$, a *1 x m* matrix, includes *m* observation surface heat inputs and (.)+ is the Moore-Penrose pseudo-inverse giving the least squares solution. This definition results in the following algebraic equation for this case [80]:

$$Q_{Cond} = \sum_{i=1}^{m} b_i F_{i,ModalCond} \tag{4.13}$$

d) *POD temperature field generation*: With calculated T_0 , ψ_i, and b_i for a new combination of design variables, the corresponding temperature field for the test case can be generated inside the entire domain from Eq. (4.1) for different numbers of used POD modes, *m*.

We should note that to solve Eq. (4.5) using Galerkin projection, the flow field and effective thermal conductivity at the dominant scales are required. The average of the velocity and effective thermal conductivity fields between two neighboring observations of each test case are used instead of the exact values in Eq. (4.5). Also, a POD based reduced order velocity model inside the domain can be obtained using flux matching process [53, 80] and used for greater accuracy. In the next section, the method outlined above is applied to an air cooled data center cell.

4.2 Illustration of Multi-scale Thermal Modeling Approach: A Data Center Example

The POD based method outlined above and illustrated in Figure 4.1 is applied to a data center cell shown in Figure 4.4 to simulate the temperature field as a function of Computer Room Air-Conditioning (CRAC) unit air delivery velocity and rack heat loads. Each CRAC unit takes in hot return air from the room and discharges cold air into a sub-floor plenum for delivery to the data center through perforated tiles. Since the air temperature field at the rack scale drives the design of a cooling system in a data center, the turbulent energy equation is solved at the rack domain, see Figure 4.2, via POD modes and Galerkin projection. Also, the effect of room scale phenomena, such as room level air re-circulation, on the rack scale modeling is considered as boundary conditions at the rack inlet/outlets in Galerkin projection. So, equations (4.5), (4.6), and (4.7) are used to obtain m algebraic equations for each rack. At the data center scale, a simple energy balance is applied across the CRAC unit, case b) in Figure 4.3 and Eq. (4.10). Also, the temperature field at the perforated tile surfaces is kept fixed at the known

constant air discharge temperature, case a) in Figure 4.3 and Eq. (4.8). Ultimately, (*m*Nracks+1+1*) equations are obtained to solve for the m POD mode coefficients, b_i . All the mentioned equations are solved together using least square approach to obtain a single set of POD coefficients, assuming the same POD temperature equation for the entire domain.

In Section 4.2.1, a data center example with 5 design variables is defined. The accuracy and efficiency of the presented method in simulating the temperature field for different sets of design parameters are examined in Section 4.2.2 and 4.2.3 through comparison with fine-mesh, full-domain CFD/HT results.

4.2.1 Example Definition

The data center cell is the same as in Section 2.4. To obtain the required observations for the POD algorithm, one-fourth of the representative data center and the plenum are simulated using CFD/HT code, Fluent v. 6.1. The geometry of this section of the data center is shown in Figure 4.4. Each rack is modeled as a volumetric heat source with 6 representative fans at its exit and a lumped pressure jump at its inlet. It is assumed that the sample data center is populated with 30 kW racks in its full capacity. The fan curve and pressure drop coefficient in the model are selected based on the characteristics of IBM eServer™ BladeCenter® compact server infrastructure installed in a rack with nominally designed 30 kW capacity [25]. Accordingly, the pressure rise-velocity relationship in the fan is modeled as:

$$P(V) = -57.961V^3 + 99.784\,\mathrm{V}^2 - 439.41\,\mathrm{V} + 744.46 \tag{4.14}$$

while the pressure drop-velocity relationship of the server system is considered as

$$P(V) = -280.68\,\mathrm{V}^2 \tag{4.15}$$

The CRAC unit is modeled with a constant inlet and exit velocity, discharging the cooling air into the plenum at 15 ^{o}C. An initial mesh contains 198,588 grid cells. The 93% refined mesh with 383,826 grid cells leads to 2.3% and 3.1% change in maximum velocity and temperature, respectively. Therefore, the mesh with 383,826 grid cells is considered fine enough and used here for CFD/HT simulations.

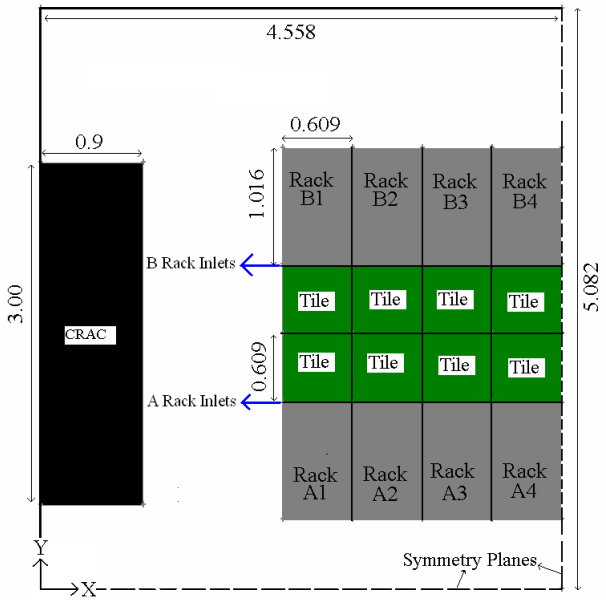

Figure 4.4. Data center cell top view; Dimensions in m. Only one quarter of the cell is shown due to symmetry.

To construct a POD based reduced order model of the temperature field, the rack heat loads and CRAC air flow rate are considered to change between 500 W - 30 kW and 0.94 m^3/s (2000 CFM) - 25.45 m^3/s (54000 CFM), respectively. To reduce the number of design variables for illustration purposes, we assume that corresponding racks in each column have the same heat load. This leads to 5 design variables for the data center cell of Figure 4.4:

1. inlet air velocity of CRAC unit, V_{in}
2. heat load of Rack A1&B1, Q_1
3. heat load of Rack A2&B2, Q_2
4. heat load of Rack A3&B3, Q_3
5. heat load of Rack A4&B4, Q_4

4.2.2 POD Temperature Field for the Example

The CRAC velocity and rack heat loads are varied to generate 19 observed temperature fields for the data center example. The design variables for these observations are collected in Table 4.1. The algorithm listed in Section 4.1 is followed to calculate the POD temperature modes and coefficients for the different test cases. The rack inlet air temperatures are usually used for thermal design of data centers. The contours of the average of all 19 observations, T_0 in Eq. (4.1), at the inlets of racks A1 through A4 and B1 through B4 of the data center cell in Figure 4.4 are shown in Figure 4.5a and Figure 4.5b, respectively. It is seen that the dominant hot spots for the data center cell occur at the middle and top of the 1st rack. As mentioned in Section 4.1, the energy captured by each POD mode in the system is proportional to the relevant eigenvalue in

Eq. (3). The energy percentage captured by each POD mode is plotted versus the mode number in Figure 4.6. The magnitude of the eigenvalue and the energy captured by each mode decreases sharply with the index of POD modes. The modes with largest eigenvalues take the shape of large scale smooth structures, e.g. see Figure 4.7a and Figure 4.7b. The modes with large index numbers include small scale structures, such as the temperature boundary layer, e.g. Figure 4.7c and Figure 4.7d. Figure 4.7 shows the contours of the first two and last two POD modes at the inlet surfaces of racks A1, A2, A3, and A4 of the data center. To solve Eq. (4.5) obtained from Galerkin projection, the velocity field inside the racks and at its boundaries is required. Here we use the CFD solution to verify the presented POD based algorithm. The effects of the velocity and effective thermal conductivities on the temperature solution are studied in Section 4.2.3.

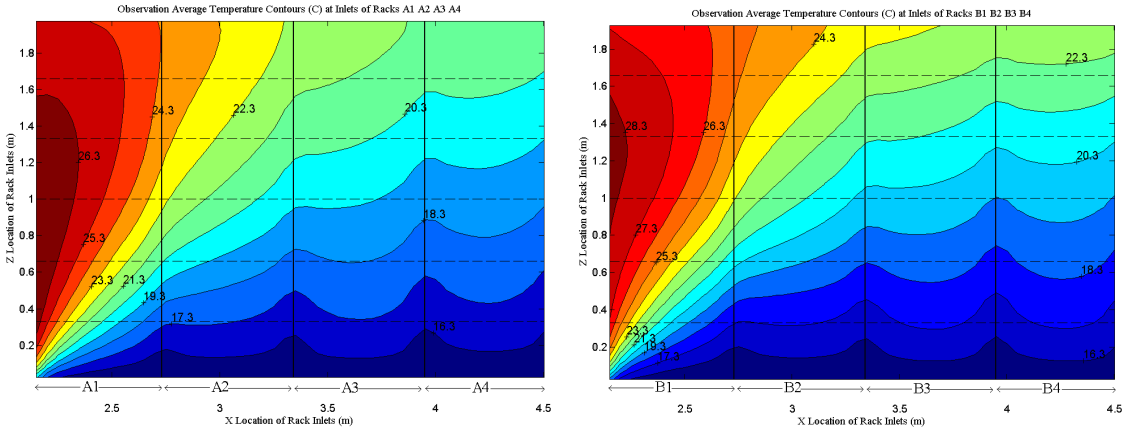

(a) Racks A1-A4 (b) Racks B1-B4.

Figure 4.5. Reference air temperature contours (^{o}C) at the racks inlets.

Table 4.1. Design parameters for the observations

Observation#	1	2	3	4	5	6	7	8	9	10	11	12	13	14	15	16	17	18	19
VCRACin (m/s)	0.4	0.6	0.8	1	1.4	1.9	2.1	2.31	2.4	2.6	3.5	4	4.8	5	6	7	8	9	9.4
RackAB 1 (Kw)	1	2	4	5	6	4	12	15	30	21	14	10	30	21	20	18	17	27	30
RackAB 2 (Kw)	1	3	3	5	7	10	8	15	5	11	22	15	30	21	20	18	13	26	30
RackAB 3 (Kw)	1	2	1	5	8	12	19	15	5	7	20	20	28	21	25	29	24	26	30
RackAB 4 (Kw)	1	1	5	5	9	16	9	15	20	6	14	30	23	21	25	29	18	26	30

The presented algorithm is used to generate temperature field for several new combinations of the design variables. For this case, there are 8*18+1+1=146 equations to be solved for the 18 unknown POD coefficients, using least square approach. POD coefficients of different modes, b_i, for 5 arbitrary test cases are shown in Figure 4.8 when all 18 modes are retained in the decomposition of Eq. (4.1). It is seen that the value of POD coefficients decreases for modes with higher index and lower energy content. So the first few terms in the decomposition of Eq. (4.1) are dominant.

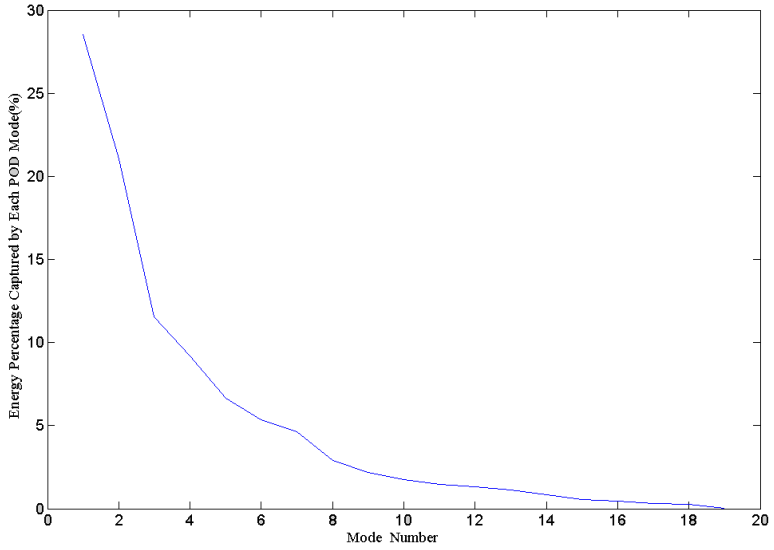

Figure 4.6. Energy percentage captured by each POD mode versus the mode number

Another parameter that shows the convergence of the POD solution is the average temperature difference between inlet and outlet of a rack. This temperature difference across all 8 racks is calculated and plotted in Figure 4.9 for 4 cases when the number of used POD modes changes from 1 to 18. It is seen that the rack temperature differences eventually converge at roughly around 10 modes for all test cases. As shown in Figure 4.6, the first 10 modes capture ~ 84% energy of the system. To study the fidelity of the POD method, the converged values for the temperature differences are compared with full CFD/HT solutions for 15 arbitrary test cases, of which 14 are distinct from the observations. The maximum error for all cases is 1.5 ^{o}C or 9% relative to the temperature differences obtained by full CFD/HT solutions, while the average error for all test cases is 4%. Additionally and more importantly, the POD temperature values within the racks and at their boundaries are compared with full numerical simulations. A mean error, $\overline{T}_{error}(x,y,z)\,(°C)$, is calculated by taking an average of the absolute values of the temperature difference between POD and full numerical predictions for all points:

$$T_{error}(x,y,z) = \left| T_{POD}(x,y,z) - T_{Fluent}(x,y,z) \right| \tag{4.16}$$

$$\overline{T}_{error}(x,y,z) = \frac{\sum_{i=1}^{N_{nodes}} T_{error}(x,y,z)}{N_{nodes}} \tag{4.17}$$

N_{nodes} is the number of nodes/points in the domain, 114,000 at the rack scale. The mean error at the rack scale is plotted for 5 different cases in Figure 4.10 when the number of used POD modes changes from 1 to 18. The converged mean error at the rack scale for these cases is less than 1.3 ^{o}C or 6%. Comparing Figure 4.10 with Figure 4.9 shows while the average temperature difference across the racks has converged after ~10 modes, the

local temperatures need ~4 additional modes to converge for the same test case. As shown in Figure 4.10, the local temperatures at the rack scale converge after ~14 modes.

To see if the POD method can predict the air temperatures at the rack inlets accurately for use in design decisions, the full field predictions, POD simulations, and the POD temperature error are shown in Figure 4.11 for racks A1 through A4 for 4 test cases. The average error is less than 1 ^{o}C, while the maximum local error is ~2.5 ^{o}C for some small regions. Considering that the error in deployed sensor measurements can be around 1 ^{o}C, the POD based method can be used effectively in solving data center thermal design problems. The mean error, the standard deviation, and the Euclidean L2 norm of the POD temperature error at all 114,000 points of the rack scale for the 15 test cases are tabulated in Table 4.2. The standard deviation and the error norm for each test case are defined by:

$$T_{Std} = \left(\frac{\sum_{i=1}^{N_{nodes}} \left(T_{error}(x,y,z) - \overline{T}_{error}(x,y,z) \right)^2}{N_{nodes} - 1} \right)^{1/2} \tag{4.18}$$

$$Error\ Norm = \frac{\left\| T_{error}(x,y,z) \right\|}{\left\| T_{Fluent}(x,y,z) \right\|} * 100\% = \left(\frac{\sum_{i=1}^{N_{nodes}} {T_{error}}^2(x,y,z)}{\sum_{i=1}^{N_{nodes}} {T_{Fluent}}^2(x,y,z)} \right)^{1/2} * 100\% \tag{4.19}$$

In the error norm, the values of temperature are in degree Celsius. As seen in Table 4.2, the mean error varies from 0.35 ^{o}C to 2.29 ^{o}C, while the average is 1.36 ^{o}C, and the average standard deviation 1.12 ^{o}C. Also, the error norm changes from 1.8% to 10.1%, while the average is 6.2%. These values confirm that the presented POD method is accurate enough at the rack scale to use for design purposes.

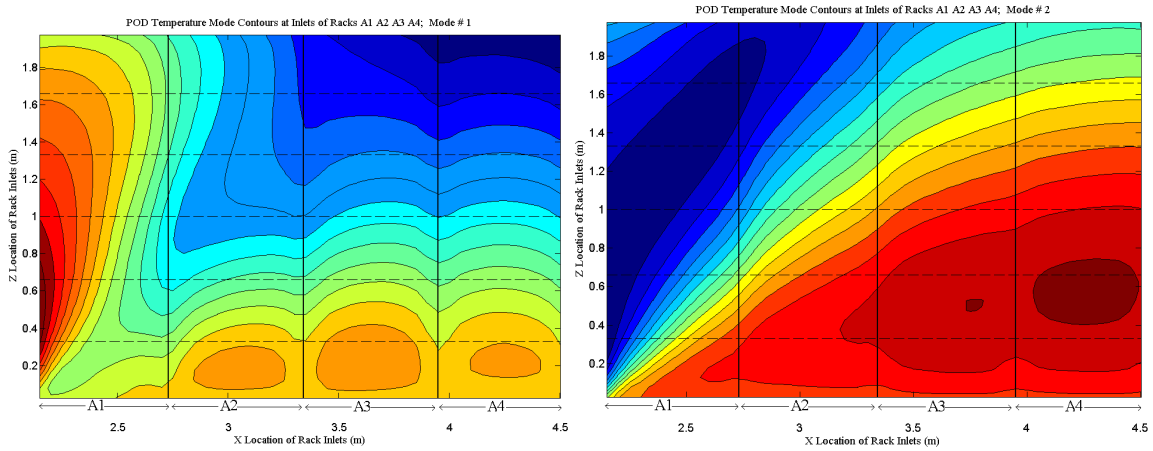

(a) Mode 1 (b) Mode 2

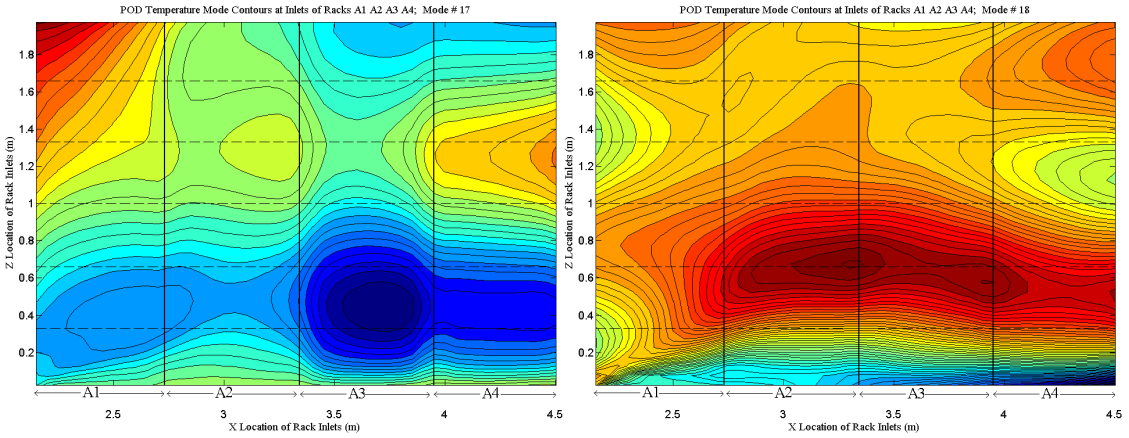

(c) Mode 17 (d) Mode 18

Figure 4.7. Contours of the first two and last two POD modes at the racks inlet surfaces for racks A1-A4.

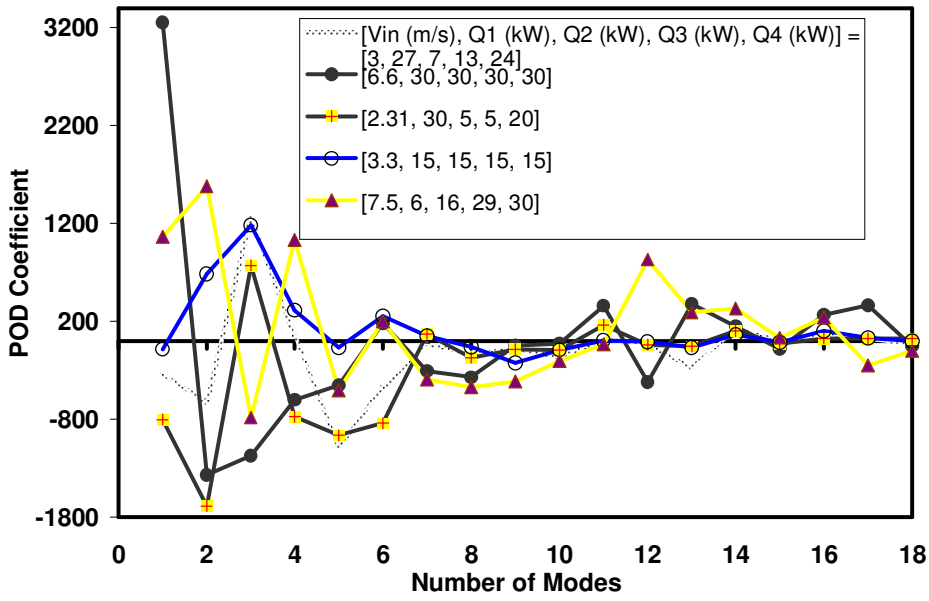

Figure 4.8. POD coefficients of different modes for five test cases which are specified in the legend.

Table 4.2. POD temperature error at rack scale and whole domain for fifteen test cases

		Rack Scale (114,000 points)			Whole Data Center (383,826 points)		
Case#	[Vin(m/s), Q1(kW), Q2(kW), Q3(kW), Q4(kW)]	Error Norm (%)	Mean Error (C)	Standard Deviation (C)	Error Norm (%)	Mean Error (C)	Standard Deviation (C)
1	*[7.5, 6, 16, 29, 30]*	6.35	1.32	1.16	19.00	3.06	2.98
2	*[2, 21, 21, 21, 21]*	3.73	0.96	0.89	30.10	8.29	5.89
3	*[2.31, 5, 5, 20, 30]*	6.59	1.61	1.02	21.07	4.39	3.94
4	*[3, 27, 7, 13, 24]*	6.08	1.21	0.99	12.75	2.32	2.19
5	*[2.31, 30, 5, 5, 20]*	1.80	0.35	0.32	15.80	2.89	2.89
6	*[3.3, 15, 15, 15, 15]*	3.51	0.54	0.60	10.73	1.64	1.76
7	*[6.6, 30, 30, 30, 30]*	4.48	1.18	0.96	23.04	4.53	4.45
8	*[5.5, 14, 23, 3, 19]*	7.39	1.35	1.25	17.74	2.78	2.70
9	*[1.5, 2, 30, 1, 3]*	8.89	1.98	1.36	18.51	3.39	3.27
10	*[4, 30, 29, 9, 28]*	10.12	2.25	1.87	19.30	3.82	3.40
11	*[7.8, 4, 8, 19, 3]*	9.11	1.40	1.17	35.67	5.39	3.36
12	*[1.155, 2.5, 2.5, 10, 15]*	8.66	2.29	1.89	30.32	6.31	6.58
13	*[4.62, 30, 30, 30, 30]*	3.93	1.00	0.91	27.69	6.04	5.79
14	*[6.5, 14, 29, 22, 28]*	6.69	1.56	1.23	16.41	2.92	2.77
15	*[1.4, 6, 7, 8, 9]*	6.23	1.33	1.13	18.06	3.44	3.12
Average		6.24	1.36	1.12	21.08	4.08	3.67

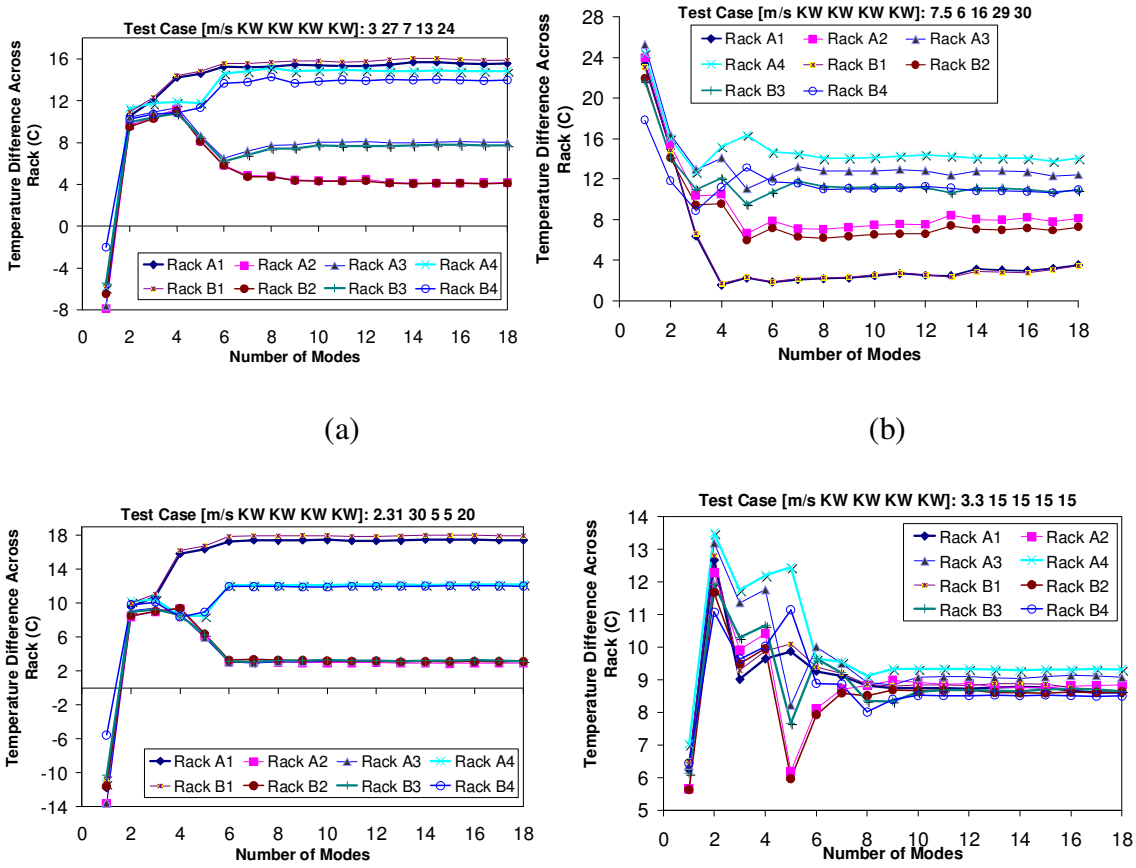

Figure 4.9. Average temperature difference (^{o}C) across eight racks for four test cases. Relevant test case is mentioned at the top of each plot

Although the suggested algorithm mainly focused on the rack scale to predict temperatures at the rack inlet/outlets and inside the racks, it would be interesting to see the POD temperature prediction for the entire data center domain. A very accurate representation of the temperature field at the room scale is not expected, since only a total energy balance and a perforated tile temperature match were used to simulate the details at the room level. The mean error for the entire domain including 383,826 points is calculated and plotted for 5 different cases in Figure 4.12, as the number of used POD modes changes

from 1 to 18. It is seen that the mean error for all cases doesn't change with the number of used POD modes. Additionally, the mean error, the standard deviation, and the Euclidean L2 norm of the POD temperature error at all 383,826 points of the entire domain are tabulated in Table 4.2 for all 15 cases considered before. The mean error changes from 1.64 ^{o}C up to 6.31 ^{o}C, while the average is 4.08 ^{o}C. The average of all standard deviations is 3.67 ^{o}C. Also, the error norm changes from 10.7% up to 35.7% while the average is 21.1%. Although all these values confirm that the presented POD method is not accurate enough at the room scale, it is worth noting that test cases#2, 11, 12, and 13 which have a mean error and error norm higher than 5 ^{o}C and 25% respectively are out of the range of observed temperature fields, or are near the extreme limits.

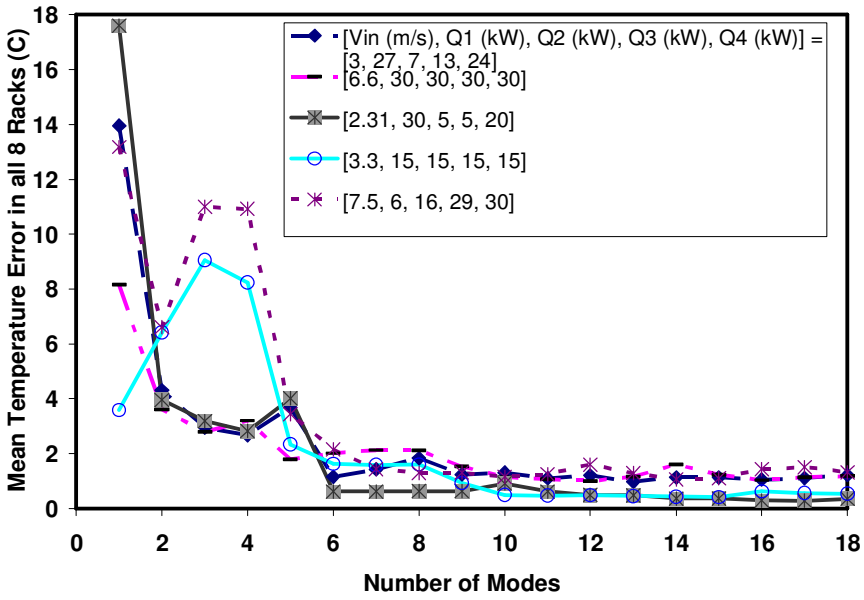

Figure 4.10. Mean temperature error (^{o}C) within eight racks and at their boundaries versus used mode numbers for five test cases which are specified in the legend

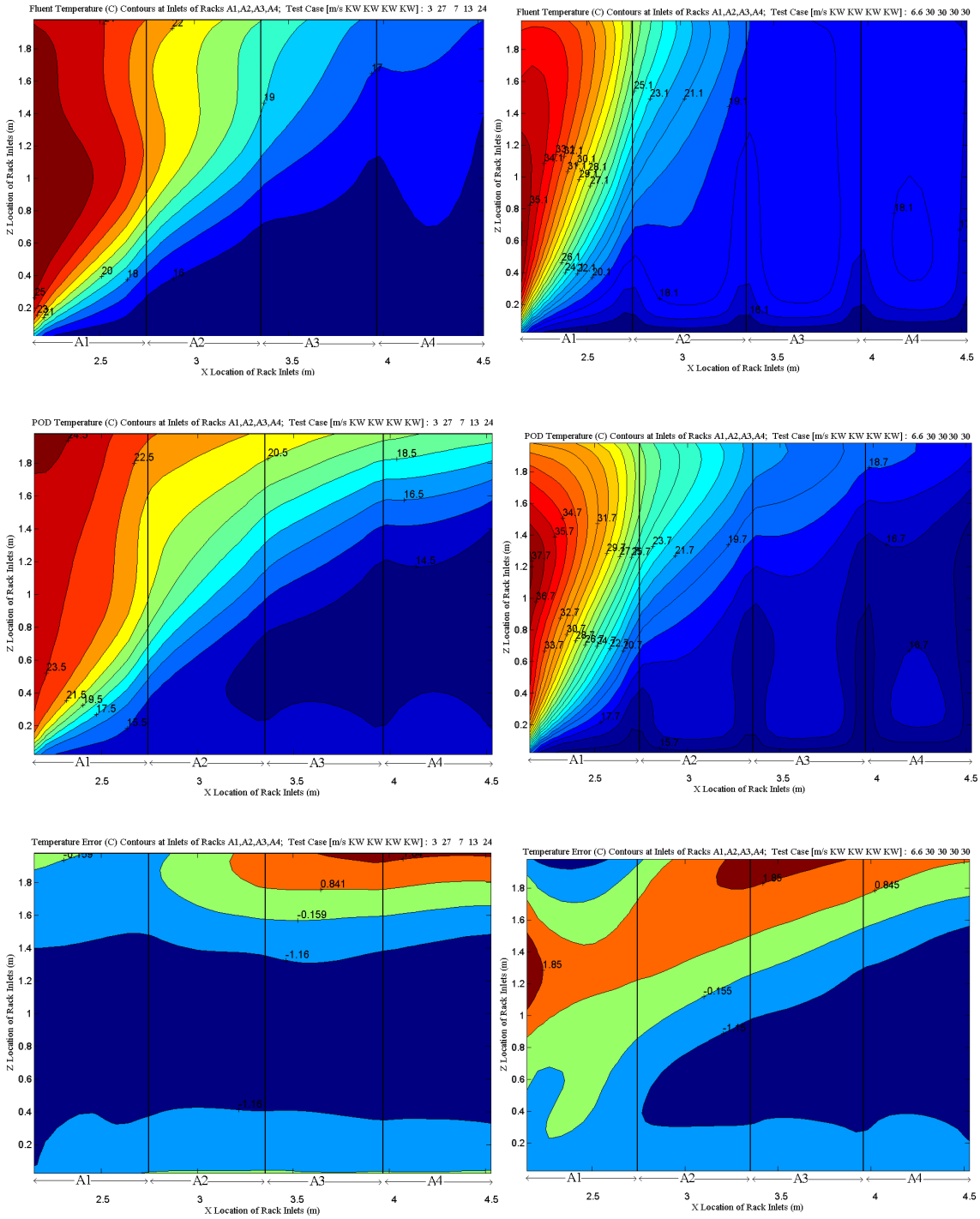

(a) (b)

Figure 4.11. Contours of CFD/HT temperature, POD temperature, and relative error (^{o}C) at racks inlets for four test cases. Relevant test case is mentioned at the top of each contour plot.

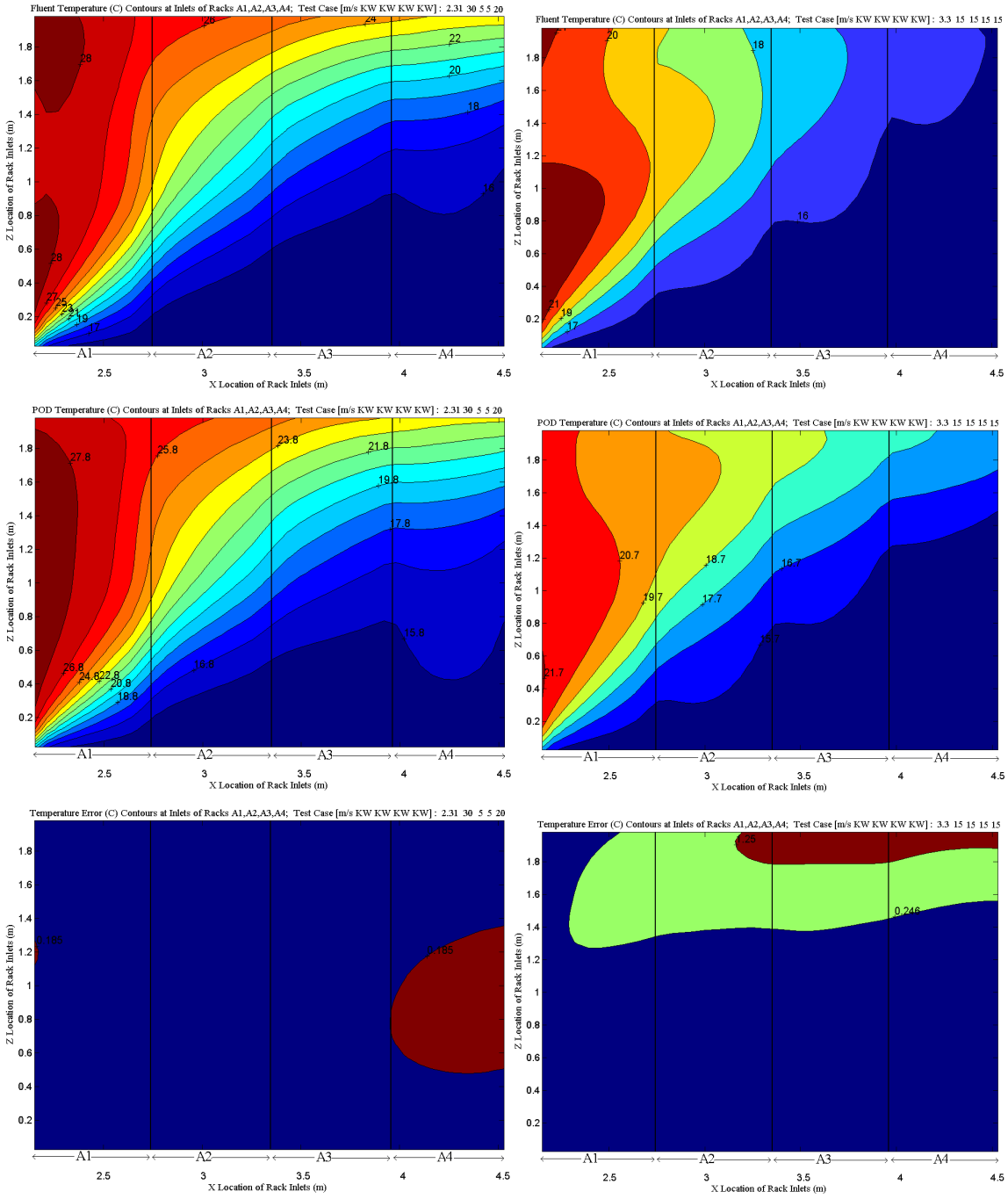

(c) (d)

Figure 4.11. Continued.

An important parameter affecting the temperature field in the data center example is the total heat load divided by the CRAC velocity. This quantity for 19 observations, tabulated in Table 4.1, changes from 18 kW.s/m up to 51.95 kW.s/m, while the average is 35.24 kW.s/m. However, this quantity for test cases#2, 11, 12, and 13 of Table 4.2 is 84, 8.72, 51.95, and 51.95 kW.s/m respectively, which are at the extreme limit or out of the range of the observed data. If we exclude these test cases, the average of norm errors for remaining 11 cases becomes 17.7%. In the next section, the computational efficiency of the algorithm for design purposes, along with the effect of velocity solution on the POD temperature results are studied.

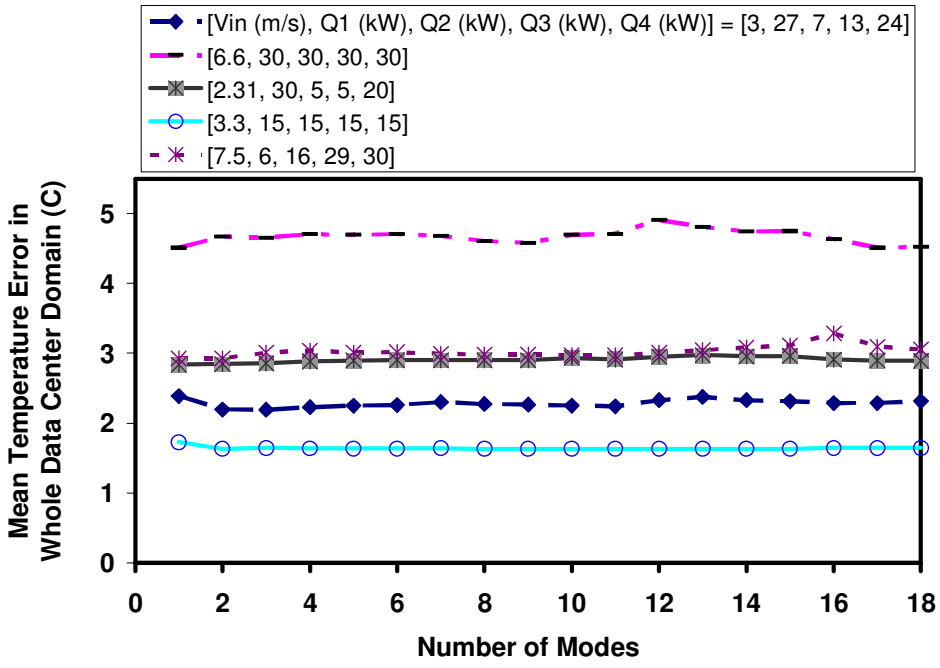

Figure 4.12. Mean temperature error (^{o}C) in whole domain versus used mode numbers for five test cases which are specified in the legend

4.2.3 Velocity Solution Effect on the Result

To solve Eq. (4.5) using Galerkin projection, the flow field and effective thermal conductivity at the rack scale are required. If the flow field has been obtained by a $k-\varepsilon$ model in the CFD/HT approach, the effective thermal conductivity can be obtained versus the turbulent kinetic energy (k) and its dissipation rate (ε):

$$k_{eff} = k_{th} + \frac{c_p \mu_t}{\mathrm{Pr}_t} = k_{th} + \frac{c_p}{\mathrm{Pr}_t}(\rho C_\mu \frac{k^2}{\varepsilon}) \tag{4.20}$$

where the constant C_μ and turbulent Prandtl number, Pr_t , are usually considered constants of 0.09 and 0.85, respectively. The flow field needs to be solved first to obtain the temperature field observations. So, the average of the velocity and effective thermal conductivity fields at the rack scales between two neighboring observations of each test case is used instead of the exact values in Eq. (4.5) to solve the temperature field for the test case. For instance, with CRAC velocity of 3 m/s, the average of the velocity fields of observation#10 with V_{in}=2.6 m/s and observation#11 with V_{in}=3.5 m/s in Table 4.1 is used in the POD algorithm. This modification has been applied to the algorithm and new results for the same 15 test cases are shown in Table 4.3 . Compared to the previous results in Table 4.2, this modification has changed the solutions for the worst cases by only ~1%. The mean error changes from 0.35 ^{o}C up to 2.39 ^{o}C for different test cases, while the average is still 1.36 ^{o}C. The average of all standard deviation is 1.10 ^{o}C. Also, the error norm still changes from 1.8% up to 10.1%, while the average is 6.2%.

Regarding the method efficiency, the POD-based algorithm generates the temperature field for a new test case with different CRAC velocity and rack heat loads in

12 minutes, while the CFD/HT simulation done by Fluent takes ~2 hours for the same test case on the same computing platform (a desktop computer with Xeon™ CPU, 2.8-GHz and 2.75 GB of RAM). Also, the most time-consuming part of the method, integrating the velocity terms in Eq. (5) over the domain, can be done once for all observed CRAC velocities, if the method is to be used for many simulations. It takes ~38 minutes to calculate these terms. After that, the algorithm is ready to obtain the POD temperature field for each new test case in only 4 seconds. So, if we assume that 100 additional runs beyond the initial observations are needed to find an optimal thermal design in data centers, the CFD/HT model by Fluent takes ~200 hours (~8 days) to find the design solution, while the POD algorithm can do it in ~(38+7=45) minutes which is ~250 times faster. This confirms the ability of the presented method to provide a quick and accurate enough thermal modeling of a multi-scale thermal-fluid system in order to design around several input parameters.

Regarding the POD computational efficiency comparison with CFD based numerical methods, it should be noted that the CFD/HT model developed and simulated by Fluent here is not an optimum numerical model. One could develop a more computationally efficient CFD based model for the data center example.

Table 4.3. Temperature error of the POD algorithm using average of neighbouring velocity solutions

		Rack Scale (114,000 points)			Whole Data Center (383,826 points)		
Case#	[Vin(m/s), Q1(kW), Q2(kW), Q3(kW), Q4(kW)]	Error Norm (%)	Mean Error (C)	Standard Deviation (C)	Error Norm (%)	Mean Error (C)	Standard Deviation (C)
1	*[7.5, 6, 16, 29, 30]*	6.36	1.33	1.15	18.99	3.06	2.98
2	*[2, 21, 21, 21, 21]*	3.68	0.95	0.86	30.23	8.31	5.93
3	*[2.31, 5, 5, 20, 30]*	6.59	1.61	1.02	21.07	4.39	3.94
4	*[3, 27, 7, 13, 24]*	5.82	1.12	0.99	12.70	2.30	2.19
5	*[2.31, 30, 5, 5, 20]*	1.80	0.35	0.32	15.80	2.89	2.89
6	*[3.3, 15, 15, 15, 15]*	4.81	0.89	0.66	10.51	1.64	1.70
7	*[6.6, 30, 30, 30, 30]*	4.29	1.15	0.90	23.32	4.61	4.48
8	*[5.5, 14, 23, 3, 19]*	7.39	1.37	1.24	17.88	2.81	2.71
9	*[1.5, 2, 30, 1, 3]*	8.97	1.99	1.40	18.52	3.40	3.26
10	*[4, 30, 29, 9, 28]*	10.12	2.25	1.87	19.30	3.82	3.40
11	*[7.8, 4, 8, 19, 3]*	9.08	1.41	1.15	35.69	5.39	3.37
12	*[1.155, 2.5, 2.5, 10, 15]*	9.11	2.39	2.01	30.25	6.31	6.56
13	*[4.62, 30, 30, 30, 30]*	2.82	0.77	0.59	27.73	6.05	5.80
14	*[6.5, 14, 29, 22, 28]*	6.68	1.56	1.22	16.41	2.90	2.79
15	*[1.4, 6, 7, 8, 9]*	6.23	1.33	1.13	18.06	3.44	3.12
Average		6.25	1.36	1.10	21.10	4.09	3.67

4.3 Chapter Closure

While time-consuming and costly, especially for iterative optimization based design, CFD/HT models are currently used to obtain the thermal fields inside multi-scale thermal-fluid systems such as data centers. A new method based on Proper Orthogonal Decomposition (POD) was presented in this chapter to develop reduced order models of the temperature field in these systems. The POD modes are obtained at the system level based on numerically or experimentally observed temperature fields, while the algebraic equations to calculate POD coefficients are obtained separately at different scales. The energy equation is solved at the dominant scales via POD modes, Galerkin projection, and special treatment of boundary conditions, while energy balance, specified temperature, and heat flux matching are used at non-dominant scales. Finally, equations of all scales are solved together using the least square approach to generate a temperature field for a new set of design parameters. The method was applied to a data center cell with five design parameters, one CRAC velocity and four racks heat loads. The method

results in average error norm of 6.2% for different sets of design parameters, while it can be up to ~250 times faster than the CFD/HT simulation done by Fluent in an iterative optimization technique.

The presented approach is centered on the integration of three constructs to solve the challenges of multi-parameter thermal modeling in complex multi-scale convective systems: a) POD basic technique, b) Galerkin projection, and c) energy balance/heat flux matching. Analysis of the obtained results shows the ability of the presented method to generate rapid and sufficiently accurate thermal modeling of a multi-scale thermal-fluid system to design around several input parameters. While the proposed method was applied to one class of multi-scale systems, these constructs should be applicable to other complex multi-scale convective systems.

The thermal modeling challenges in developing the open design method in Figure 3.1 is solved through using the developed POD based modeling approach in this chapter. In Chapter 5, the integration of the three constructs of POD based method, cDSP, and robust design as a practical open design method is demonstrated through application to a data center cell design.

CHAPTER 5

OPEN DESIGN APPROACH FOR ENERGY EFFICIENT DATA CENTERS

In Section 3.1, three main challenges were identified to develop a design method for open multi-scale systems, as shown in Figure 3.1. Robust design principles and cDSP were explained in Sections 3.2 and 3.3 as the two available tools to use in this research in order to overcome the challenges in inherent variability management and having multiple objectives. Also, the third and main challenge, thermal modeling, was solved through development of a POD based reduced order thermal modeling approach in Chapter 4. As shown in Figure 3.1, a simulation-based open thermal design approach is developed based on the integration of these three tools to bring adaptability and robustness, two main features of open engineering systems, to multi-scale convective systems. In Chapter 5, the application of this design method for open energy efficient air-cooled data centers is explained. In Section 5.1, the design problem for open energy efficient thermal management of air-cooled data centers is described. In Section 5.2, the open design method of Figure 3.1 is demonstrated through application to a data center cell in which there is an annual increase in the power consumption for the next 10 years. The results using both traditional and open design methods are compared and discussed. Finally, the chapter synopsis is presented in Section 5.3.

5.1 Baseline and Open Design Methods for Energy Efficient Data Centers

The typical approach currently used for the thermal management of data centers utilizes computer room air conditioning (CRAC) units that deliver cold air to the racks arranged in alternate cold/hot aisles through perforated tiles placed over an under-floor plenum, as shown in Figure 5.1. The CRAC units themselves are cooled by a chilled water loop, transferring the data center heat load to an outdoor chiller and ultimately to the ambient. In the traditional design, the required CRAC air flow rate is calculated based on an acceptable temperature difference across the servers, ΔT , typically 11 ^{o}C (20 ^{o}F):

$$V_{in} A_{CRAC} = \frac{Q_{total}}{\beta \rho c_p \Delta T} \tag{5.1}$$

where V_{in} is the average velocity of the supply air from the CRAC unit's discharge surface, A_{CRAC}. Also, Q_{total} is the data center heat load. Coefficient $\beta > 1$ is a rule-of-thumb parameter which accounts for the air recirculation effect on the temperature field in the data centers with cold/hot aisle arrangement. The CRAC supply temperature is fixed for intended data center heat load, while the work/heat load among the servers and racks are distributed randomly. As explained in Chapter 2 in addressing the firs research question while the heat generated by the electronic equipment in data centers is increasing year after year due to demands for higher processor speeds and miniaturization, sustainable and reliable operation of data centers is possible through energy-efficient and open design of cooling systems for containing operating costs and promoting sustainability. In this regard, the main design requirements of the air-cooled systems can be classified into [101]:

a) *Operating temperature limits*: The cooling system must keep the operating temperature in a specified range, below a typical value of 85 °C for silicon components. To analyze the thermal performance of the typical air-cooling systems in data centers, a corresponding criterion may be to maintain the inlet cooling air temperature to the servers, considering the possible changes in the system parameters, under 32 °C [102].

b) *Energy efficiency*: Total cooling energy consumption of the data center, which is the summation of CRAC and chiller consumed work, $W_{Cooling} = W_{CRAC} + W_{Chiller}$, determines the operating cost of the data center cooling system, which should be minimized. Also, the cooling system should be designed to remove the actual data center heat load, rather than planned occupancy, to have an energy efficient design which is neither under-cooled nor overcooled.

c) *Robustness*: This requires maintaining the energy efficiency, effectiveness, reliability, and performance stability of the equipment, in spite of large uncertainty and variability. The typical variability sources are variations of CRAC supply air flow rate and rack heat loads.

d) *Adaptability*: This allows additional flexibility to adjust and adapt to future technology, changes in environment and changes in customer demands. Air-cooled systems should be designed to be adaptable to these changes through, for example, intelligent rack heat load re-allocation and changes in supply temperature and air flow rates of CRAC units to handle the lifecycle mismatch between the IT equipment and facility thermal management systems.

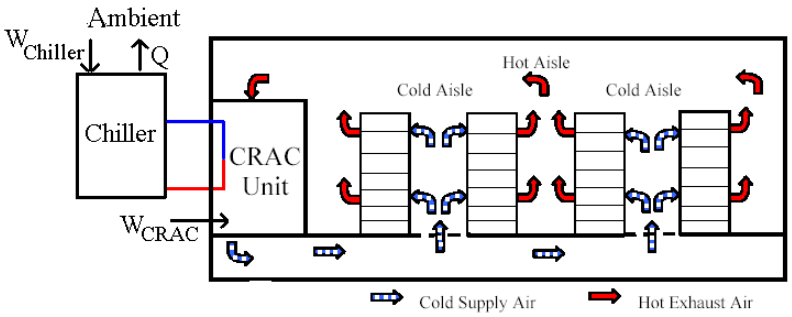

Figure 5.1. State-of-the-art configuration in cooling data centers

Previous application of simulation based design for data centers is limited to ad hoc analyses based on experience and simple correlations [17, 55], simple data center level Computational Fluid Dynamics/Heat Transfer (CFD/HT) modeling with some comparison of configurations [1, 2, 4, 22, 54], and some limited geometric optimization using design of experiments to create coarse response surface models with very few variables [5, 14-16]. All this previous work utilizes the single objective of temperature minimization. An exploration of possible different data centers configurations and thermal characteristics requires a quick and accurate compact thermal model. Simulation methods based on learning machine methodology to predict the air temperature at some discrete points such as server inlets/outlets for a new heat load distribution among the data center racks have been explored [93-96]. This method has been used to find the optimum heat load distribution among racks for different data center capacity utilization. These methods require a large number of data points for interpolation and usually need a long calibration for each data center of interest before it can be used for simulation and optimization. These "smart" thermal solutions are completely based on experimental measurement and online control of the specified parameters [20, 95]. Rolander [52] presented a simulation-based design approach centered on POD and the cDSP for robust

design of turbulent convective systems and applied it to a single electronic rack of an air-cooled data center. This approach was shown to provide 50% more efficiency by re-allocation of the server heat loads and adapting the inlet air flow rate [52].

In Section 5.2, the method of Figure 3.1 for open design of multi-scale convective systems is demonstrated through application for an air-cooled data center cell. A data center example is defined first in Section 5.2.1. Then, a reduced order thermal modeling of the data center using the POD based method, explained in Chapter4, is developed in Section 5.2.2. The design problem is formulated using the cDSP in Section 5.2.3. Finally, the results and discussion are presented in Section 5.2.4.

5.2 Open Design of a Data Center Example

5.2.1 Example Definition

An adaptable robust and energy efficient design of an air-cooled data center cell which will be used for the next 10 years is considered. The data center cell is the same as in Section 4.2.1. One-forth of the data center cell is shown in Figure 5.2. The data center will house 1,033 Watt/m^2 (96 Watt/ft^2) for the first year of the operation, which is equal to 10% utilization of the full capacity. New IT equipment is integrated into the data center annually so that the data center will cope with 10,355 Watt/m^2 (962 Watt/ft^2) during the 10^{th} year of the operation at 100% utilization.

Considering the requirements of an air-cooled data center, explained in Section 5.1, the design problem can be summarized as in Figure 5.3. This diagram shows a design methodology to handle the actual momentary total heat load with minimum

cooling energy consumption and maximum efficiency, through adaptable changes in the rack heat load allocation, and CRAC supply air flow rate and temperature. The method also seeks minimum variation in the rack inlet temperature due to changes in CRAC supply air flow rate and temperature and rack heat loads. The heat load re-allocation can be implemented through physical relocation of the hardware, and/or by distributing the processing tasks among the servers through virtualization technology [20]. The air flow rate of CRAC units can be varied using variable frequency drive motors. Also, the CRAC supply temperature can be easily changed in operational data centers.

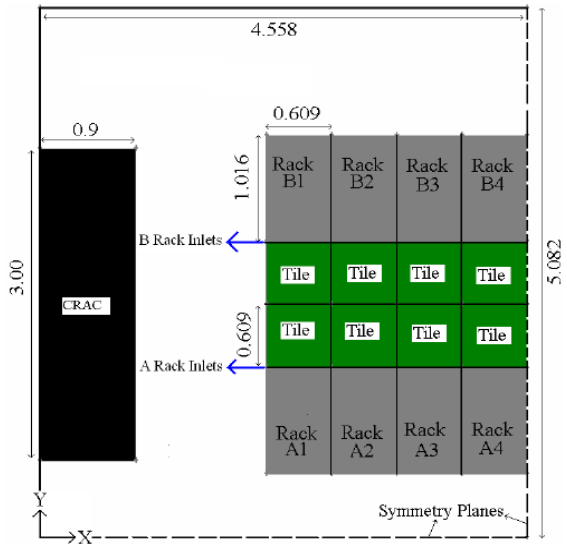

Figure 5.2. Data center cell top view; Dimensions in m. Only one quarter of the cell is shown due to symmetry.

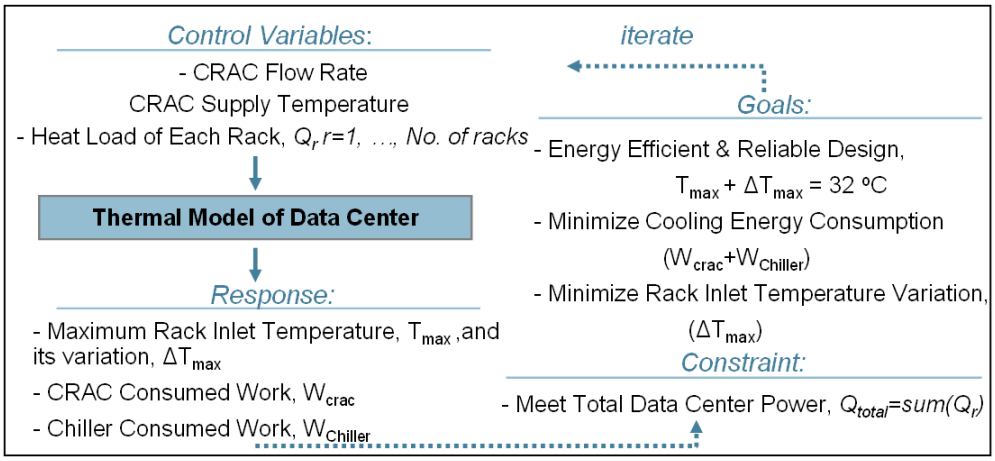

Figure 5.3. Adaptable robust design in energy efficient data centers

As explained in the following, we do not directly consider the CRAC supply temperature as a control variable in iterative optimization. Also, to reduce the number of design variables for illustration purposes, we assume that corresponding racks in each column of the data center cell have the same heat load. This leads to 5 design variables, x_i, for the data center cell of Figure 5.2:

1. inlet air velocity of CRAC unit, V_{in}
2. heat load of Rack A1&B1, Q_1
3. heat load of Rack A2&B2, Q_2
4. heat load of Rack A3&B3, Q_3
5. heat load of Rack A4&B4, Q_4

The rack heat loads and CRAC air velocity are considered to change between 500 W - 30 kW and 0.35 m/s – 9.4 m/s, respectively. This causes the CRAC air flow rate to change from 0.94 m^3/s (2000 CFM) - 25.45 m^3/s (54000 CFM). Depending on the

thermal capacity of the CRAC heat exchanger, the CRAC unit must provide a minimum flow rate to be able to remove a given data center heat load. The typical relationship between the heat removal capacity of a CRAC unit as a function of air flow rate is shown in Figure 5.4. Accordingly, the following relationship is used to calculate the minimum required CRAC velocity (in m/s) as a function of total heat load (in kW):

$$V_{in,\min imum} = \frac{-0.01 + \sqrt{(0.0001) - (28E-8)Q_{total}}}{-0.0008} \tag{5.2}$$

For a given data center heat load and initial CRAC supply temperature (15 ^{o}C in this study) , the maximum inlet cooling air temperature to the servers, considering the possible changes in the system parameters, is designed to be equal to 32 °C in order to have reliable, and neither overcooled nor under-cooled data center based on ASHRAE standards [102]. For this purpose, the initial data center air temperatures, obtained at the CRAC initial supply temperature, are increased by a specific value $(32 - (T_{max} + \Delta T_{max}))$.

$$T_{Supply,\,new} = T_{Supply,\,initial} + (32 - (T_{max} + \Delta T_{max})) \tag{5.3}$$

Considering the new CRAC supply temperature, the chiller work is calculated by:

$$W_{Chiller} = \frac{Q}{COP} \tag{5.4}$$

Where the Coefficient of Performance (COP) of the chiller-CRAC loop as a function of CRAC supply temperature can be calculated by modeling the chiller performance and the CRAC heat exchanger. This relationship for a water-chilled CRAC unit in a Hewlett-Packard (HP) Utility Data Center [103] is shown in Figure 5.5. At higher supply

temperatures, the COP increases and the chiller consumes less energy to remove a given center heat load. This relationship from [103] is also used here for COP calculation.

$$COP = 0.0068T_{Supply}^2 + 0.0008T_{Supply} + 0.458 \tag{5.5}$$

In addition to the chiller work, the work consumed by the CRAC blower motor should be calculated. The consumed work by CRAC is usually a linear function of the air flow rate. The following equation, obtained from the available data for typical CRAC units, is used in this study to calculate W_{CRAC}:

$$W_{CRAC}(kW) = 2.7V_{in}(m/s) \tag{5.6}$$

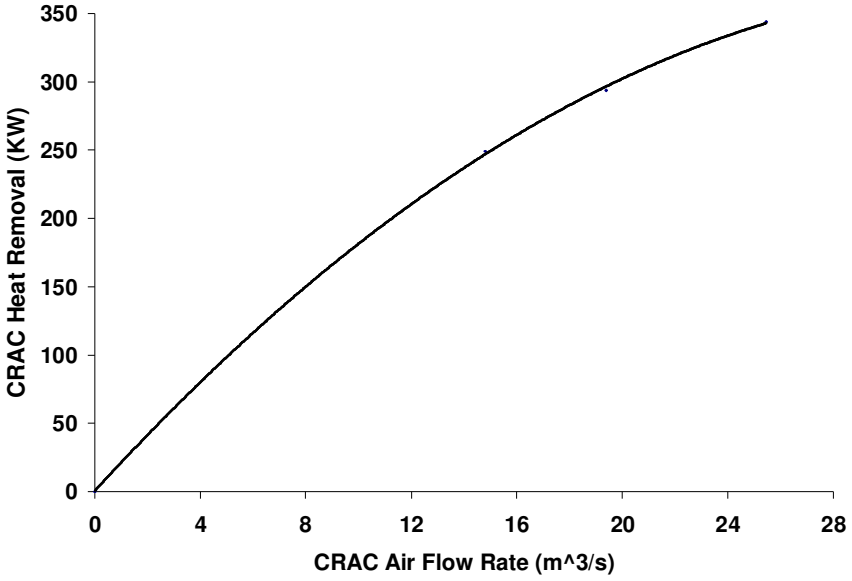

Figure 5.4. CRAC heat removal capacity as a function of air flow rate

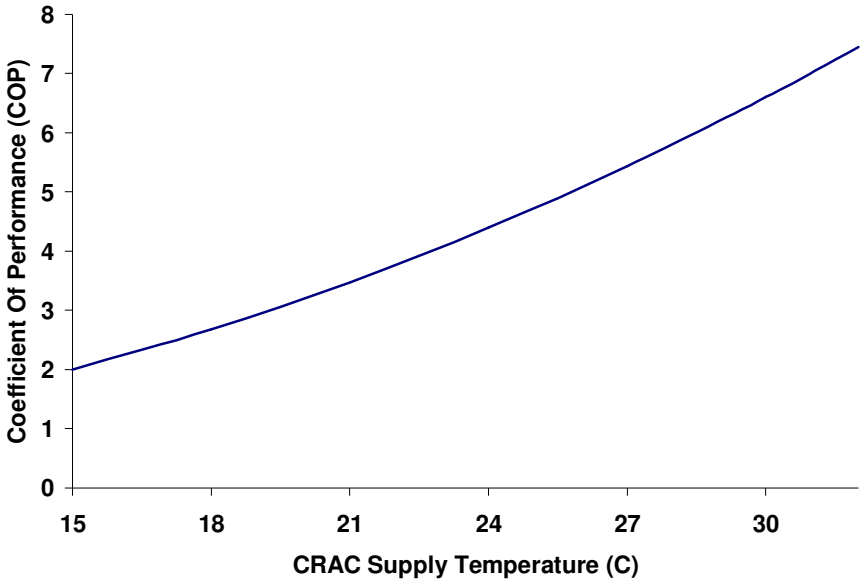

Figure 5.5. COP of a chilled water loop in the HP Utility Data Center [103]

At each iteration of the design problem in Figure 5.3, the chiller and CRAC work are calculated as explained above. Then, iteration continues to find optimal and robust values of the control variables to minimize the cooling energy consumption and rack inlet temperature variation. In order to model the temperature field inside the data center and obtain T_{max}, the POD based algorithm explained in Chapter 4 is used. Also, for Type-II robust design, the variability of the response, $\Delta T_{\max}$, is calculated by Taylor expansions of the system response, considering the worst variation scenario in the design variables:

$$\Delta T_{\max} = \sum_{i=1}^{5} \left| \frac{\delta T_{\max}}{\delta x_i} \Delta x_i \right| \tag{5.7}$$

The derivatives are computed using first order difference technique since no closed form solution exists.

To summarize, the following steps are taken to solve the design problem in Figure 5.3 for the data center example:

1. Find the maximum rack inlet temperature T_{max} as a function of control variables of CRAC velocity and racks heat loads:

   1.1. For known CRAC initial supply temperature (15 ^{o}C), generate observations by varying the control variables, i.e. CRAC velocity and racks heat loads

   1.2. Obtain POD modes and coefficients for a new set of control variables

   1.3. Find T_{max}

   1.4. Calculate $\Delta T_{\max}$, $T_{supply,\, new}$, $W_{Chiller}$, W_{crac} using Eqs. (5.3) - (5.7)

2. Using cDSP and designer's preferences over the goals, W_i , formulate and solve the design problem for a given data center heat load at different years, Q_{total}

3. Save the results for energy efficient and robust operation of the data center at each year:

   3.1. optimal/robust CRAC flow rate and racks heat loads

   3.2. optimal/robust CRAC supply temperature

Following the listed steps, the POD based algorithm is applied to the data center cell in Section 5.2.2. Then, the design problem is formulated by cDSP in Section 5.2.3. The design problem is solved and results for the examplpe are discussed in Section 5.2.4.

5.2.2 POD Based Thermal Modeling of the Data Center Cell

To obtain the required observations for the POD algorithm summarized in Figure 4.1, one-fourth of the data center cell and the plenum, shown in Figure 5.2, are simulated using CFD/HT code, Fluent v. 6.1, similarly to the model in Section 4.2.1. As mentioned in Section 4.2.1, the pressure rise-velocity relationship in the fan is modeled as:

$$P(V) = -57.961V^3 + 99.784\,\mathrm{V}^2 - 439.41\,\mathrm{V} + 744.46 \tag{5.8}$$

while the pressure drop-velocity relationship of the server system is considered as

$$P(V) = -280.68\,\mathrm{V}^2 \tag{5.9}$$

The CRAC velocity and rack heat loads are varied to generate 25 observed temperature fields for the data center cell. The design variables for these observations are collected in Table 5.1. The contours of the average of all 25 observations, T_0 in Eq. (2), at the inlets of racks A1 through A4 and B1 through B4 of the data center in Figure 5.2 are shown in Figure 5.6a and Figure 5.6b, respectively.

Table 5.1. Design parameters for the observations

Observation#	1	2	3	4	5	6	7	8	9	10	11	12	13	14	15	16	17	18	19	20	21	22	23	24	25
Vin (m/s)	0.4	0.6	0.8	1	1.2	1.4	1.6	2	2.1	2.4	2.6	3	3.25	3.5	3.75	4	4.25	4.5	5	5.5	6	7	8	9	9.4
Q1 (KW)	1	2	4	5	7	6	11	4	12	30	21	17	4	14	15	10	10	21	21	29	20	18	17	27	30
Q2 (KW)	1	3	3	5	4	7	11	10	8	5	11	6	7	22	16	15	10	16	21	28	20	18	13	26	30
Q3 (KW)	1	2	1	5	8	8	11	12	19	5	7	22	10	20	16	20	30	27	21	16	25	29	24	26	30
Q4 (KW)	1	1	5	5	9	9	11	16	9	20	6	20	8	14	25	30	30	23	21	26	25	29	18	26	30

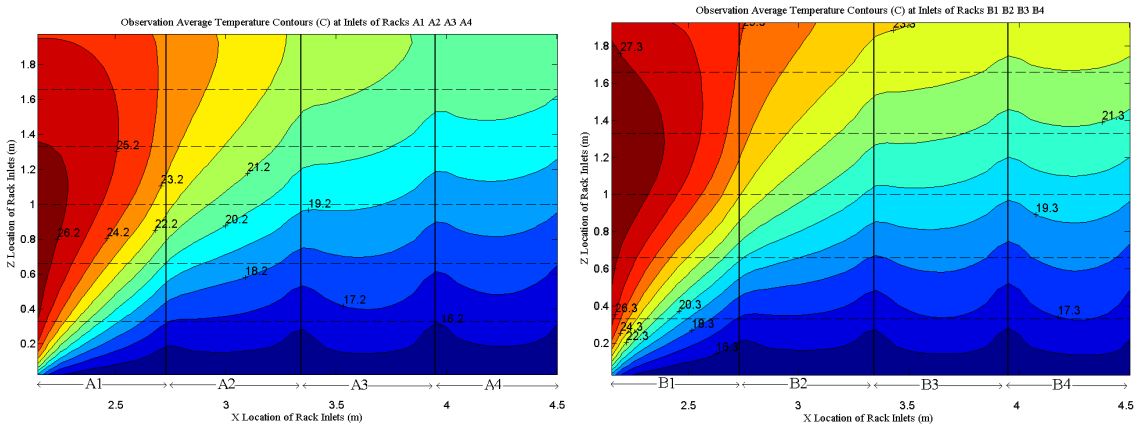

(a) Racks A1-A4. (b) Racks B1-B4.

Figure 5.6. Reference air temperature contours (^{o}C) at the racks inlets.

Similarly to Section 4.2.1 and Section 4.4.2, the POD based algorithm is used to generate temperature field for several new combinations of the design variables. The resulting POD based thermal model has only 24 DOF, representing a 5 order of magnitude decrease from the CFD/HT model. The POD-based algorithm generates the temperature field for a new test case with different CRAC velocity and rack heat loads in 12 minutes, while the CFD/HT simulation by Fluent takes ~2 hours for the same test case on the same computing platform (a desktop computer with Xeon™ CPU, 2.8-GHz and 2.75 GB of RAM). Since the algorithm is to be used for many simulations, the most time-consuming part of the method, integrating the velocity terms in Eq. (4.5) over the domain, is done once for all observed CRAC velocities. It takes ~92 minutes to calculate these terms. After that, the algorithm is ready to obtain the POD temperature field for each new test case in only 5 seconds. As explained in Chapter 4, comparing the temperature field from the POD based method with the CFD/HT simulations for the sample data center shows that the method can predict the temperature field at the rack scale with the average error norm of ~6% for different sets of design parameters [104]. In

this section, only the comparison between the maximum rack inlet temperature, T_{max}, obtained by POD and CFD/HT is presented since T_{max} drives the thermal design decision as discussed before and shown in Figure 5.3.

The maximum rack inlet temperatures obtained by POD are compared with full CFD/HT solutions in Table 5.2 for 41 arbitrary test cases, of which 36 are distinct from the observations. As seen in Table 5.2, the average of the error for all test cases is 1.3 ^{o}C or 4.6% while the error for few test cases, especially for the cases out of the range of observed temperature fields or near the extreme limits, is higher than 2.5 ^{o}C. To be used within the iterative robust design problem of Figure 5.3, the compact model of the data center must predict the effect of the total center heat load, rack heat load allocation, and the CRAC velocity on T_{max} accurately.

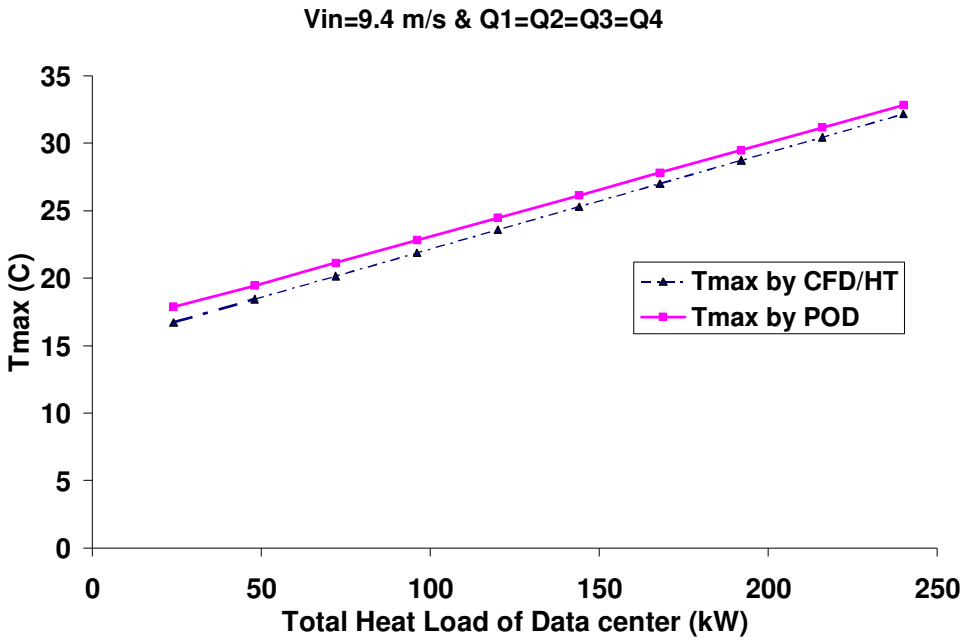

Figure 5.7. T_{max} obtained by POD and CFD/HT for CRAC velocity of 9.4 m/s and uniform distribution of the data center heat load

In Figure 5.7, the T_{max} obtained by POD and CFD/HT simulations are compared when the total heat load of the data center varies from 24 kW (10% utilization) to 240 kW (100% utilization). For these results, the CRAC velocity is fixed at 9.4 m/s and the total center heat load is distributed uniformly among all 8 racks. The maximum temperature increases with the center heat load linearly. As seen in the figure, the POD predicts the effect of the total heat load on T_{max} accurately.

The effect of the racks heat load distribution is shown in Figure 5.8 when the CRAC velocity is fixed at 2.31 m/s and the total center heat load is 120 kW but with different distributions among 8 racks. It is interestingly seen that a simple work load distribution change among the racks can decrease the maximum temperature at the rack inlets as much as 10 ^{o}C, which could be translated to significant energy saving in the chiller work. This shows there are opportunities to save energy in air-cooled data centers through intelligent workload re-allocation if an efficient design method is applied. As seen in the figure, the POD based method predicts this trend accurately.

The effect of the CRAC velocity on the T_{max} obtained by POD is shown in Figure 5.9 for 6 different center heat loads with a uniform distribution among the racks. Also, T_{max} is obtained by CFD/HT simulation for some limited velocities when Q_{total}=120, 168, and 240 kW as shown in this figure. It is seen that the trend and values of T_{max} obtained by POD are in a good agreement with CFD/HT simulations. The design constraint (T_{max} = 32 ^{o}C) is shown in this figure as well.

Table 5.2. Error in the maximum rack inlet temperature obtained by POD compared with CFD/HT

Case#	[Vin (m/s), Q1 (kW), Q2 (kW), Q3 (kW), Q4 (kW)]	Tmax by CFD/HT	Tmax by POD	Error (C)	Absolute of Error (C)	Relative Error (%)
1	*[7.5, 6, 16, 29, 30]*	25.99	28.27	2.29	2.29	8.80
2	*[2, 21, 21, 21, 21]*	43.38	43.43	0.05	0.05	0.12
3	*[2.31, 5, 5, 20, 30]*	38.47	39.16	0.70	0.70	1.81
4	*[3, 27, 7, 13, 24]*	28.60	28.36	-0.24	0.24	0.86
5	*[2.31, 30, 5, 5, 20]*	29.84	28.72	-1.12	1.12	3.74
6	*[3.3, 15, 15, 15, 15]*	25.21	26.34	1.13	1.13	4.50
7	*[6.6, 30, 30, 30, 30]*	38.75	37.33	-1.42	1.42	3.66
8	*[5.5, 14, 23, 3, 19]*	28.96	29.68	0.72	0.72	2.48
9	*[1.5, 2, 30, 1, 3]*	31.75	34.03	2.28	2.28	7.19
10	*[4, 30, 29, 9, 28]*	36.19	37.48	1.29	1.29	3.57
11	*[7.8, 4, 8, 19, 3]*	19.96	22.84	2.88	2.88	14.45
12	*[6.5. 14. 29. 22. 28]*	31.27	33.53	2.26	2.26	7.22
13	*[2.31, 10, 10, 20, 20]*	33.31	34.68	1.37	1.37	4.10
14	*[2.31, 20, 20, 10, 10]*	30.42	29.97	-0.45	0.45	1.47
15	*[2.31, 15, 15, 15, 15]*	30.73	32.24	1.51	1.51	4.91
16	*[8, 30, 30, 30, 30]*	34.96	34.01	-0.94	0.94	2.70
17	*[4, 15, 15, 15, 15]*	26.72	28.67	1.95	1.95	7.29
18	*[3, 21, 21, 21, 21]*	30.83	30.57	-0.25	0.25	0.82
19	*[4.5, 18, 12, 23, 7]*	30.67	30.40	-0.28	0.28	0.90
20	*[2.31, 18, 12, 23, 7]*	29.79	30.54	0.75	0.75	2.53
21	*[7.5, 18, 12, 23, 7]*	26.21	24.94	-1.27	1.27	4.85
22	*[4.3, 4, 8, 19, 3]*	21.15	24.75	3.60	3.60	17.00
23	*[2.31, 4, 8, 19, 3]*	24.29	26.08	1.80	1.80	7.39
24	*[6.5, 14, 29, 22, 28]*	31.27	33.53	2.26	2.26	7.22
25	*[0.5, 1.5, 0.5, 1.5, 2.5]*	26.19	26.50	0.30	0.30	1.16
26	*[0.66, 3, 2.5, 2.5, 1.5]*	26.95	26.32	-0.63	0.63	2.34
27	*[0.73, 3, 3, 6, 4]*	36.47	34.85	-1.62	1.62	4.45
28	*[1.1, 27, 1, 1, 1]*	34.72	31.60	-3.12	3.12	8.98
29	*[1.3, 5, 6, 7, 6]*	32.89	30.34	-2.55	2.55	7.75
30	*[1.5, 12, 12, 5, 5]*	30.22	30.14	-0.08	0.08	0.27
31	*[1.6, 11, 11, 11, 11]*	37.88	35.86	-2.02	2.02	5.33
32	*[2.8, 17, 14, 13, 10]*	26.09	25.97	-0.13	0.13	0.49
33	*[3, 17, 6, 22, 20]*	27.13	27.98	0.85	0.85	3.15
34	*[3.25, 4, 7, 10, 8]*	19.85	23.31	3.45	3.45	17.40
35	*[3.75, 15, 16, 16, 25]*	26.63	26.71	0.08	0.08	0.29
36	*[4.25, 10, 10, 30, 30]*	27.17	28.37	1.20	1.20	4.40
37	*[4.5, 21, 16, 27, 23]*	34.56	33.66	-0.91	0.91	2.63
38	*[7.5, 28, 29, 30, 29]*	35.31	34.23	-1.08	1.08	3.07
39	*[8.5, 15, 27, 27, 27]*	28.95	29.09	0.15	0.15	0.51
40	*[2.31, 30, 28, 1, 1]*	31.76	29.61	-2.16	2.16	6.79
41	*[2.31, 1, 1, 28, 30]*	40.40	40.24	-0.16	0.16	0.40
Average					1.30	4.61

As seen in Figure 5.9, the change trend of the maximum rack inlet temperature with CRAC velocity is highly nonlinear, having at least one local minimum and maximum for each total heat load. For example, when Q_{total}=168 kW, the maximum inlet temperature decreases from ~43 ^{o}C gradually to reach ~29 ^{o}C, a local minimum, by

increasing the inlet velocity from 2 m/s to ~3.4 m/s. Increasing the CRAC velocity more than ~3.4 m/s increases the temperature unexpectedly to reach a local maximum, ~35 ^{o}C, at ~4.6 m/s. Afterwards, T_{max} decreases linearly by increasing the velocity. As seen in the figure, the POD based method predicts this trend accurately. This trend shows that the thermal management of data centers cannot be done by simply increasing the cooling air flow rate of CRAC units. As seen in Figure 5.9, increasing the CRAC velocity by 129% from 2.8 m/s to 6.4 m/s, requires 129% more power, but does not change the maximum rack inlet temperature or the thermal performance of the center when Q_{total}=168 kW. This confirms that there are opportunities to save energy in air-cooled data centers through intelligent changes in CRAC velocity if an efficient design method is applied.

The reason for the nonlinear changes in T_{max} with CRAC velocity in Figure 5.9 is the change of the air recirculation pattern in the data center around 3.8 m/s. The operating point of the server fans calculated from Eqs. (5.8) and (5.9) is ~1.07 m/s or equivalently ~0.21 m^3/s (455 CFM). So, the required air flow rate for each rack is ~1.28 m^3/s (2730 CFM) and for all 8 racks is ~10.26 m^3/s (21840 CFM). If we assume the CRAC air flow rate is distributed uniformly among all 8 perforated tiles in Figure 5.2, the CRAC unit needs to provide at least 10.26 m^3/s (21840 CFM) air flow to match the required rack air flow rates. This is equal to providing the velocity of 3.8 m/s by the CRAC unit. Below this limit, air recirculation from the hot aisle to the cold aisle will provide the rest of the required rack flow rate. On the other hand, at velocities much above this limit, the extra rate of flow provided by the CRAC unit will re-circulate mainly between the CRAC and the closest racks, i.e. Racks A1 and B1 in Figure 5.2. We see an unexpected increase in T_{max} as a result of increasing the CRAC velocity in some regions in Figure 5.9, where a

transition in the air recirculation pattern occurs inside the center. This trend can start at CRAC velocities as low as ~3 m/s and end at velocities as large as ~5m/s depending on the total heat load and its distribution.

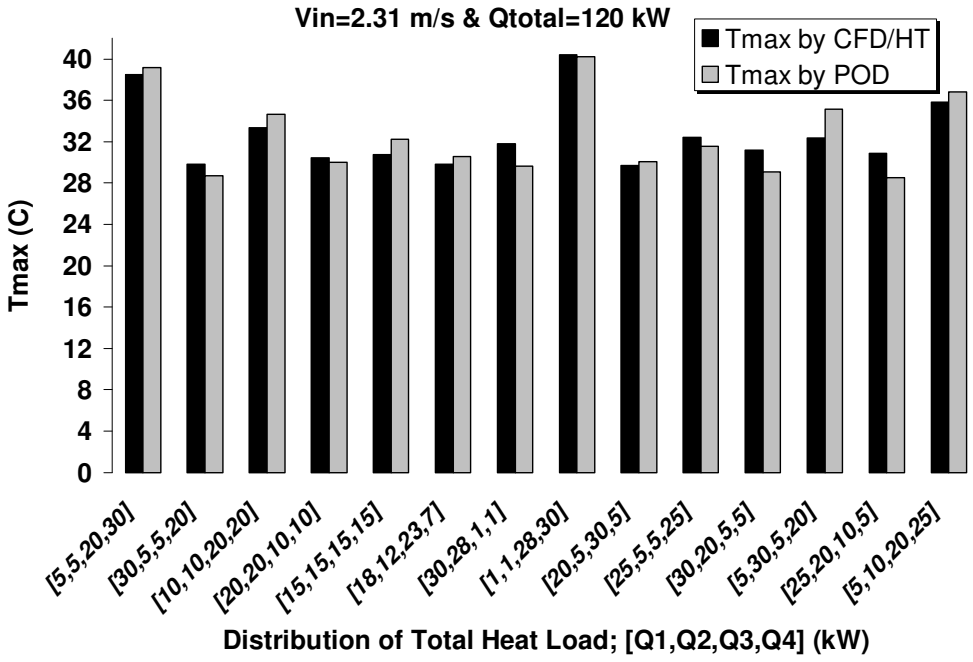

Figure 5.8. T_{max} obtained by POD and CFD/HT for CRAC velocity of 2.31 m/s and different distributions of the data center heat load, 120 kW

Accurate and computationally efficient prediction of the effects of the CRAC velocity, total data center heat load, and rack heat load allocation on T_{max} by the POD based method makes it a suitable tool to be used within the cDSP in order to design around the 5 design variables. The cDSP for this example is constructed in the next section.

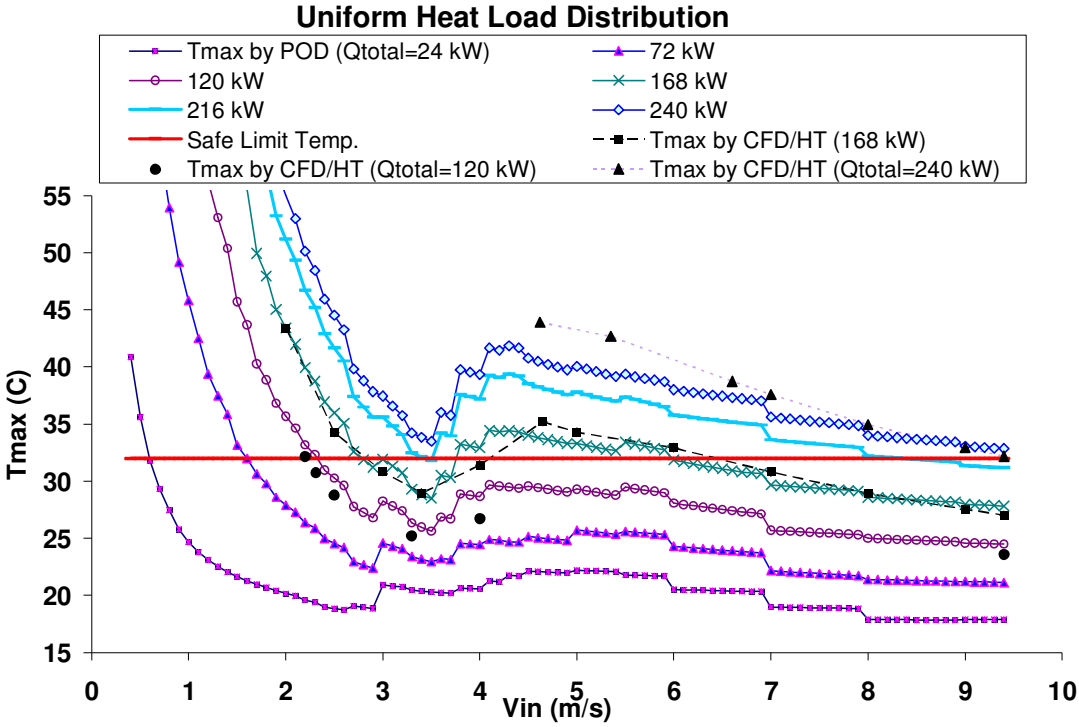

Figure 5.9. T_{max} obtained by POD and CFD/HT versus CRAC velocity for different data center heat loads with uniform distributions among racks

5.2.3 CDSP for the Data Center Cell Design

Using the cDSP construct in Figure 3.2, the cDSP for an adaptable robust and energy efficient design of the data center cell shown in Figure 5.2 is constructed. The mathematical formulation of the cDSP is shown in Table 5.3 while each section of it is explained in the following.

Given

The POD based method explained in Section 4.2 is used to calculate T_{max} as a function of control variables. The initial CRAC supply temperature is 15 ^{o}C while the

new CRAC supply temperature after each iteration is obtained from Eq. (5.3). The total cooling energy consumption, $W_{Cooling}$, is the summation of the CRAC work, calculated from Eq. (5.6), and the chiller work, calculated from Eqs. (5.5) and (5.4) at the new supply temperature. The variation of the control variables is determined by literature review and experience. For a more accurate representation, manufacturers' or experimental statistical data can also be used if available. As stated before, the given total data center power increases annually by 10% from 24 kW to 240 kW during 10 years of operation. Since at 100% utilization, when Q_{total}=240 kW, the heat loads of all racks must be 30 kW and there is no space for energy efficient design, this is not considered in the cDSP.

The target cooling energy is the minimum possible energy consumption of the data center for a given Q_{total}. The minimum of W_{crac} in Eq. (5.6) is obtained if the minimum possible inlet velocity, Eq. (5.2), is provided by the CRAC unit. The chiller work is minimal if there is no air recirculation in the center and so the supply temperature is equal to T_{max} and equal to 32 ^{o}C. Using Eq. (5.5), the maximum COP of the center can be 7.45 and accordingly the minimum chiller work is calculated from Eq. (5.4).

The variability of the response, $\Delta T_{\max}$, is calculated by Eq. (5.7) and the maximum possible value of this variation, $Max(\Delta T_{\max})$, is obtained by searching the domain for different design variables.

Find

The design variables and the associated deviations from the target values are the parameters to be found.

Satisfy

There are three constraints for this problem. The maximum temperature at the rack inlet considering the worst scenario, $T_{\max} + \Delta T_{\max}$, must be less than the limit, 32 ^{o}C, in Eq. (5.11). Also, the CRAC velocity must be at least equal to the required velocity based on the CRAC capacity and the center heat load, calculated from Eq. (5.2). The final constraint is keeping the total data center heat load at the given Q_{total}, Eq. (5.13).

There are two goals associated with 1) minimization of the cooling energy consumption for an energy efficient design and 2) minimization of the variation of T_{max} for a robust operation. As explained in Section 5.1, the maximum air temperature at the rack inlets for the worst possible changes is designed as 32 ^{o}C in order to have a not overcooled design, Eq. (5.14), while the cooling energy is minimized to reach the target, Eq. (5.15). Deviation variable d_1 in Eq. (5.15) represents the overachievement of the goal since the minimum possible energy consumption of the data center for a given Q_{total} has been considered as the target in Eq. (5.10). In fact, d_1 shows how much larger the cooling energy consumption of the center is than the possible minimum. Also, the variation of T_{max} respect to the changes in the design variables is minimized to reach zero, Eq. (5.16). Deviation variable d_2 in Eq. (5.16) represents the overachievement of the goal since the minimum possible T_{max} variation is zero. In fact, d_2 shows how larger the system response variation is than zero, considering the worst possible instability, $Max(\Delta T_{\max})$, as the comparison reference.

Minimize

Both d_1 and d_2 need to be minimized, ideally zero, to reach the associated goals. In the cDSP formulation, the designer's preferences over the goals are applied through weighting each deviation variable. The total deviation function, defined by Eq. (5.17), is minimized to calculate the control variables.

5.2.4 Results and Discussion

Two different scenarios are studied here. In the first scenario, robustness is not considered and optimal solution is obtained by minimizing the cooling energy consumption function. In the second scenario, the effects of variations in the control variables and robustness on the solution are studied through solving the cDSP in Table 5.3. The optimal solution and the minimum of the objective function in Eq. (5.17) for solving the cDSP are found through a pattern search [105] using the MATLAB Genetic Algorithm and Direct Search Toolbox. The objective functions were minimized using several initial guesses to make sure the pattern search has found the absolute minima. Also, several simpler forms of the cDSP of Table 5.3 having only two design variables were solved first and the solutions were examined using graphical illustrations such as Figure 5.8 and Figure 5.9 to verify that the pattern search converges correctly to the optimal solutions.

Table 5.3. The mathematical formulation of the cDSP for the adaptable robust and energy efficient design of the data center cell

Given

• Response model of maximum rack inlet temperature, T_{max} , new CRAC supply temperature, and total cooling energy as functions of $x_1, x_2, x_3, x_4, x_5 = V_{in}(m/s), Q_1(kW), Q_2(kW), Q_3(kW), Q_4(kW)$

• $T_{Supply,iniial} = 15^{\circ}C$

• $\Delta V_{in}(m/s) \,\&\, \Delta Q_i(kW) \quad i = 1,...,4$

• Total data center power, Q_{total} =24, 48, 72, 96, 120, 144, 168, 192, 216 kW

• Target cooling energy consumption,

$$G_{CoolingEnergy}(kW) = 2.7V_{in,\min imum}(m/s) + \frac{Q_{total}(kW)}{7.45} \qquad (5.10)$$ Where

$$V_{in,\min imum}(m/s) = \frac{-0.01 + \sqrt{(0.0001) - (28E-8)Q_{total}(kW)}}{-0.0008} \qquad (5.2)$$

• Target for total maximum possible variation, $Max(\Delta T_{\max})(^{\circ}C)$

Find

•The values of control factors:

x_1, CRAC inlet velocity, Vin

x_2, Heat load of Rack A1&B1,Q_1 ; x_3, Heat load of Rack A2&B2,Q_2,

x_4, Heat load of Rack A3&B3,Q_3; x_5, Heat load of Rack A4&B4,Q_4

•The values of deviation variables: $d_i^+, d_i^- \quad i = 1,2$

Satisfy

• *The constraints*:

- The maximum rack inlet temperature cannot exceed 32 ^{o}C

$$T_{\max} + \sum_{i=1}^{n} \left| \frac{\delta T_{\max}}{\delta x_i} \Delta x_i \right| \le 32^{\circ}C \qquad (5.11)$$

- CRAC inlet velocity must be higher than the minimum required CRAC velocity to cope with the total center heat load:

$$V_{in,\min imum} \le x_1 \qquad (5.12)$$

- The total heat load of the center must equal Q_{total}

$$2x_2 + 2x_3 + 2x_4 + 2x_5 = Q_{total} \qquad (5.13)$$

• *The goals:*

- Minimize cooling energy consumption for a neither overcooled nor under-cooled design:

$$T_{\max,new} + \sum_{i=1}^{n} \left| \frac{\delta T_{\max}}{\delta x_i} \Delta x_i \right| = 32 \qquad (5.14)$$

$$\frac{G_{CoolingEnergy}}{W_{CRAC} + W_{Chiller}} + d_1 = 1 \qquad (5.15)$$

- Minimize variation of T_{max}

$$\frac{\sum_{i=1}^{n} \left| \frac{\delta T_{\max}}{\delta x_i} \Delta x_i \right|}{Max(\Delta T_{\max})} - d_2 = 0 \qquad (5.16)$$

• *The bounds:*

$0.4m/s \le x_1 \le 9.4m/s$

$0.5kW \le x_i \le 30kW \quad i = 2,...,5$

$d_i \ge 0 \;\; i = 1,2$

Minimize

• The Archimedean objective function:

$$f = \sum_{i=1}^{2} W_i d_i \;, with \;\; \sum_{i=1}^{2} W_i = 1 \;,\; W_i \ge 0, i = 1,2 \qquad (5.17)$$

5.2.4.1 Optimal VS. Baseline Design

First, we assume there is no variation in the design parameters, i.e., $\Delta V_{in} = \Delta Q_i = 0$. The optimal solutions are obtained to have an adaptable and energy efficient data center for 10 years. Five design variables, one CRAC flow rate and four racks heat loads, along with new CRAC supply temperature are found to change each year to cope with the annual total data center work load increase to guarantee the data center remains reliable and energy efficient, neither overcooled nor under-cooled. The obtained variables and cooling energy consumptions for 9 years are shown in Table 5.4. Also, the adaptable energy efficient design is compared with the traditional design in Table 5.4 and Figure 5.10. In the traditional design, the required CRAC air flow rate is calculated using Eq. (5.1) with recirculation effect of $\beta = 1.15$, while the total data center heat load each year is distributed randomly among all racks, as listed in Table 5.4, to represent today's data centers. The CRAC supply temperature is fixed in the traditional design, while the adaptable design results in new higher supply temperatures for each year to avoid overcooling the center and have the maximum rack inlet temperature equal to the limit, $T_{max,\ new}$ = 32 ^{o}C, according to Eq. (5.3). As shown in the table and figure, the traditional design of the data center cell fails to meet the reliability constraint after two years, i.e., T_{max} > 32 ^{o}C, while the adaptable design method application guarantees that the IT equipment operation remains safe for all years. Additionally, through adaptable intelligent changes in the rack heat loads and computer room air conditioning unit flow rate and supply temperature, the energy consumption and cost of powering the required cooling systems is always kept minimal. As shown in the table and figure, the adaptable

design consumes 12-46% less energy than the traditionally designed cooling system during different years of the operation.

Table 5.4. Adaptable optimal design versus baseline/traditional design

	Year#	1st	2nd	3rd	4th	5th	6th	7th	8th	9th
	Data Center Utilization	10%	20%	30%	40%	50%	60%	70%	80%	90%
	Data Center Heat Load (kW)	24	48	72	96	120	144	168	192	216
Traditional/ Baseline Design	Vin (m/s)	0.76	1.51	2.27	3.03	3.79	4.54	5.30	6.06	6.82
	Q1 (kW)	2	8.4	4.8	7.5	14.8	9.9	4.8	25.7	27.3
	Q2 (kW)	6.1	5.1	3.4	13.5	11.7	15.1	29.7	23.2	28.5
	Q3 (kW)	2.8	7.1	2.1	18	14.8	17.7	28	29.7	22.8
	Q4 (kW)	1.1	3.4	25.7	9	18.7	29.3	21.5	17.4	29.4
	Tmax	27.74	26.08	34.41	26.32	28.06	31.85	39.09	33.19	35.56
	Supply Temp. (C)	15	15	15	15	15	15	15	15	15
	Wcrac (kW)	2.05	4.09	6.14	8.18	10.23	12.27	14.32	16.36	18.41
	Wchiller (kW)	12.00	24.00	36.00	48.00	60.00	72.00	84.00	96.00	108.00
	Wtotal (kW)	14.05	28.09	42.14	56.18	70.23	84.27	98.32	112.36	126.41
Adaptable Optimal Design	Vin (m/s)	1.12	1.93	3.00	3.00	3.71	3.24	3.39	9.40	9.38
	Q1 (kW)	8.35	12.9	3.8	9.5	2.725	11.1	9.3	11.9	18
	Q2 (kW)	1.05	4.5	29.8	29.9	15.625	29.9	29.7	24.7	30
	Q3 (kW)	1.55	3.3	1	2.3	29.925	13.9	26.9	29.9	30
	Q4 (kW)	1.05	3.3	1.4	6.3	11.725	17.1	18.1	29.5	30
	Tmax	21.48	21.90	21.29	23.33	23.72	26.55	27.14	27.40	29.69
	New Supply Temp. (C)	25.52	25.10	25.71	23.67	23.28	20.45	19.86	19.60	17.31
	Wcrac (kW)	3.03	5.22	8.10	8.10	10.01	8.74	9.16	25.38	25.33
	Wchiller (kW)	4.89	10.08	14.48	22.40	28.84	43.41	53.22	62.22	86.04
	Wtotal (kW)	7.92	15.30	22.58	30.50	38.85	52.15	62.39	87.60	111.37
	Energy Saving (%)	43.6	45.5	46.4	45.7	44.7	38.1	36.5	22.0	11.9

As shown in Table 5.4, optimal value of the CRAC velocity and the distribution of the heat load among the racks are different for different years, depending on the total center heat load. To minimize the cooling energy consumption, the summation of CRAC and chiller work needs to be minimized. CRAC work is minimum at lower CRAC velocities, V_{in}, based on Eq. (5.6), while the chiller work becomes minimum at lower T_{max} based on Eqs. (5.3)-(5.5) and Figure 5.5. Considering the nonlinear change of T_{max} with V_{in} shown in Figure 5.9, lowering V_{in} in a specific range, roughly between 3 m/s and 5

m/s depending on the total heat load and its distribution, will unexpectedly reduce T_{max} and also the chiller work in addition to reducing the CRAC work. This is the reason that the design solution has resulted in an optimal V_{in} between 3-3.7 m/s in the 3rd year through the 7th year of the operation, as shown in Table 5.4. When the data center heat load increases from 72 kW in the 3rd year to 168 kW in the 7th year, the optimal CRAC velocity changes slightly between 3-3.7 m/s and even decreases in the 6th year. On the other hand, in the 1st and 2nd years, the optimal velocities happen at 1.12 m/s and 1.93 m/s. In these cases, the reduction in the CRAC work as a result of having lower velocities than 3 m/s has been larger than the reduction in the chiller work as a result of having a minimum T_{max} at ~ 3 m/s. In the 8th and 9th years, the competition between the effects of V_{in} and T_{max} on the CRAC and chiller work will result in an optimal velocity around the upper bound of V_{in}, 9.4 m/s. This happens since T_{max} is very close to the limit of 32 ^{o}C at velocities ~3-4 m/s and so there is almost no gain on the chiller work compared with the gain at higher velocities close to the upper bound, as seen in Figure 5.9.

Although the optimal heat load distribution in a data center depends on the details of the center flow/temperature fields at different CRAC velocities and heat load distributions, being obtained through the exact solution of the governing equations, some general conclusions can be obtained based on the results of Table 5.4 and the air recirculation pattern around the racks in Figure 5.2. As explained at the end of Section 5.2.2, the air recirculation pattern of the center changes at roughly 3.8 m/s. As seen in Table 5.4, in the 1st and 2nd years with the optimal velocities of 1.12 and 1.93 m/s, when the provided flow rate by the CRAC unit is much lower than the required flow rate by the racks, the best place to put most of the heat is the first racks, A1 and B1 in Figure 5.2. In

these years, the air-recirculation happens largely from the tops of the racks and slightly from the sides of the first racks. On the other hand, in the 3rd, 4th, 6th, and 7th years, when the transition in the recirculation pattern is happening at the associated optimal velocities, the best racks to put most of the total heat on are the second racks, A2 and B2. Conversely, in the 5th, 8th, and 9th years, when the optimal V_{in} is 3.71, 9.4, 9.38 m/s and the CRAC flow rate is at least equal to the required flow rate, the best racks to put most of the total heat on is the third racks, Racks A3 and B3, while the worst racks to put heat on is the first racks, Racks A1 and B1. In these years, the air recirculation happens largely between the CRAC and the closest racks, i.e., Racks A1 and B1.

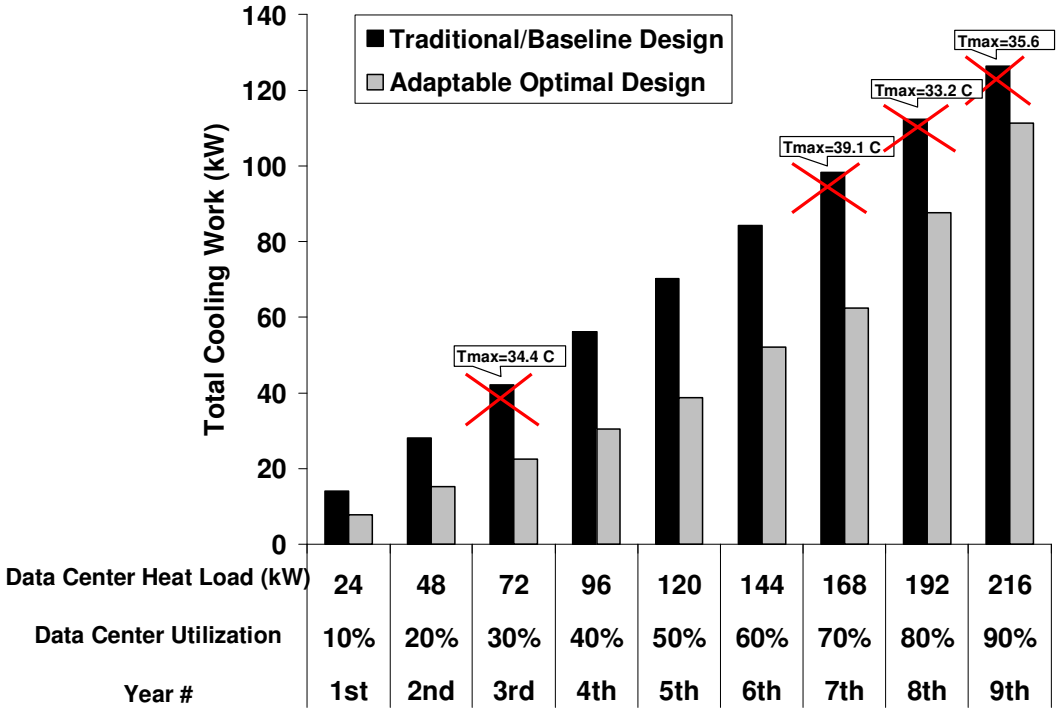

Figure 5.10. Total cooling energy consumption of adaptable and traditional designs for 9 years. Cross signs show that the reliability requirement has been failed to meet, i.e., $T_{max} > 32\ ^{o}C$, by the traditional design at years# 3, 7, 8, and 9.

5.2.4.2 Robust VS. Optimal Design

In the first scenario, an energy efficient data center was designed to have the maximum rack inlet temperature, $T_{max,new}$, equal to the limit 32 ^{o}C in each year. Although it is the most energy efficient configuration, small changes in the system parameters can cause $T_{max,new}$ to increase and IT equipment operation to fail. For illustration purpose, we consider the operation of the data center cell in the 5th year when Q_{total}=120 kW. If we assume each control variable can vary by ±5% during operation, i.e. $\Delta V_{in} = \pm 0.05 V_{in}$ and $\Delta Q_i = \pm 0.05 Q_i \quad i = 1,...,4$, the variation in $T_{max}, \Delta T_{\max}$ in Eq. (5.7), can be as high as 3.68 ^{o}C. This maximum possible variation, $Max(\Delta T_{\max})$, obtained by searching the domain, happens at {x_1, x_2, x_3, x_4, x_5}={2.707 m/s, 1 kW, 29.8 kW, 28.2 kW, 1 kW}. As seen in Table 5.4, the design variables, {x_1, x_2, x_3, x_4, x_5}, at the optimal energy efficient configuration are {3.71 m/s, 1 kW, 29.8 kW, 28.2 kW, 1 kW}. In this configuration, T_{max} variation, calculated by Eq. (5.7), is 2.31 ^{o}C and the maximum temperature at the rack inlets can reach 34.31 ^{o}C because of the small variations in the control variables, making the IT equipment not satisfy the reliability design constraint. To handle this issue, robustness in design constraints as illustrated in Figure 3.3b must be considered in solving the design problem. For this purpose, the maximum air temperature at the rack inlets for the worst scenario, $T_{\max} + \Delta T_{\max}$, is considered in the associated constraints in Eqs. (5.11) and (5.14) of the cDSP in Table 5.3, while the weighing coefficient associated with the robustness in the goals, minimizing T_{max} variation, is zero, i.e., W_1=1 and W_2=0. The cDSP is solved for the total heat load, Q_{total}=120 kW. The new values of the control variables, energy consumption, and T_{max} variation are compared with the results of the optimal energy

efficient design in Table 5.5, see Case#1 and Case#2. As seen in Table 5.5, considering robustness in constraints guarantees that the maximum possible rack inlet temperature remains 32 ^{o}C despite the changes in the design variables. Also, comparing Case#2 and Case#1 in Table 5.5 shows that the variation in T_{max} is reduced by 69.4% from 2.31 ^{o}C to 0.71 ^{o}C. This might be unexpected since the weighing coefficients associated with the minimization of $\Delta T_{\max}$ are zero in this scenario, i.e. W_1=1 and W_2=0 in Eq. (5.17). This reduction happens because lower value of $\Delta T_{\max}$ results in a higher new supply temperature, based on Eq. (5.3), and as a result, lower chiller work. So, satisfying only the first goal in the cDSP, Eq. (5.14), indirectly considers $\Delta T_{\max}$ minimization and the second goal, Eq. (5.16), somewhat as well. This is one example showing the linear weighting system used in the cDSP does not accurately translate the designer's preferences over different goals in complex design problems. Generally, a Pareto frontier [106] should be developed between two extreme solution points in order to investigate the tradeoffs between robust and optimal solutions in designing highly nonlinear complex systems such as data centers.

The Pareto frontier is made through changing the weights in Eq. (5.17) in the cDSP to determine the design specifications as the goal changes from an optimal solution, when W_1=1 and W_2=0, to a robust solution, when W_1=0 and W_2=1. Six different cases with the associated weighing coefficients and design specifications are shown in Table 5.5 for the data center cell with 120 kW total heat load. Case#1 in the table is the optimal design, when T_{max} has the highest variation, 2.31 ^{o}C, in the Pareto frontier but the energy consumption is minimal, W_{total}=38.85 kW. While the first case

denies the design constraint and IT equipment reliability limit with small changes in the design variables, Case#2 considers the robustness in constraints, as explained above. This results in a 69.41% reduction in $\Delta T_{\max}$ but 8.44% increase in the energy consumption. To have a more stable IT operation, the variation in T_{max} should be reduced. This is done by increasing the associated weighing coefficient, W_2, in Eq. (5.17), and reducing the energy efficiency weighing coefficient. Cases#3 through #6 in Table 5.5 show the design specifications as the data center design becomes more robust. As the weighing coefficients change linearly through the frontier, nonlinear changes in the T_{max} variation and energy consumption, W_{total}, are observed. The last two cases have the same design specifications with the lowest $\Delta T_{\max}$, 0.46 ^{o}C (80.16% reduction compared with the optimal solution), and so the most stability and robustness in the operation. But, they consume 37.8% more energy than the optimal solution. If a data center is loosely controlled or needs a high level of reliability and stability, the last case should be selected as the final solution. However, Case#3, when W_1=0.75 and W_2=0.25, results in a better balance between energy efficiency and robustness; it brings 73.77% reduction in $\Delta T_{\max}$ but only 7.76% increase in W_{total} compared with the optimal solution, as seen in Table 5.5. Overall, the Pareto frontier in Table 5.5 gives designers a much greater amount of information and freedom in configuring the data center for their desired goals over a single application of the weighted sum approach.

Table 5.5. Pareto frontier; robust design vs. optimal design specifications in the 5th year with Q_{total}=120 kW

Case#	1- Optimal Energy Efficient Design	2- Energy Efficient Design with Robustness in Constraints	3- Energy Efficient Design with Robustness in Constraints and Goals	4- Energy Efficient Design with Robustness in Constraints and Goals	5- Energy Efficient Design with Robustness in Constraints and Goals	6- Energy Efficient Design with Robustness in Constraints and Goals
Energy Efficeincy Weighing Coefficient, W1	1	1	0.75	0.5	0.25	0
Robustness, Minimizing Tmax Variation, Weighing Coefficient, W2	0	0	0.25	0.5	0.75	1
Vin (m/s)	3.707	3.507	3.507	8.307	9.4	9.4
Q1 (kW)	2.725	2.1	1.3	7.6	9	9
Q2 (kW)	15.625	22.1	22.5	14	11.2	11.2
Q3 (kW)	29.925	26.5	28.7	14	22.6	22.6
Q4 (kW)	11.725	9.3	7.5	24.4	17.2	17.2
Tmax (C)	23.72	24.90	24.83	24.22	22.95	22.95
New Supply Temp. (C)	23.28	21.69	21.79	22.24	23.60	23.60
Wcrac (kW)	10.01	9.47	9.47	22.43	25.38	25.38
Wchiller (kW)	28.84	32.66	32.39	31.26	28.14	28.14
Wtotal (kW)	*38.85*	*42.13*	*41.86*	*53.69*	*53.52*	*53.52*
Maximum Variation in Tmax (C)	*2.31*	*0.7066*	*0.6059*	*0.5426*	*0.4583*	*0.4583*
New Tmax plus the worst possible variation (C)	34.31	32	32	32	32	32
Reduction in Variability (%) Compared with Optimal Design	-	*69.41*	*73.77*	*76.51*	*80.16*	*80.16*
Increase in Wtotal (%) Compared with Optimal Design	-	*8.44*	*7.76*	*38.20*	*37.76*	*37.76*

Although the Pareto frontier results in Table 5.5 have been obtained for the dynamic rack heat load allocation, their general trend can be validated through investigating a graphical illustration of T_{max} versus the CRAC velocity for the uniform distribution of the total heat load Q_{total}=120 kW, shown in Figure 5.9. Comparing the obtained CRAC velocity and T_{max} for different weighing coefficients in Table 5.5 with the associated graph for Q_{total}=120 kW in Figure 5.9 shows an agreement in the trend of the results when changing from optimal to robust solution. For more optimal and more energy efficient solutions, i.e. Case#1, 2, and 3 in Table 5.5, the obtained CRAC velocity is ~3.5 m/s. As seen in Figure 5.9, T_{max} is almost a minimum at ~3.5 m/s and so the chiller and data center operation will be relatively efficient in these cases. On the other hand, in order to have more robustness in the equipment operation, we should look for

the flat regions, where T_{max} slightly changes with changes in the variables. As seen in Figure 5.9, variation of T_{max} with the CRAC velocity becomes weak after ~8 m/s, while T_{max} is also relatively small. This is the reason that the solution for Case#4, when both robustness and energy efficiency are important for designer, happens at 8.3 m/s, as shown in Table 5.5. Also, as seen in Figure 5.9, T_{max} reaches its minimum variation at upper bound of 9.4 m/s, where the most robust solutions, Case#5 and 6 in Table 5.5, happen as well. Small discrepancy of the results in Table 5.5 with the trend of T_{max} variation in Figure 5.9 is due to the effect of the dynamic heat load allocation. The nonlinear behavior of the data center energy efficiency and robustness with the associated weighing coefficients in the cDSP confirms the necessity of obtaining a Pareto frontier for complex nonlinear systems.

5.3 Chapter Closure

Developing open energy-efficient air-cooled data centers that are readily adaptable to changes through continuous improvement of an existing base is necessary in today's global market. In this chapter, a simulation-based design approach is presented to bring adaptability and robustness in the multi-scale convective systems, solving the challenges in thermal-fluid modeling, inherent variability management, and having multiple objectives. The presented approach is centered on the integration of three constructs: a) POD based multi-scale modeling, b) cDSP, and c) robust design. The method is applied for an adaptable robust thermal design of an energy efficient air-cooled data center cell with an annual increase in the power consumption for the next 10 years. The results show a 12-46% reduction in the energy consumption of the center in addition

to being adjustable to the newer IT equipment and higher heat loads compared with a traditional design. Also, a family of solutions along a Pareto frontier is generated by the cDSP to give the designer great information and freedom in configuring the data center to move between an optimal energy efficient and a robust operation. Compared with an optimal solution, a robust solution can reduce the variability in the thermal response by 73.8% with only 7.8% increase in the center energy consumption. While the proposed method has been successfully applied to one class of multi-scale systems, the three constructs and their integration should be applicable to other complex multi-scale convective systems.

So far, the design part of the second research question has been addressed to design energy efficient open thermal solution in data centers. But, as shown in Figure 1.8 and explained in Section 1.2, the realization of such an open design in operational data centers need some modification and validation. In Chapter 6, the design method of Figure 3.1 is modified to be able to use with virtualization technology in future operational data centers. The modification and experimental validation of the POD method are discussed in Chapters 7 and 8.

CHAPTER 6

COORDINATED OPTIMIZATION OF COOLING AND IT POWER

As mentioned in Sections 1.2 and 2.5 and shown in Figure 1.8, concurrency and exchanging design knowledge among the thermal and IT management are required to realize an open energy efficient operational data center in the near future. This realization must be considered to address the second research question completely. In this chapter, the design method of Figure 3.1 is modified to bring adaptability and concurrency for coordinated minimization of cooling and IT power consumption in data centers. The modified method is based on the developed POD based thermal modeling approach in Chapter 4 and power profiling of the IT equipment. The cDSP is not used here and robustness is not considered as a goal. In Section 6.1, the design problem is reviewed and summarized. In Section 6.2, the design method is demonstrated through application for an energy efficient data center cell with different rack and server architectures. Then, the results are presented and discussed. The chapter is summarized in Section 6.3.

6.1 Coordinated IT and Cooling Energy Efficiency Design Problem

The power consumption of data center facilities can be in the range of tens of MW. Recent surveys have identified that IT hardware alone can consume from 33% to 75% of datacenter power [10]. Also, a significant fraction, from 22% to 54%, of the energy costs associated with the operation of a typical data center can be ascribed to the

cooling hardware [52]. To achieve an energy efficient operational data center concurrency and exchanging design knowledge among the thermal and IT management are required [101].

Regarding the IT energy efficiency, there has been significant recent work focused on power management of compute resources. Methods have been developed to utilize capabilities such as processor voltage/frequency scaling for reduced power profiles of processors and platforms [107]. Storage resources have also provided a strong opportunity to reduce power and thermal usage in enterprise systems [108]. The importance and benefits of being able to manage heterogeneous compute resources in the IT space have been documented from low level processor management to multi-platform management [109, 110]. At the datacenter level, power consumption can be reduced by turning servers off and bringing them online based on demand [111].

Energy efficiency in data centers can increase substantially by minimizing the power consumed by IT equipment and cooling systems together. Coordinated management of IT and cooling systems has been done mainly based on the heuristic based thermal prediction approaches for temperature-aware workload placement in data centers [103, 112, 113]. Emulation tools that estimate the thermal implications of power management can aid in the offline design of management policies as well [114]. Also, Raghavendra et.al [115] leveraged a feedback mechanism to federate five individual power management solutions, currently available commercially, to monitor individual power consumptions across a collection of machines and dynamically re-provision power across systems to maintain a group power budget. Using simulations based on 180 server

traces from nine different real-world enterprises, they demonstrated the correctness, stability, and efficiency advantages of the proposed solution. Nathuji et.al [98] through simulation-based results demonstrated that substantial efficiencies in datacenter power consumption can be attained by coordinating the operation of the IT and the cooling management subsystems. In [98], cooling management was enabled by variable CRAC air velocities and using an ambient intelligence-based load management (AILM) approach [99] while IT management was based on modern virtualization technologies [116], [117], [118]. Although they have showed the importance of the coordination, they do not demonstrate how two technologies can be coordinated for power optimization in data centers.

All previous studies on coordinated cooling and IT power management simulate the interactions among the temperature field in the data center, the system parameters, and the facility power consumption based on some heuristic approaches. However, minimizing over-provisioning and designing neither overcooled or under-cooled data centers with different configurations and thermal characteristics are possible only if a deterministic and quick modeling of the data center temperature field is available in terms of the involved system parameters.

Considering the requirements of an open air-cooled data center, explained in Chapter 3, a design method for adaptable coordinated cooling and IT power management can be developed similarly to the adaptable design approach in Chapter 5. The diagram in Figure 6.1 shows a design methodology to handle the actual momentary data center average computational task utilization with minimum total energy consumption of IT and

cooling systems and maximum efficiency, through adaptable changes in the rack level task utilization, and CRAC supply air flow rate and temperature. The task utilization allocation can be assigned to the servers of the different racks through modern virtualization technologies [116], [117], [118]. As mentioned in Chapter 5, the air flow rate of CRAC units can be varied using variable frequency drive motors. Also, the CRAC supply temperature can be easily changed in operational data centers.

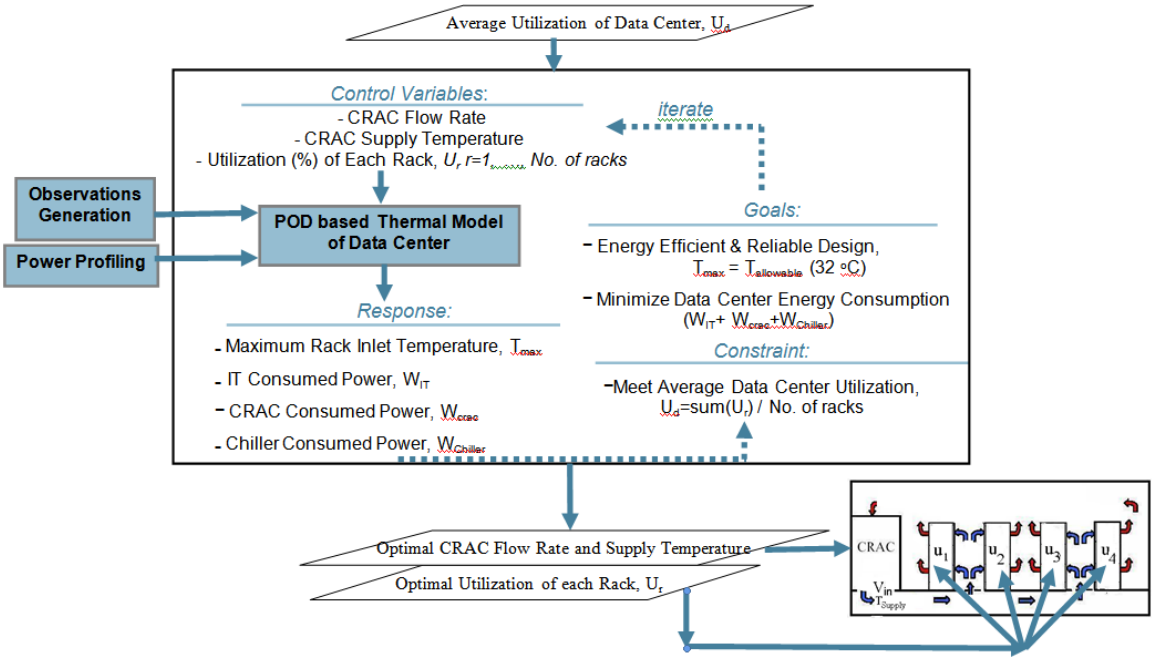

Figure 6.1. Adaptable Coordinated IT and Thermal design in energy efficient data centers

In the design approach shown in Figure 6.1, the developed POD based reduced order thermal modeling approach in Chapter 4 is used. Also, power profiling of the IT equipment is used to obtain the relationship between the server utilization and the IT

power consumption. To the best knowledge of the authors, this work presents the first deterministic design approach for adaptable energy efficient coordinated management of IT and cooling systems at the data center level. In Section 6.3, it is demonstrated how power profiling and the POD based method can be used together according to the diagram in Figure 6.1 to minimize the total power consumed by IT and cooling systems of a data center example.

6.2 Coordinated Design of a Data Center Example

In Section 6.2.1, an example with different scenarios is defined. Then in Section 6.2.2, the approach for power profiling of the IT equipment is briefly explained and the corresponding power-CPU utilization relation of the servers are obtained. In Section 6.2.3, a POD based reduced order modeling of the data center cell is obtained using the method developed in Chapter 4. Finally in Section 6.2.4, the optimization design problem is solved and the results are discussed for different scenarios.

6.2.1 Example Definition

An adaptable energy efficient design of an air-cooled data center cell is considered through coordinated IT and cooling power optimization. The data center cell is the same as in Chapter 5. One-fourth of the data center cell is shown in Figure 6.2. The approach illustrated in Figure 6.1 is applied to the data center cell of Figure 6.2 for four different scenarios, depending on the architecture and number of servers per each rack. Each rack can have either 42 rack mounted 1U (47.6 mm) servers or 84 blade servers

housed in 6 7U (311.15 mm) server infrastructure. Also, two different architectures for the servers in each rack are considered here:

1- *Dell 4-core*: The machine has 4 cores with Intel ® Core ™ 2 Extreme CPU X9650 @ 3.00 GHZ and 6 MB cache size, Total RAM of 7.2 GB and 1 TB SATA hard disk.

2- *Dell 2-core*: The machine has 2 cores with Intel ® Pentium ® D CPU @ 3.20 GHZ and 1 MB cache size, Total RAM of 512 MB and 80 GB SATA hard disk.

As mentioned before, we assume that all servers in a specific rack have the same architecture but the racks can be different from each other. Also, to reduce the number of design variables for illustration purposes, we assume that corresponding racks in each column of the data center cell (e.g. A1 and B1 in Figure 6.2) have the same workload utilization and architecture. Accordingly, four scenarios defined as:

Scenario#1: All 8 racks have 42 Dell 2-core servers.

Scenario#2: All 8 racks have 84 Dell 2-core servers.

Scenario#3: Each rack has 42 servers. But, racks A1, B1, A3, and B3 have Dell 4-core servers while racks A2, B2, A4, and B4 have Dell 2-core servers.

Scenario#4: The rack configurations remain the same as Scenario#3 except that each rack has 84 servers in this scenario.

In the next sections, the steps need to take according to the diagram in Figure 6.1 for the data center example is demonstrated and the results are presented.

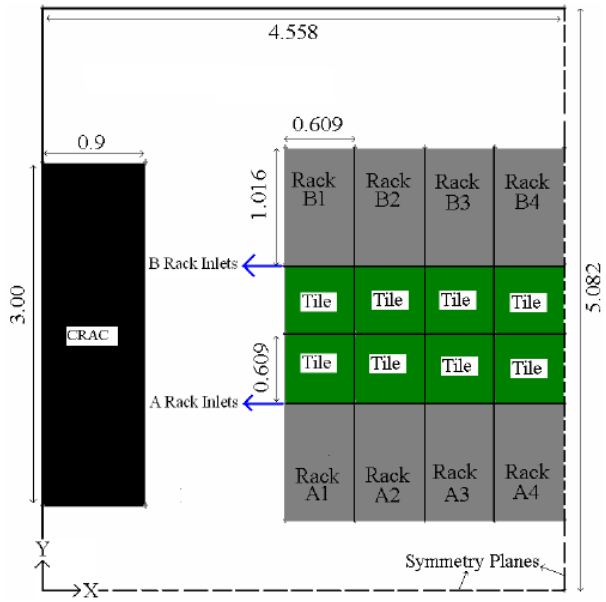

Figure 6.2. Data center cell top view; Dimensions in m. Only one quarter of the cell is shown due to symmetry

6.2.2 Power Profiling of the Servers

A mapping from CPU utilization to power consumption is obtained to calculate the IT power, W_{IT}, in terms of the server utilization in each rack. This step has been done by Hrishikesh Amur and Bhavani Krishnan, Dr. Karsten Schwan's students in the College of Computing at Georgia Tech. So, the used approach and the results are presented briefly.

Assuming a heterogeneous environment in the data center, the power profiles are obtained for each kind of server. Since all the servers are assumed to be virtualized, the mapping from server utilization to power depends on the power management algorithm in the hypervisor. The test machines were profiled using the methods outlined in [117] as well as the stock algorithm in Xen 3.3. The mappings which are approximated to linear

curves are shown in Figure 6.3. In general, a linear relation can be assumed between power and server power consumption. The corresponding linear equations to relate between Dell-4 core server and Dell-2 core server utilizations with the server consumed power are expressed in Figure 6.3 as well. As seen in Figure 6.3, the Dell-4 core machine is more energy efficient than the 2-core machine.

Assuming that all the power consumed by IT dissipates to the heat, the heat load of each rack is obtained simply by adding the consumed powers of all housed servers at the corresponding server utilization.

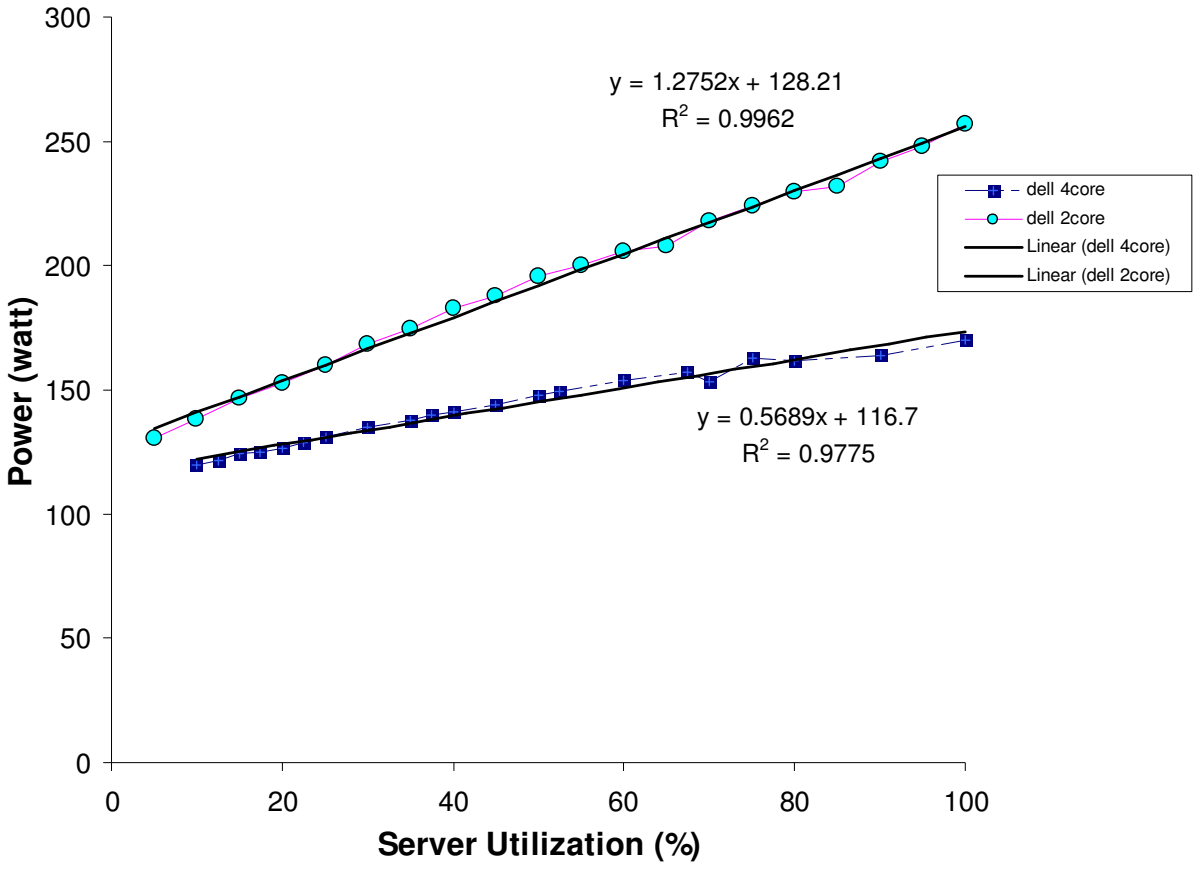

Figure 6.3. Power profiling results for two servers (courtesy of Hrishikesh Amur and Bhavani Krishnan)

6.2.3 POD Based Thermal Modeling of the Data Center Cell

The thermal and energy modeling required in the design approach of Figure 6.1 are obtained using the POD method developed in Chapter 4. The modeling process and its application for the data center example are the same as presented in Section 5.2.1, where the data center cell was considered for an open energy efficient design. The POD based results were presented in Section 5.2.2 as well.

6.2.4 Optimization Design Solution for the Example

We present the optimization results for different average data center utilizations. It is assumed that the data center cell experiences momentary average utilizations equal to 10, 30, 50, 70, or 90% over time. The optimization problem in Figure 6.1 is solved through a pattern search [105], using the MATLAB Genetic Algorithm and Direct Search Toolbox, to find the optimal CRAC inlet velocity and supply temperature and optimal distribution of the workload among the racks for each data center average center utilization. The optimal results are compared with a baseline design to identify the energy saving in the total power of the data center cell achieved by the coordinated design approach.

6.2.4.1 Baseline Design

In the baseline design which traditionally is used in today data center design, the required CRAC air flow rate is calculated using Eq. (5.1). Also, the average utilization is distributed uniformly among all racks of the data center. The baseline design results for the data center cell for the four defined scenarios are tabulated in Table 6.1 and Table 6.2,

Table 6.3, and Table 6.4. For each data center average utilization, the corresponding rack utilization and consumed power (equal to the dissipated heat), CRAC air velocity and supply temperature, the power consumed by CRAC and chiller, and the total data center power consumption have been listed in the tables. As expected, the IT, cooling, and total consumed power is higher at higher utilizations. Also, using Dell-4 core instead of 2 core servers reduces the IT, cooling, and total power consumption.

Table 6.1. Baseline design results for Scenario#1

	Rack Architecture Layout	All Racks: 2core				
	Data Center Average Utilization	10%	30%	50%	70%	90%
Baseline Design	Vin (m/s)	1.49	1.77	2.04	2.31	2.58
	Ut1 (%)	10.00	30.00	50.00	70.00	90.00
	Ut2 (%)	10.00	30.00	50.00	70.00	90.00
	Ut3 (%)	10.00	30.00	50.00	70.00	90.00
	Ut4 (%)	10.00	30.00	50.00	70.00	90.00
	QR1 (kW)	5.92	6.99	8.06	9.13	10.21
	QR2 (kW)	5.92	6.99	8.06	9.13	10.21
	QR3 (kW)	5.92	6.99	8.06	9.13	10.21
	QR4 (kW)	5.92	6.99	8.06	9.13	10.21
	Tmax (C)	27.28	26.91	26.48	25.96	25.35
	Data Center Heat Load (kW)	47.36	55.93	64.50	73.07	81.64
	T Discharge (C)	15.00	15.00	15.00	15.00	15.00
	Wcrac (kW)	4.04	4.77	5.50	6.23	6.96
	Wchiller (kW)	23.68	27.97	32.25	36.54	40.82
	Wcooling (kW)	27.72	32.73	37.75	42.76	47.78
	Wtotal (kW)	75.08	88.66	102.25	115.83	129.42

6.2.4.2 Optimal Design

The results obtained by solving the optimization problem for different data center utilization are shown in Table 6.5, Table 6.6, Table 6.7, and Table 6.8 for the four scenarios. At each table, the optimal values of required CRAC inlet velocity, utilization

and associated IT power of each rack to meet the center utilization, data center IT power consumption, CRAC air supply temperature, CRAC and chiller work and their summation, and the minimum possible total power consumption of the data center cell are listed. The initial maximum rack inlet temperature is listed as well while the final maximum temperature is designed to be 32°C for all cases. Also, the total power consumption obtained by the coordinated design approach is compared with that of the baseline design and the achieved energy saving is shown. As seen in the tables, the design approach for coordinated optimization of IT and cooling power results in 12-24% saving in the total energy consumption of the data center cell in different scenarios.

Table 6.2. Baseline design results for Scenario#2

	Rack Architecture Layout	All Racks: 2core				
	Data Center Average Utilization	10%	30%	50%	70%	90%
Baseline Design	Vin (m/s)	2.99	3.53	4.07	4.61	5.15
	Ut1 (%)	10.00	30.00	50.00	70.00	90.00
	Ut2 (%)	10.00	30.00	50.00	70.00	90.00
	Ut3 (%)	10.00	30.00	50.00	70.00	90.00
	Ut4 (%)	10.00	30.00	50.00	70.00	90.00
	QR1 (kW)	11.84	13.98	16.13	18.27	20.41
	QR2 (kW)	11.84	13.98	16.13	18.27	20.41
	QR3 (kW)	11.84	13.98	16.13	18.27	20.41
	QR4 (kW)	11.84	13.98	16.13	18.27	20.41
	Tmax (C)	24.15	26.31	30.60	31.80	32.60
	Data Center Heat Load (kW)	94.73	111.87	129.00	146.14	163.28
	T Discharge (C)	15.00	15.00	15.00	15.00	15.00
	Wcrac (kW)	8.07	9.53	10.99	12.45	13.91
	Wchiller (kW)	47.36	55.93	64.50	73.07	81.64
	Wcooling (kW)	55.43	65.46	75.49	85.52	95.55
	Wtotal (kW)	150.16	177.33	204.50	231.67	258.83

Due to the nonlinearity of the effects of CRAC velocity and rack heat load distribution on the temperature field and maximum rack inlet temperature and as a result

on the total power consumption of the data center, the optimal CRAC velocities and the best racks to assign more workload to varies nonlinearly for different center utilizations and rack architectures. However, some general trends can be concluded from the presented results:

Table 6.3. Baseline design results for Scenario#3

	Rack Architecture Layout	AB1:4core / AB2:2core / AB3:4core / AB4:2core				
	Data Center Average Utilization	10%	30%	50%	70%	90%
Baseline Design	Vin (m/s)	1.40	1.59	1.79	1.98	2.18
	Ut1 (%)	10.00	30.00	50.00	70.00	90.00
	Ut2 (%)	10.00	30.00	50.00	70.00	90.00
	Ut3 (%)	10.00	30.00	50.00	70.00	90.00
	Ut4 (%)	10.00	30.00	50.00	70.00	90.00
	QR1 (kW)	5.14	5.62	6.10	6.57	7.05
	QR2 (kW)	5.92	6.99	8.06	9.13	10.21
	QR3 (kW)	5.14	5.62	6.10	6.57	7.05
	QR4 (kW)	5.92	6.99	8.06	9.13	10.21
	Tmax (C)	27.89	27.53	27.32	27.04	26.66
	Data Center Heat Load (kW)	44.24	50.44	56.64	62.83	69.03
	T Discharge (C)	15.00	15.00	15.00	15.00	15.00
	Wcrac (kW)	3.77	4.30	4.83	5.35	5.88
	Wchiller (kW)	22.12	25.22	28.32	31.42	34.51
	Wcooling (kW)	25.89	29.52	33.14	36.77	40.40
	Wtotal (kW)	70.13	79.96	89.78	99.60	109.42

- While the CRAC air flow rate is increased to meet higher center utilizations and heat loads in the traditional design, the CRAC flow rate changes slightly with higher utilization in the optimal design. Actually, in most of the cases in the optimal design, the higher utilization is met by simply changing the workload distribution among the racks.

- In Scenarios#1 and 2, when all racks have the same 2 core servers, the optimal workload distribution is decided based on the thermal effects of the workload distribution since the IT power consumption for all racks is equal. As seen in Table 6.5 and Table 6.6, it is generally concluded the second racks, Racks A2 and B2 in Figure 6.2, are the best place to put most of the workload on, considering only cooling energy consumption. Also, the worst places for load allocation are either the third racks, when number of servers is 42 in Sceanrio#1, or the first racks, when number of servers is 84 in Sceanrio#2, are the worst place.

Table 6.4. Baseline design results for Scenario#4

	Rack Architecture Layout	AB1:4core / AB2:2core / AB3:4core / AB4:2core				
	Data Center Average Utilization	10%	30%	50%	70%	90%
Baseline Design	Vin (m/s)	2.79	3.18	3.57	3.97	4.36
	Ut1 (%)	10.00	30.00	50.00	70.00	90.00
	Ut2 (%)	10.00	30.00	50.00	70.00	90.00
	Ut3 (%)	10.00	30.00	50.00	70.00	90.00
	Ut4 (%)	10.00	30.00	50.00	70.00	90.00
	QR1 (kW)	10.28	11.24	12.19	13.15	14.10
	QR2 (kW)	11.84	13.98	16.13	18.27	20.41
	QR3 (kW)	10.28	11.24	12.19	13.15	14.10
	QR4 (kW)	11.84	13.98	16.13	18.27	20.41
	Tmax (C)	24.54	25.90	25.85	28.58	30.86
	Data Center Heat Load (kW)	88.49	100.88	113.27	125.66	138.06
	T Discharge (C)	15.00	15.00	15.00	15.00	15.00
	Wcrac (kW)	7.54	8.60	9.65	10.71	11.76
	Wchiller (kW)	44.24	50.44	56.64	62.83	69.03
	Wcooling (kW)	51.78	59.04	66.29	73.54	80.79
	Wtotal (kW)	140.27	159.91	179.56	199.20	218.85

- As mentioned before and shown in Figure 6.3, racks with 4-core servers are more energy efficient than racks with 2-core servers. So, racks with 4-core servers are better places to put most of the work load on if we consider only power consumption in

the data center. But when the goal is minimizing the total power consumption, the thermal effects and IT effects compete with each other. This competition is seen in Scenarios#3 and 4, where IT efficient 4-core servers have been housed in the first and third racks which are the worst places from the thermal effect perspective, as concluded in the previous paragraph. In contrast, the second racks, the best place from the thermal effect perspective, in these scenarios house 2-core servers with lower IT energy efficiency.

Table 6.5. Optimal design results for Scenario#1

	Rack Architecture Layout	All Racks: 2core				
	Data Center Average Utilization	10%	30%	50%	70%	90%
Optimal Design / Efficient Distribution	Vin (m/s)	2.6	2.9	2.9	2.9	2.925
	Ut1 (%)	6.50	11.50	52.00	96.00	100.00
	Ut2 (%)	32.50	99.50	100.00	100.00	100.00
	Ut3 (%)	0.50	1.50	4.00	2.00	60.00
	Ut4 (%)	0.50	7.50	44.00	82.00	100.00
	QR1 (kW)	5.73	6.00	8.17	10.53	10.74
	QR2 (kW)	7.13	10.71	10.74	10.74	10.74
	QR3 (kW)	5.41	5.47	5.60	5.49	8.60
	QR4 (kW)	5.41	5.79	7.74	9.78	10.74
	Tmax (C)	21.00	20.79	21.54	22.29	23.15
	Optimum Data Center Heat Load (kW)	47.36	55.93	64.50	73.07	81.64
	Tnew of Discharge (C)	26.00	26.21	25.46	24.71	23.85
	Wcrac (kW)	7.02	7.83	7.83	7.83	7.90
	Wchiller (kW)	9.33	10.86	13.20	15.78	18.79
	Wcooling (kW)	16.35	18.69	21.03	23.61	26.69
	Wtotal (kW)	63.72	74.62	85.53	96.68	108.33
Baseline Design	Wtotal (kW)	75.08	88.66	102.25	115.83	129.42
	Energy Saving (%)	15.14	15.84	16.35	16.54	16.29

- In Scenario#3, when each rack has 42 servers, the results in Table 6.7 show that the IT power consumption drives the final optimal solution; i.e. IT effect > thermal effect. In this scenario, the third racks receive most of the workload while the

second racks have the lowest workload, which is completely in opposition to the results of Scenario#1.

- In Scenario#4, when each rack has 84 servers (so higher heat load and larger range of heat load change per rack compared with Scenario#2), the thermal effect is as important as or even more important than the IT effect to drive the final optimal solution. As seen in Table 6.8, the thermal effect is dominant and the second racks are the best place to put most of the heat when data center utilization is equal to 30%, 70%, and 90%. At 10% utilization, IT effect is dominant and at 50% utilization both IT and thermal effects have shown the same importance.

Table 6.6. Optimal design results for Scenario#2

	Rack Architecture Layout	All Racks: 2core				
	Data Center Average Utilization	10%	30%	50%	70%	90%
Optimal Design / Efficient Distribution	Vin (m/s)	3.5	3.4	3.4	3.7	3.5
	Ut1 (%)	0.50	0.25	4.00	3.99	60.00
	Ut2 (%)	38.50	73.25	100.00	75.99	100.00
	Ut3 (%)	0.50	31.25	44.00	99.99	100.00
	Ut4 (%)	0.50	15.25	52.00	99.99	100.00
	QR1 (kW)	10.82	10.80	11.20	11.20	17.20
	QR2 (kW)	14.89	18.62	21.48	18.91	21.48
	QR3 (kW)	10.82	14.12	15.48	21.48	21.48
	QR4 (kW)	10.82	12.40	16.34	21.48	21.48
	Tmax (C)	23.57	24.54	25.43	26.52	27.87
	Optimum Data Center Heat Load (kW)	94.73	111.87	129.00	146.13	163.28
	Tnew of Discharge (C)	23.43	22.46	21.57	20.48	19.13
	Wcrac (kW)	9.45	9.18	9.18	9.99	9.45
	Wchiller (kW)	22.51	28.65	35.46	43.91	55.14
	Wcooling (kW)	31.96	37.83	44.64	53.90	64.59
	Wtotal (kW)	126.68	149.69	173.65	200.03	227.87
Baseline Design	Wtotal (kW)	150.16	177.33	204.50	231.67	258.83
	Energy Saving (%)	15.63	15.58	15.09	13.65	11.96

One general conclusion obtained from the optimization solutions for different scenarios is that more energy saving could obtain due to the thermal effect if the range of

possible heat load change per rack becomes higher, for example if the server power at the idle situation with zero utilization was much more lower than the power at 100% utilization in Figure 6.3. This conclusion motivates us to consider the standby situation at the server operation in data centers. If we can put some servers at standby instead of zero utilization, the energy efficiency becomes higher due to both IT and thermal effects. The optimization result for this scenario is presented in the following.

Table 6.7. Optimal design results for Scenario#3

Optimal Design / Efficient Distribution	Rack Architecture Layout	AB1:4core / AB2:2core / AB3:4core / AB4:2core				
	Data Center Average Utilization	10%	30%	50%	70%	90%
	Vin (m/s)	2.20	2.40	2.60	2.90	2.91
	Ut1 (%)	2.50	46.50	99.00	99.50	99.50
	Ut2 (%)	0.50	0.50	1.00	7.50	69.50
	Ut3 (%)	36.50	72.50	99.00	99.50	99.50
	Ut4 (%)	0.50	0.50	1.00	73.50	91.50
	QR1 (kW)	4.96	6.01	7.27	7.28	7.28
	QR2 (kW)	5.41	5.41	5.44	5.79	9.11
	QR3 (kW)	5.77	6.63	7.27	7.28	7.28
	QR4 (kW)	5.41	5.41	5.44	9.32	10.29
	Tmax (C)	22.43	21.76	21.43	21.60	22.51
	Optimum Data Center Heat Load (kW)	43.12	46.94	50.82	59.33	67.90
	Tnew of Discharge (C)	24.57	25.24	25.57	25.40	24.49
	Wcrac (kW)	5.94	6.48	7.02	7.83	7.85
	Wchiller (kW)	9.41	9.76	10.32	12.19	14.90
	Wcooling (kW)	15.35	16.24	17.34	20.02	22.75
	Wtotal (kW)	58.47	63.18	68.16	79.36	90.65
Baseline Design	Wtotal (kW)	70.13	79.96	89.78	99.60	109.42
	Energy Saving (%)	16.64	20.99	24.08	20.33	17.16

Table 6.8. Optimal design results for Scenario#4

Optimal Design / Efficient Distribution	Rack Architecture Layout	AB1:4core / AB2:2core / AB3:4core / AB4:2core				
	Data Center Average Utilization	10%	30%	50%	70%	90%
	Vin (m/s)	3	3.4	3.40	3.4	3.5
	Ut1 (%)	34.25	3.00	65.49	80.50	99.75
	Ut2 (%)	0.25	67.00	49.49	80.50	99.75
	Ut3 (%)	5.25	39.00	75.49	70.50	68.75
	Ut4 (%)	0.25	11.00	9.49	48.50	91.75
	QR1 (kW)	11.44	9.95	12.93	13.65	14.57
	QR2 (kW)	10.80	17.95	16.07	19.39	21.45
	QR3 (kW)	10.05	11.67	13.41	13.17	13.09
	QR4 (kW)	10.80	11.95	11.79	15.96	20.60
	Tmax (C)	23.26	23.93	24.75	25.43	25.90
	Optimum Data Center Heat Load (kW)	86.17	103.01	108.40	124.36	139.42
	Tnew of Discharge (C)	23.74	23.07	22.25	21.57	21.10
	Wcrac (kW)	8.10	9.18	9.18	9.18	9.45
	Wchiller (kW)	20.00	25.15	28.21	34.17	39.82
	Wcooling (kW)	28.10	34.33	37.39	43.35	49.27
	Wtotal (kW)	114.27	137.35	145.79	167.71	188.69
Baseline Design	Wtotal (kW)	140.27	159.91	179.56	199.20	218.85
	Energy Saving (%)	18.54	14.11	18.81	15.81	13.78

6.2.4.3 Optimal Design with Standby Servers

Power profiling the Dell servers shows that the consumed power for both 2-core and 4-core servers at the standby situation is 6 watt, which is very low compared with the server powers at the zero utilizations in Figure 6.3. In this regard, the optimization design problem is solved again for Scenarios#1 and 2, assuming that servers can be at standby situations. The new results are presented in Table 6.9 and Table 6.10. The total power obtained from the baseline design and optimal design are listed in the tables as well. Compared with the baseline design, the optimal design with standby servers results in 12-70% saving in the total energy consumption of the data center cell, which is much higher than the saving obtained by the previous optimal results. The energy saving at lower data center utilizations, when we can have more servers at standby, is higher than the saving

in higher utilizations. As seen in Table 6.9 and Table 6.10, three racks has standby servers at 10% utilization of the data center and the energy saving is very high around 70%. At 30% and 50% utilization, two racks house standby servers resulting in 47% energy saving. At 70% utilization only one rack has standby servers resulting in 27% energy saving. When the utilization of the data center is 90%, we cannot have any servers at standby and the obtained results and energy saving are equal to the previous optimal results.

Table 6.9. Optimal design with standby servers; results for Scenario#1

	Rack Architecture Layout	All Racks: 2core with 42 servers				
	Data Center Average Utilization	10%	30%	50%	70%	90%
Baseline Design	Wtotal (kW)	75.08	88.66	102.25	115.83	129.42
Optimal Design	Wtotal (kW)	63.72	74.62	85.53	96.68	108.33
	Energy Saving (%)	15.14	15.84	16.35	16.54	16.29
Optimal With Satndby Servers	Vin (m/s)	1	1.5	1.8	3	2.925
	Ut1 (%)	StandBy	22.5	100.00	99.00	100.00
	Ut2 (%)	40.00	97.5	100.00	99.00	100.00
	Ut3 (%)	StandBy	StandBy	StandBy	StandBy	60.00
	Ut4 (%)	StandBy	StandBy	StandBy	82.00	100.00
	QR1 (kW)	0.252	6.59	10.74	10.69	10.74
	QR2 (kW)	7.53	10.61	10.74	10.69	10.74
	QR3 (kW)	0.252	0.252	0.252	0.252	8.60
	QR4 (kW)	0.252	0.252	0.252	9.78	10.74
	Tmax (C)	22.18	22.79	22.30	21.25	23.15
	Optimum Data Center Heat Load (kW)	16.57	35.40	43.97	62.81	81.64
	Tnew of Discharge (C)	24.82	24.21	24.70	25.75	23.85
	Wcrac (kW)	2.70	4.05	4.86	8.10	7.90
	Wchiller (kW)	3.55	7.93	9.51	12.60	18.79
	Wcooling (kW)	6.25	11.98	14.37	20.70	26.69
	Wtotal (kW)	22.82	47.38	58.34	83.50	108.33
	Energy Saving (%)	69.61	46.56	42.94	27.91	16.30

Table 6.10. Optimal design with standby servers; results for Scenario#2

	Rack Architecture Layout	All Racks: 2core with 84 servers					
	Data Center Average Utilization	10%		30%	50%	70%	90%
Baseline Design	Wtotal (kW)	150.16	150.16	177.33	204.50	231.67	258.83
Optimal Design	Wtotal (kW)	126.68	126.68	149.69	173.65	200.03	227.87
	Energy Saving (%)	15.63	15.63	15.58	15.09	13.65	11.96
Optimal With Satndby Servers	Vin (m/s)	1.5	1.8	2.9	3.4	3.5	3.5
	Ut1 (%)	40.00	StandBy	StandBy	StandBy	StandBy	60.00
	Ut2 (%)	StandBy	40.00	97	100.00	89.00	100.00
	Ut3 (%)	StandBy	StandBy	23.00	100.00	99.50	100.00
	Ut4 (%)	StandBy	StandBy	StandBy	StandBy	91.50	100.00
	QR1 (kW)	15.05	0.504	0.504	0.504	0.504	17.20
	QR2 (kW)	0.504	15.05	21.16	21.48	20.30	21.48
	QR3 (kW)	0.504	0.504	13.23	21.48	21.43	21.48
	QR4 (kW)	0.504	0.504	0.504	0.504	20.57	21.48
	Tmax (C)	22.47	22.92	22.18	22.61	25.70	27.87
	Optimum Data Center Heat Load (kW)	33.13	33.13	70.80	87.94	125.61	163.28
	Tnew of Discharge (C)	24.53	24.08	24.82	24.39	21.30	19.13
	Wcrac (kW)	4.05	4.86	7.83	9.18	9.45	9.45
	Wchiller (kW)	7.25	7.50	15.17	19.45	35.30	55.14
	Wcooling (kW)	11.30	12.36	23.00	28.63	44.75	64.59
	Wtotal (kW)	44.44	45.49	93.81	116.57	170.36	227.87
	Energy Saving (%)	70.41	69.71	47.10	43.00	26.46	11.96

From the operational point in real-world data centers, standby servers need a wakeup time, e.g. 38 seconds for the Dell servers, to come back to the operation. So, generally some knowledge about the momentary change time in the data center utilization is needed to be able to put some servers at standby situations confidently and bring them back to the operation reliably. As seen in Table 6.9 and Table 6.10, each rack except the first rack in Table 6.10 remains standby continuously from low data center utilization until a specific higher utilization. For example, the third racks in the scenario of Table 6.9 remain standby until data center utilization becomes 90% while the fourth racks stay satndby until 70% data center utilization. This trend is not true for the first racks in Table

6.10, when it should be on at 10% utilization, then should become standby from 20-70% and again should come back to operation at 90% utilization in order to achieve optimal results. But, as seen in Table 6.10, we can obtain another solution close to the optimal point with a little increase in the power consumption to have the first racks at standby like its situation at higher utilization until 90%. With having this done by optimization algorithm, fewer numbers of servers need to go on or standby successively and less knowledge about the utilization change time in the data center is needed.

6.3 Chapter Closure

The realization and application of the open design method in operational data centers must be considered to answer the second research question completely. As shown in Figure 1.8 and discussed in Section 2.5, concurrency and exchanging design knowledge among the thermal and IT management are required to realize an open energy efficient operational data center in operational data centers. In this chapter, the open design approach is modified to bring adaptability and concurrency for coordinated minimization of cooling and IT power consumption in data centers. The modified approach is centered on the POD based reduced order thermal modeling and power profiling of IT equipment to distribute the data center average task utilizations among servers and adjust the CRAC design variables intelligently. The method is validated through application to a data center cell considering different rack architectures. The results show the design approach results in 12-24% saving in the total energy consumption of the data center cell in different scenarios, compared with traditional design of data centers. Also, if we can have the option of putting the servers at standby

situation, the energy saving is much higher. In this case, we could save up to 70% in the total power consumption of the data center cell.

Although the presented results in this chapter are based on a simulated data center cell, the approach can be extended and applied for online control of modern data centers with virtualization technology.

Concurrency with IT designers, one of the realization requirements of the open design method shown in Figure 1.8, has been considered in this chapter. Two other requirements, the POD method modification and validation, are considered in the next two chapters. In Chapter 7, the POD method is modified to develop a simpler reduced order thermal modeling approach to be used for realization of open design approach in operational data centers.

CHAPTER 7

POD AND ENERGY BALANCE FOR THERMAL MODEL REDUCTION IN DATA CENTERS

As explained in Section 1.2 and shown in Figure 1.8, the POD based method should be modified to be used more efficiently in operational data centers in order to address one of the realization requirements in the second research question. In this chapter, a POD based reduced order thermal modeling approach is presented to predict the effect of the involved parameters on the temperature field in complex practical systems such as operational data centers. A complex system here means a system with multiple convective components. The physical phenomena in different components can interact internally and do not need to happen in a specific order. The key features of the study in this chapter include:

- using the basic POD technique with simple energy balance equations, heat flux matching [80], and/or surface temperature matching for temperature field generation

- conducting an explicit study on the effects of the retained POD modes and available thermal information on the accuracy of the POD based thermal field

- illustrating the approach to predict the temperature field within an entire operational air-cooled data center in terms of the involved design variables, based on observations from the minimum required thermal sensors

In Section 7.1, the new POD based method to simulate the temperature field in complex thermal-fluid systems is explained. In Section 7.2, the method is applied to an air-cooled data center cell with 5 design variables. The accuracy and computational speed of the POD generated temperature field for different test cases and scenarios are examined through comparison with CFD/HT results. The effects of the quantity of the known thermal information and number of components in the system on the POD solution are studied as well. In Section 7.3, the presented method is compared with the POD based method developed in Chapter 4. Finally, the chapter is summarized in Section 7.4.

7.1 POD and Energy Balance Based Thermal Modeling Method

The new POD based method for the thermal modeling of multi-scale systems has been illustrated in Figure 7.1. The same POD temperature equation is assumed for the entire domain:

$$T = T_0 + \sum_{i=1}^{m} b_i \psi_i \tag{7.1}$$

So, the first and second steps in Figure 7.1 are similar to the basic POD technique, as explained in Section 3.4.2.2 and Figure 3.4. The difference is where the POD coefficients, b_i , must be calculated. In this method, appropriate algebraic equations to calculate the POD coefficients are obtained by simply energy balance equations, heat flux matching [80], and/or surface temperature matching for all convective components of the complex system. Finally, all equations are subsequently solved together using the least square approach to obtain a single set of POD coefficients.

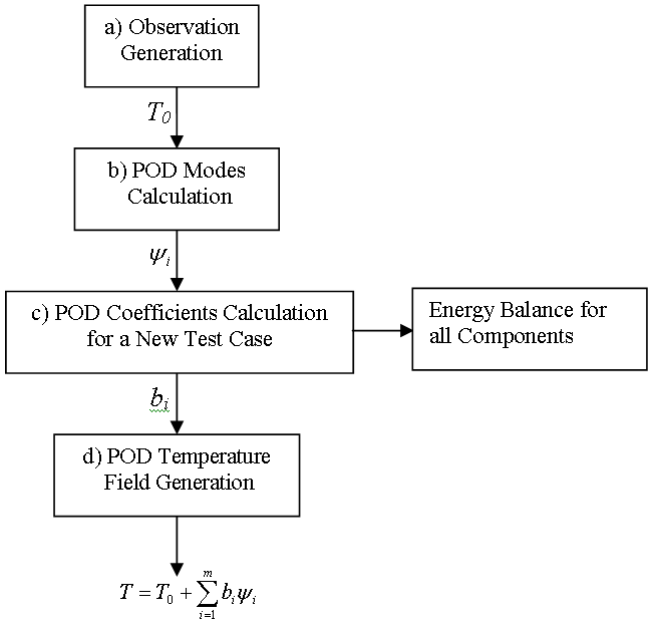

Figure 7.1. POD and Energy Balance based thermal modeling method

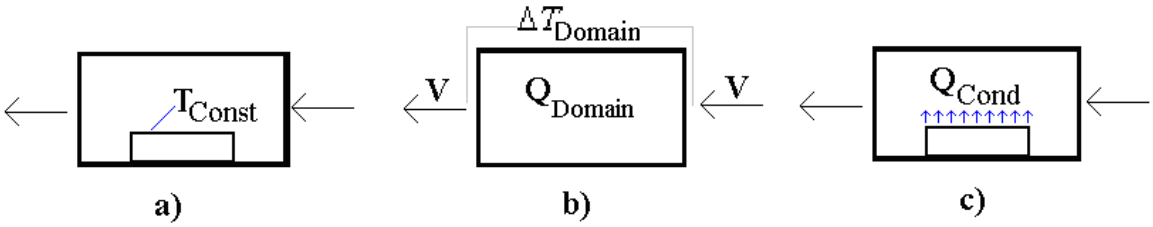

Figure 7.2. Convective components in a complex system

As explained in Chapter 4 as well, the key convective phenomena at each component or subsystem of the main system can be classified as illustrated in Figure 7.2. The corresponding equations for the different cases in Figure 7.2 was explained before in Chapter 4. In the following, these equations are briefly summarized. For case a) in Figure 7.2, the fluid temperature at a specific surface of the domain is kept at a known constant value of T_{Const}:

$$T_{Const} = \overline{T}_0 + \sum_{i=1}^{m} b_i \overline{\psi}_{i,Surf} \tag{7.2}$$

We get one algebraic equation for each constant temperature surface of the domain.

For components like case b) in Figure 7.2, one equation is obtained to satisfy the conservation of the energy across the domain:

$$\frac{Q_{Domain}}{VA\rho c_p} = \Delta T_{Domain} = \overline{T}_{0,DomianOutlet} - \overline{T}_{0,DomainInlet} + \sum_{i=1}^{m} b_i (\overline{\psi}_{i,DomainOutlet} - \overline{\psi}_{i,DomainInlet}) \tag{7.3}$$

Sometimes, especially if the method is used for thermal modeling of real-world systems, the inlet velocity and/or heat load in case b) of Figure 7.2 is not known, but the temperature difference across the domain is measured and known instead. In this case, Eq. (7.3) can be still used to find the appropriate POD coefficients associated with the measured temperature difference.

For components like case c) in Figure 7.2, one equation is obtained by defining a modal heat conduction function, $F_{i,ModalCond}$, in the POD space:

$$Q_{Cond} = \sum_{i=1}^{m} b_i F_{i,ModalCond} \tag{7.4}$$

After the algebraic equations have been obtained for all components of the system, they are solved together to find the associated POD coefficients for a new set of design variables.

We should note that the number of obtained algebraic equations, *s*, in this method, can be less, equal, or more than the number of available POD modes, *n-1*. *n* is the number

of observations. Since we need at least the same number of equations as the number of unknown POD coefficients to avoid an underdetermined system of equations, the maximum possible number of POD modes to use, *m* in $T = T_0 + \sum_{i=1}^{m} b_i \psi_i$, is limited by the number of available equations, *s*, in addition to the number of available modes, *n-1*. Accordingly, *m* can be 1 up to *min(n-1, s)* in this method. On the other hand, the number of available equations is limited by the number of convective components and available thermal information for the components in the system. This brings a limitation to the presented method whose effect on the results for a data center cell is studied in Section 7.2.3 and 7.2.4. While this limitation exists in the flux matching process [53] as well, it has not been explicitly studied in the previous applications of the POD method [21, 52, 53, 80, 91, 92]. In the next section, the method outlined above is applied to an air cooled data center cell.

7.2 Illustration of Thermal Modeling Approach: A Data Center Example

The POD based method illustrated in Figure 7.1 is applied to an air-cooled data center cell with multiple convective components to simulate the temperature field as a function of Computer Room Air-Conditioning (CRAC) unit air delivery velocity and rack heat loads. In Section 7.2.1, a data center example with 5 design variables is defined. The accuracy and computational speed of the presented method in simulating the temperature field for different sets of design variables are examined in Section 7.2.2 through comparison with fine-mesh, full-domain CFD/HT results. The effects of the quantity of the known thermal information and number of components in the system on the POD solution are studied in Section 7.2.3 and 7.2.4, respectively.

7.2.1 Example Definition

The data center cell, whose specifications were explained in Section 4.2.1, is modeled here, see Figure 7.3a. However, each server here is modeled as a uniform volumetric heat source (Q'''_{server}) with a representative fan at its exit and a lumped pressure jump at its inlet, as shown in Figure 7.3b. The walls of all 48 servers are modeled as adiabatic surfaces. A mesh with 431,120 grid cells when compared with a 334,972 grid-cell mesh leads to only 0.35% change in the maximum temperature. The change for the 334,972 grid-cell mesh compared with a coarser mesh containing 182,000 grid cells was 23%. Therefore, the mesh with 431,120 grid cells is considered fine enough and used here for CFD/HT generation of observations.

To construct a POD based reduced order model of the temperature field, the rack heat loads and CRAC air flow rate are considered to change between 500 W - 30 kW and 1 m^3/s (2128 CFM) – 16.2 m^3/s (34500 CFM), respectively. To reduce the number of design variables for illustration purposes, we assume that all 6 servers housed in a specific rack have the same heat load. Also, corresponding racks in each column are assumed to have the same heat load. This leads to the same 5 design variables as in Chapter 4 for the data center example of Figure 7.3:

1. inlet air velocity of CRAC unit, V_{in}
2. heat load of Rack A1&B1, Q_1
3. heat load of Rack A2&B2, Q_2
4. heat load of Rack A3&B3, Q_3
5. heat load of Rack A4&B4, Q_4

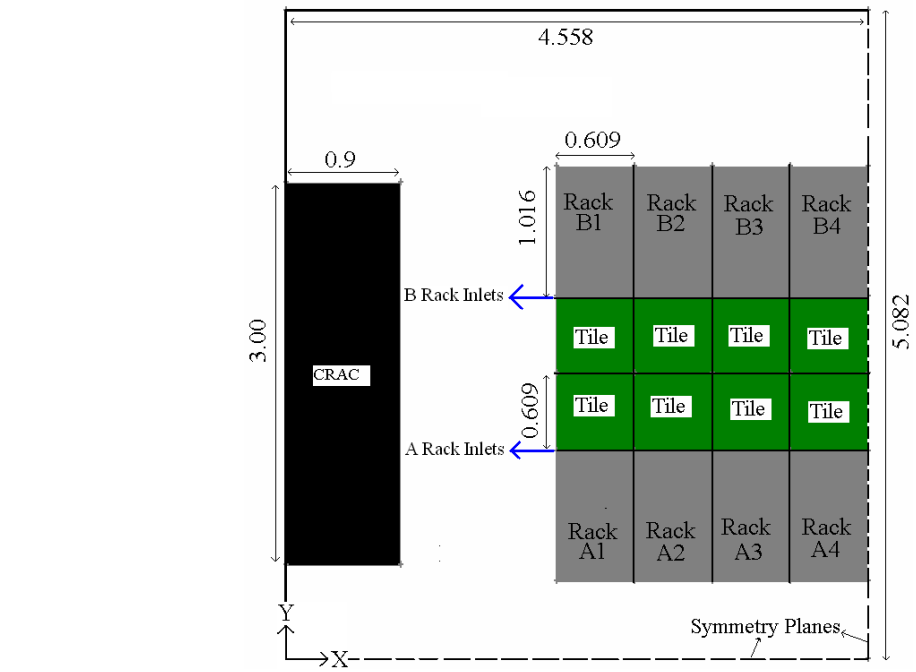

(a)

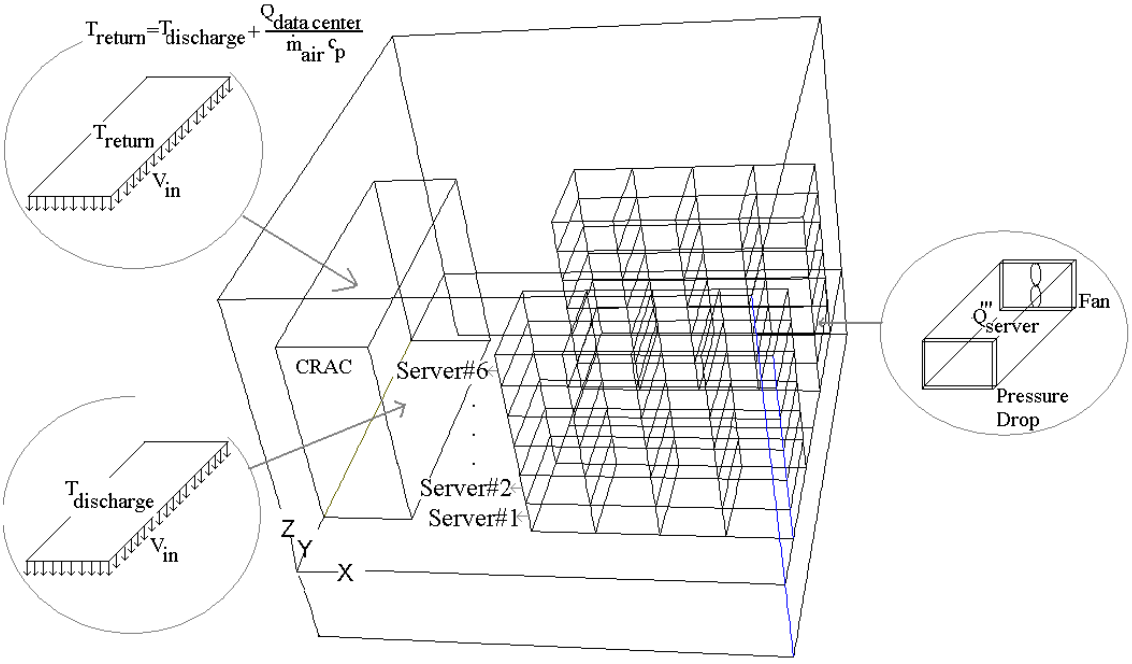

(b)

Figure 7.3. Data center cell; (a) Top view. Dimensions are in m. (b) 3D model

7.2.2 POD Temperature Field for the Data Center Example

The method illustrated in Figure 7.1 is followed to predict the temperature field for the data center example. The CRAC velocity and rack heat loads are varied to generate 21 observed temperature fields throughout the data center cell. The design variables for these observations are collected in Table 7.1. The contours of the average of all 21 observations, T_0 in Eq. (1), at the inlets of racks A1 through A4 and B1 through B4 of the data center in Figure 7.3 are shown in Figure 7.4a and Figure 7.4b, respectively. All 20 POD modes for the data center cell are calculated through Eqs. (3.8) and (3.7). The energy percentage captured by each POD mode is plotted versus the mode number in Figure 7.5. The contours of the first two and last two POD modes are shown in Figure 7.6 at the inlet surfaces of racks A1, A2, A3, and A4 of the data center.

To obtain the appropriate algebraic equations to calculate the POD coefficients for a test case with new design variables, Eq. (7.3) associated with case b) in Figure 7.2 is applied to each server in the data center. As mentioned following Eq. (7.3), heat load and inlet air velocity for each server need to be known to obtain the POD coefficients and finally the temperature field for the new test case. Alternatively, as mentioned before, the temperature difference across each server for the new test case can be measured and used in Eq. (7.3), which is more practical in an operational data center. In this study, we use the temperature differences obtained by CFD/HT solution to verify the presented algorithm. In Section 7.2.3, the effect of the number of known temperature differences across servers on the predicted temperature field is discussed. Having applied Eq. (7.3) to all servers, $N_{servers}$ equations are obtained; $N_{servers}$ is 48 here. Similarly, energy balance

equation, Eq. (7.3), is applied for the CRAC unit with known total heat load of the data center and CRAC inlet velocity for the new test case. Also, the temperature field at the perforated tile surfaces is kept fixed at the known constant air discharge temperature by applying Eq. (7.2) for case a) in Figure 7.2. Ultimately, ($N_{servers}+1+1=50$) equations are obtained to solve for 20 POD mode coefficients. All the obtained equations are solved together using least square approach to obtain a single set of POD coefficients for a new set of design variables.

Table 7.1. Design variables for the observations

Observation#	1	2	3	4	5	6	7	8	9	10	11	12	13	14	15	16	17	18	19	20	21
Vin (m/s)	0.4	0.6	0.8	1	1.2	1.4	1.6	1.9	2.1	2.4	2.6	3	3.25	3.5	3.75	4	4.25	4.5	5	5.5	6
Q1 (KW)	1	2	4	5	7	6	11	4	12	30	21	17	4	14	15	10	10	21	21	29	20
Q2 (KW)	1	3	3	5	4	7	11	10	8	5	11	6	7	22	16	15	10	16	21	28	20
Q3 (KW)	1	2	1	5	8	8	11	12	19	5	7	22	10	20	16	20	30	27	21	16	25
Q4 (KW)	1	1	5	5	9	9	11	16	9	20	6	20	8	14	25	30	30	23	21	26	25

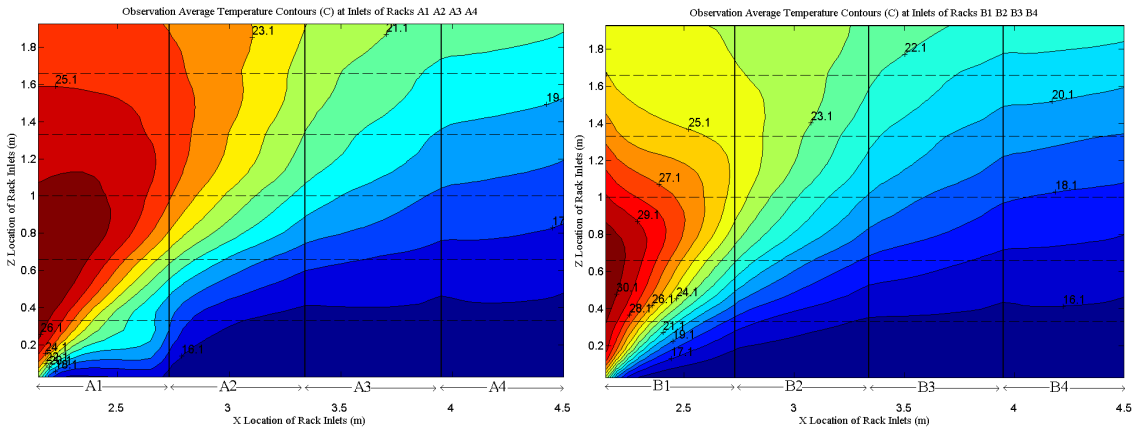

(a) Racks A1-A4 (b) Racks B1-B4

Figure 7.4. Reference air temperature contours (^{o}C) at the racks inlets

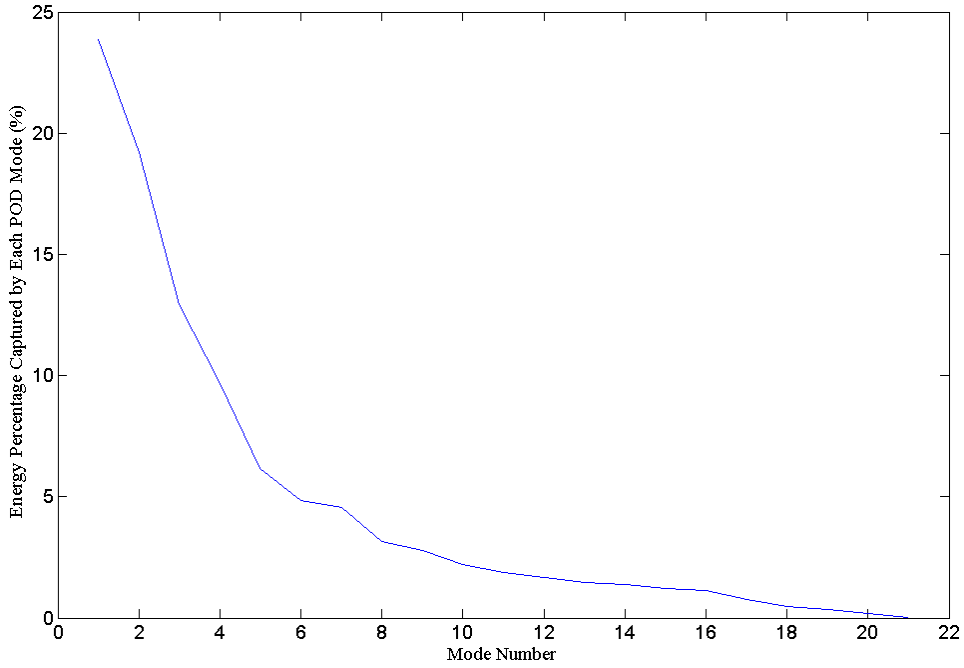

Figure 7.5. Energy Percentage (%) captured by each POD mode for the data center example

POD coefficients associated with different modes, b_i, are shown in Figure 7.7 for four arbitrary test cases, which are distinct from the observations. These coefficients have been obtained when all 20 modes are retained in the POD reconstruction in Eq. (7.1). It is seen that the value of POD coefficients decreases for modes with higher index and lower energy content. Also, the last mode coefficients are almost zero. So, the first few terms in the decomposition of Eq. (7.1) are dominant. Also, the changes in the POD coefficients after using ~10 modes are much less than the coefficient changes in the initial part of the graph in Figure 7.7. It seems that the solution has been converged after ~10 modes.

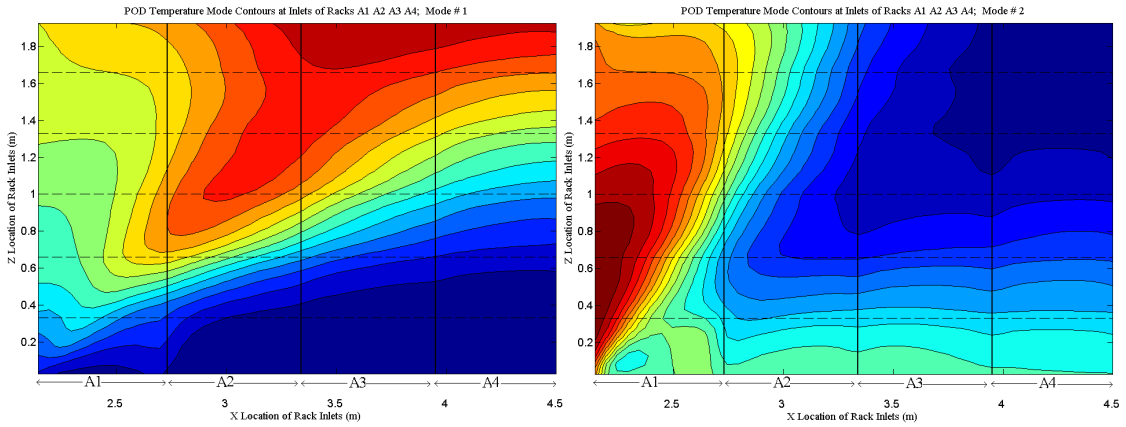

(a) Mode 1 (b) Mode 2

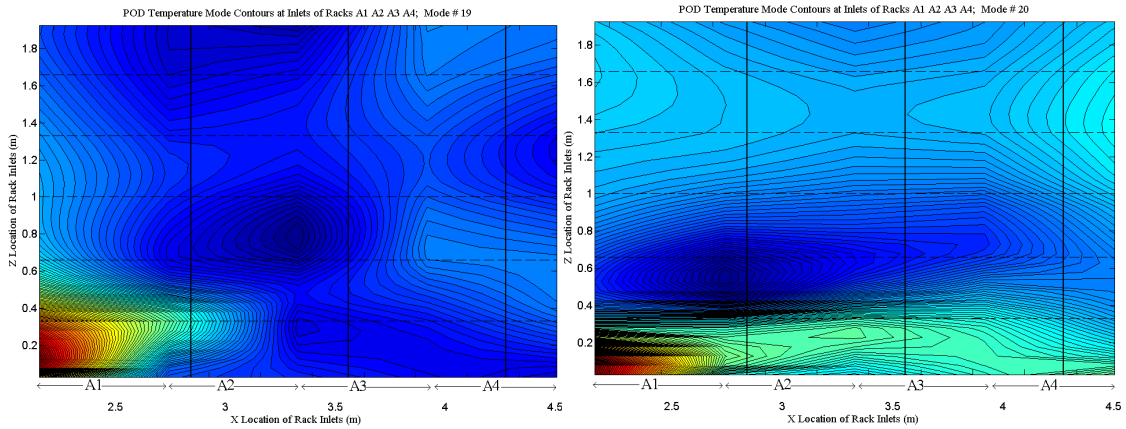

(c) Mode 19 (d) Mode 20

Figure 7.6. Structures of the first two and last two POD modes at the rack inlets

To study the convergence of the solution with the number of used POD modes, the solution is first examined at the CRAC unit, perforated tile, and servers' boundaries, for where the algebraic equations were obtained. The effect of the number of retained POD modes in Eq. (7.1) on the error in the energy conservation at the system boundaries is shown in Figure 7.8, for the four test cases. The differences between right and left hand side terms in Eq. (7.2) for the perforated tile, and Eq. (7.3) for the 48 servers and one

CRAC unit are calculated for each number of used modes. The average of these discrepancies is shown in Figure 7.8 versus the number of used modes. It is seen that after ~7 modes, the error becomes almost zero and adding more modes to the POD reconstruction does not have any effect on the energy conservation at the system boundaries. This is interesting considering that the available equations to satisfy, 50, is significantly larger than the number of modes and unknown POD coefficients. It shows that only 7 POD modes are enough to satisfy all 50 energy conservation equations at the boundaries. However, the convergence of the POD solution at local points throughout the data center is more important.

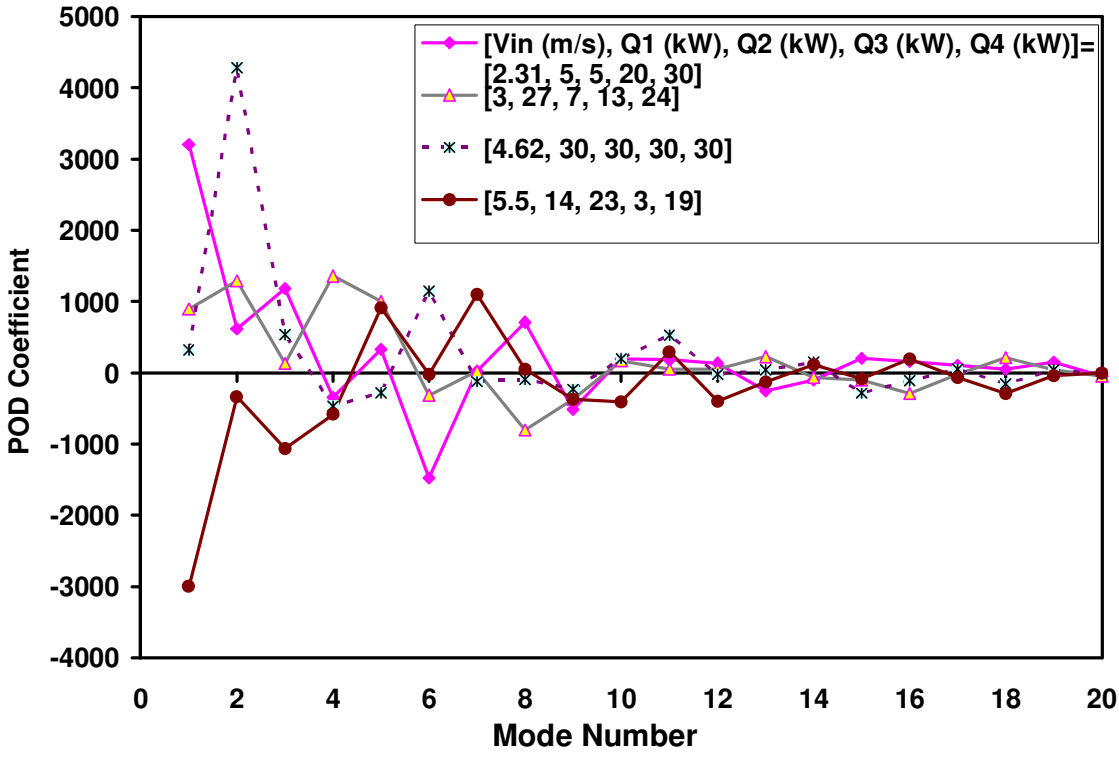

Figure 7.7. POD coefficients of the associated modes for four test cases, when all 20 modes are used in the POD reconstruction

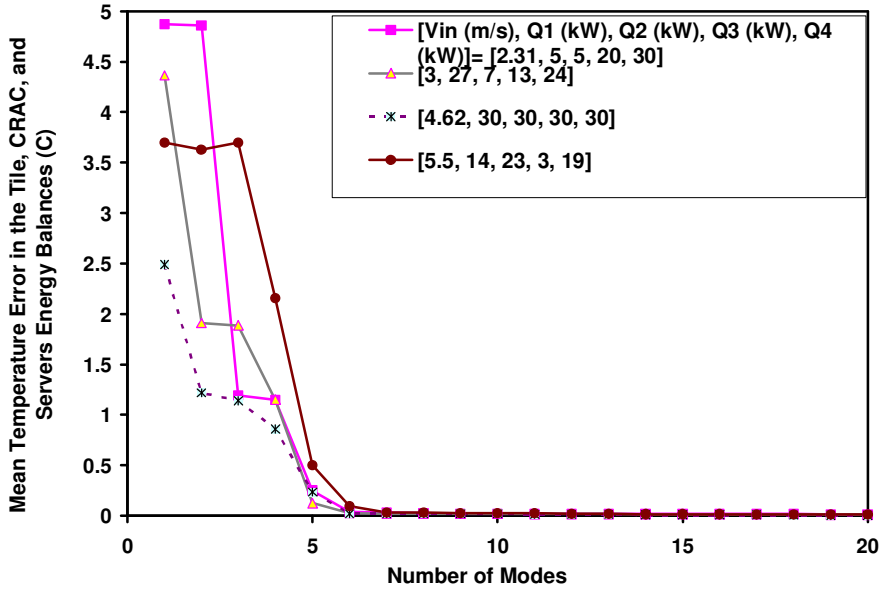

Figure 7.8. Effect of the number of retained POD modes on the error (^{o}C) in the energy conservation in the component boundaries of the data center cell for four test cases

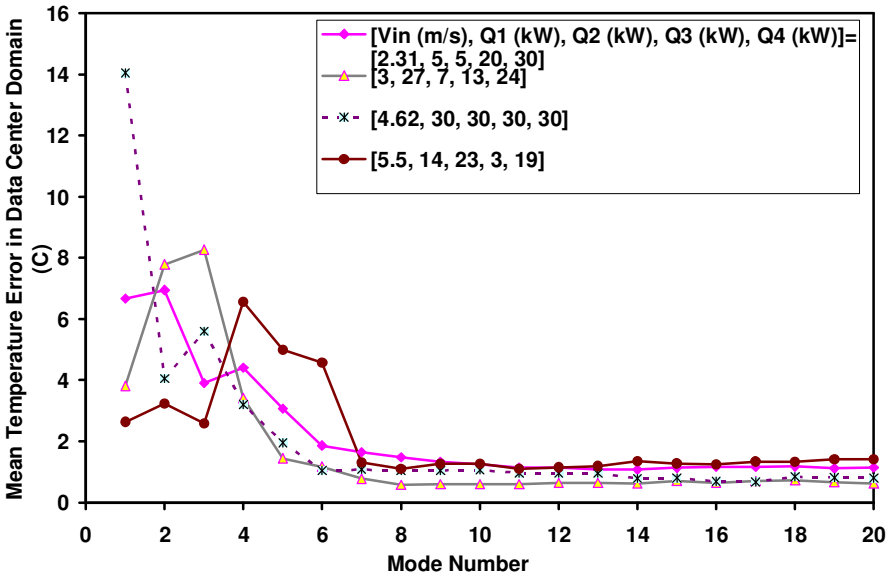

Figure 7.9. Effect of the number of retained POD modes on the mean POD temperature error (^{o}C) for the entire data center for four test cases

To study the convergence of the obtained local temperatures with the mode numbers and also to examine the fidelity of the POD method, the POD temperatures are compared with full CFD/HT simulations. A mean error, $\overline{T}_{error}(x,y,z)\,(°C)$, is calculated using Eq. (4.17). N_{nodes} in Eq. (4.17) is 431,120 for the studied data center cell in Figure 7.3. The mean error is plotted for the four test case cases in Figure 7.9 when the number of used POD modes changes from 1 to 20. Comparing Figure 7.9 with Figure 7.8 shows while the temperature difference across the system components has converged after ~7 modes, the local temperatures need ~3 additional modes to converge for the same test case. As shown in Figure 7.9, the local temperatures converge after ~10 modes. This is consistent with the relative flattening in the POD coefficient changes after ~10 modes in Figure 7.7, as discussed above. Also, the converged mean error for the entire domain for these cases is less than 1.4 ^{o}C or 7.2%, as seen in Figure 7.9.

To see if the POD method can predict the air temperatures at the rack inlets accurately for use in design decisions, the full field predictions, POD simulations, and the POD temperature error are shown in Figure 7.10 for racks A1 through A4 for 4 test cases. The average error is less than 1.5 ^{o}C, while the maximum local error is ~2.5 ^{o}C for some small regions. Since the uncertainty in deployed sensor measurements can be around 1 ^{o}C, the POD based method can be used effectively in solving data center thermal design problems. The mean error (Eq. (4.17)), the standard deviation in the error (Eq. (4.18)), and the mean relative error (Eq. (4.19)) of the POD temperature field at all 431,120 points of the domain for six test cases, which are distinct from the observations, are tabulated in Table 7.2.

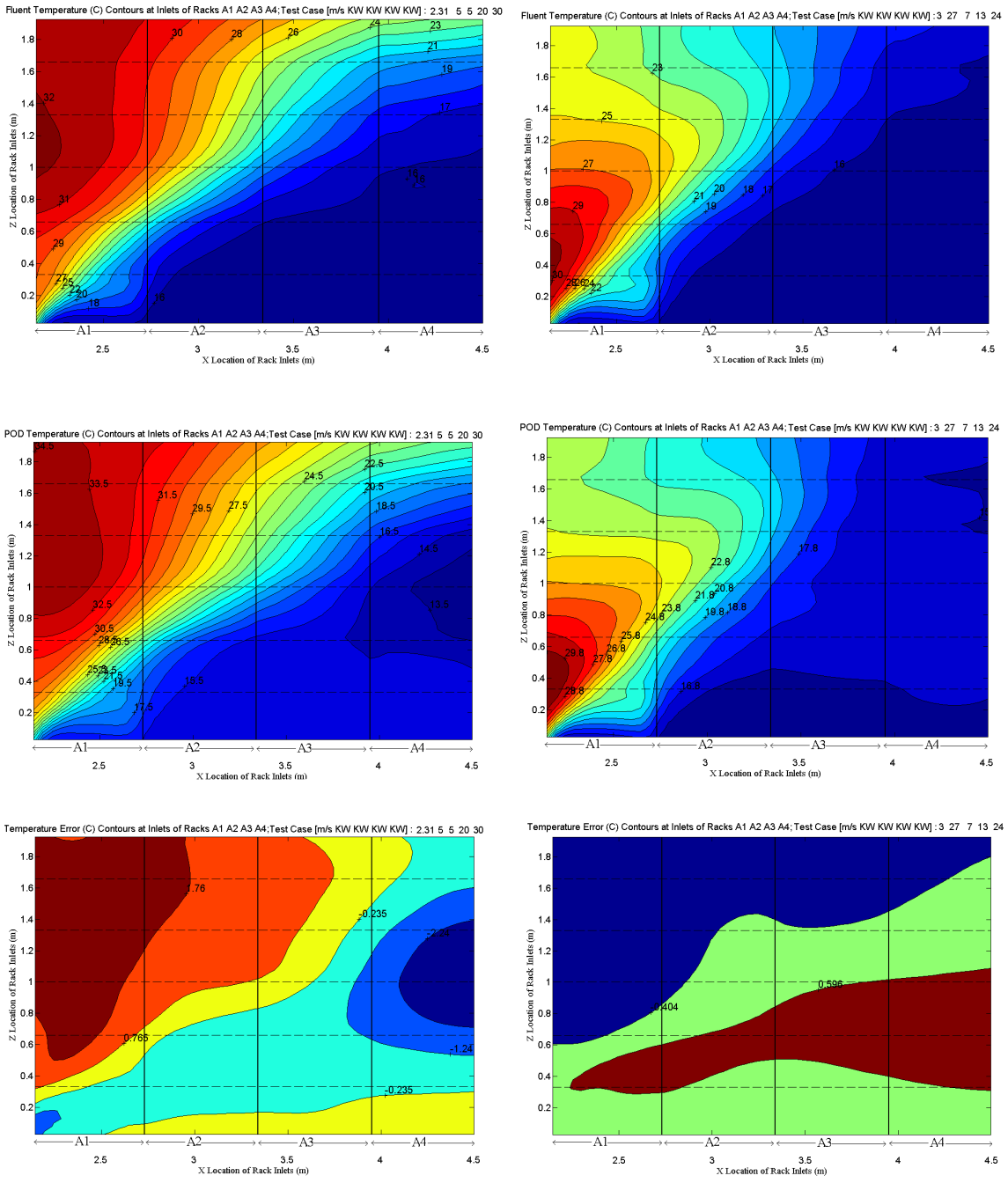

(a) (b)

Figure 7.10. Contours of CFD/HT temperature, POD temperature, and relative error (^{o}C) at racks inlets for four test cases. Relevant test case is mentioned at the top of each contour plot.

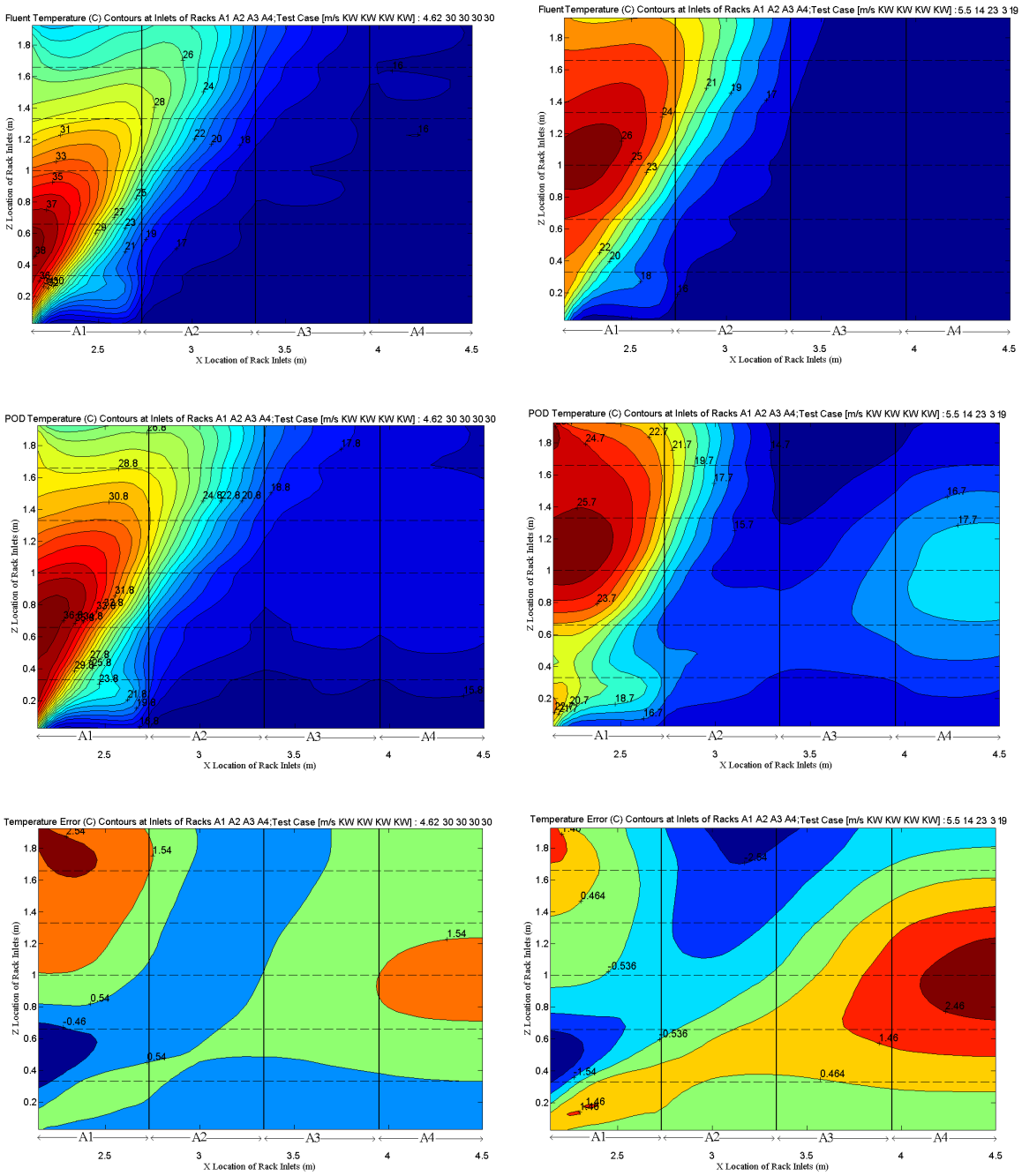

(c) (d)

Figure 7.10. Continued.

Table 7.2. POD temperature error and its standard deviation compared with CFD/HT solution for six test cases

Case#	[Vin (m/s), Q1 (kW), Q2 (kW), Q3 (kW), Q4 (kW)]	Mean Relative Error (%)	Mean Error (C)	Standard Deviation (C)
1	[1.5, 2, 30, 1, 3]	8.35	2.13	2.02
2	[2.31, 5, 5, 20, 30]	3.59	1.14	1.39
3	[3, 27, 7, 13, 24]	2.39	0.63	0.76
4	[4, 30, 29, 9, 28]	4.77	1.31	1.99
5	[4.62, 30, 30, 30, 30]	3.05	0.80	0.94
6	[5.5, 14, 23, 3, 19]	7.23	1.41	1.63
Average		4.90	1.24	1.46

As seen in Table 7.2, the mean error for the six test cases varies from 0.63 ^{o}C or 2.4% to 2.13 ^{o}C or 8.4%. The average in the mean absolute and relative error for all cases is 1.24 ^{o}C and 4.9% while the average standard deviation is 1.46 ^{o}C. These values confirm that the presented POD method is reasonably accurate at the entire data center cell.

Regarding the computational speed of the POD based method, it should be noted that the POD based thermal model has only 20 DOF, representing a 5 order of magnitude decrease compared to the CFD/HT model. The CFD/HT simulation done by Fluent takes ~2 hours to obtain the temperature field for a new test case on a desktop computer with Xeon™ CPU, 2.8-GHz and 2.75 GB of RAM. However, it takes only ~48 seconds to obtain the POD temperature field for the same test case on the same computing platform, which is ~150 times faster.

In the next section, the effect of the number of known temperature differences across the servers on the POD temperature results is studied.

7.2.3 Effect of the Known Thermal Information Quantity on the POD Results

In the previous section it was shown that the POD based method can predict a new temperature field in the entire data center cell of Figure 7.3 with an average error of 5% if the temperature differences across the 48 servers are given as known information, in addition to the CRAC air velocity and discharge temperature. One interesting question is how the POD solution and error change if lesser thermal information about the components such as the server temperature differences is supplied. This information is useful in reducing the number of required thermal sensors at the server inlets/outlets in the operational data centers to be able to predict the entire temperature field with the lowest cost.

For this purpose, four different scenarios are considered, as listed in Table 7.3:

Secenario1: Temperature differences for all 6 servers per rack in Figure 7.3 are measured and given to the method. In this situation, 50 equations are obtained to solve for the POD coefficients. The results are as presented in Section 3.2.

Secnario2: Temperature differences for only 4 servers, Server#1, 3, 4, and 6 in Figure 7.3, per rack are given to the POD method. So, there are 34 equations in this scenario.

Scenario3: Temperature differences for only three servers, Server#1, 4, and 6 in Figure 7.3, per rack are used and totally 26 equations are solved to obtain the POD coefficients.

Scenario4: Temperature differences for only two servers, Server#1 and 6 in Figure 7.3, per rack are given and totally 18 equations are solved to obtain the POD coefficients. In this scenario, the maximum possible number of retained modes in Eq. (1) is limited to 18, following the discussion in Section 2.2, while in the previous scenarios all 20 modes can be used.

Table 7.3. Specifications of Scenarios 1 through 8 for the data center example

Scenario#	No. of Components per Rack	No. of Known Temperature Differences per Rack	No. of Total Equations in Data Center	Maximum Possible No. of POD Modes to Use
1, 5	6	6	50	20
2	6	4 (for Servers#1, 3, 4, 6)	34	20
3	6	3 (for Servers#1, 4, 6)	26	20
4	6	2 (for Servers#1, 6)	18	18
6	3	3	26	20
7	2	2	18	18
8	1	1	10	10

The effect of the number of used modes on the mean error for the four scenarios is shown in Figure 7.11 for two test cases. As seen in the figure, the solution starts to diverge when the number of used server temperature differences is reduced. However, complete divergence is only seen in Scenario4 when the information of only 2 servers per rack is used in the method. In Figure 7.12, the error contours of the POD temperature field, when all possible modes are used, at the inlets of rack A1 through A4 are shown for the four scenarios and the two test cases. It is seen that the error increases as the specified

information is reduced. Also, the mean absolute and relative errors with the associated standard deviation are shown in Table 7.4 for the four scenarios and six test cases. As seen in the table, the average error for all test cases increases from 1.2 ^{o}C (4.9%) to 1.45 ^{o}C (5.7%), 2.5 ^{o}C (10%), and 3.3 ^{o}C (13.25%), as the number of known temperature differences decreases from 6 servers to 4, 3, and 2 per rack, respectively. In the results presented in Figure 7.12 and Table 7.4, all possible modes, 20 for Scenarios 1, 2, and 3 and 18 for Scenario 4, have been used in the POD reconstruction.

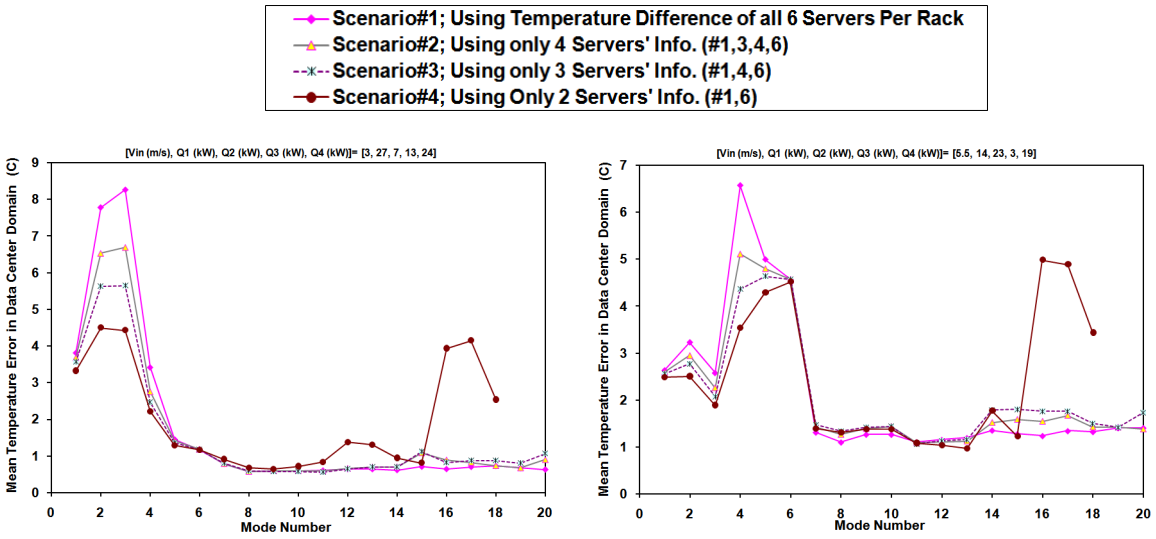

(a) (b)

Figure 7.11. Mean POD temperature error (^{o}C) versus used mode number for Scenarios 1, 2, 3, and 4; (a) Test case of [3 m/s, 27 kW, 7 kW, 13 kW, 24 kW] (b) Test case of [5.5 m/s, 14 kW, 23 kW, 3 kW, 19 kW]

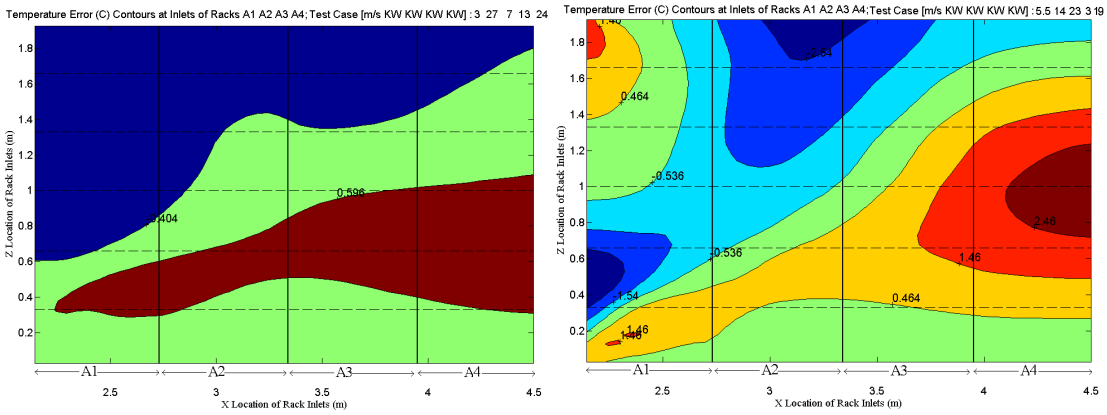

(a) Scenario1; thermal information for 6 servers per rack, totally 50 equations and 20 modes

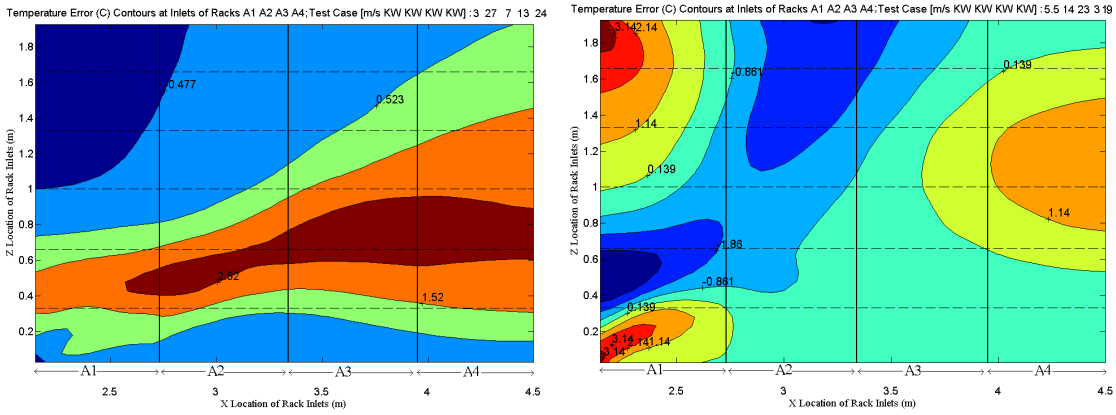

(b) Scenario 2; thermal information for 4 servers per rack, totally 34 equations and 20 modes

Figure 7.12. Contours of POD temperature error (^{o}C) at racks inlets for Scenarios 1, 2, 3, and 4 for two test cases. The results have been obtained using all possible modes. Relevant test case is mentioned at the top of each contour plot.

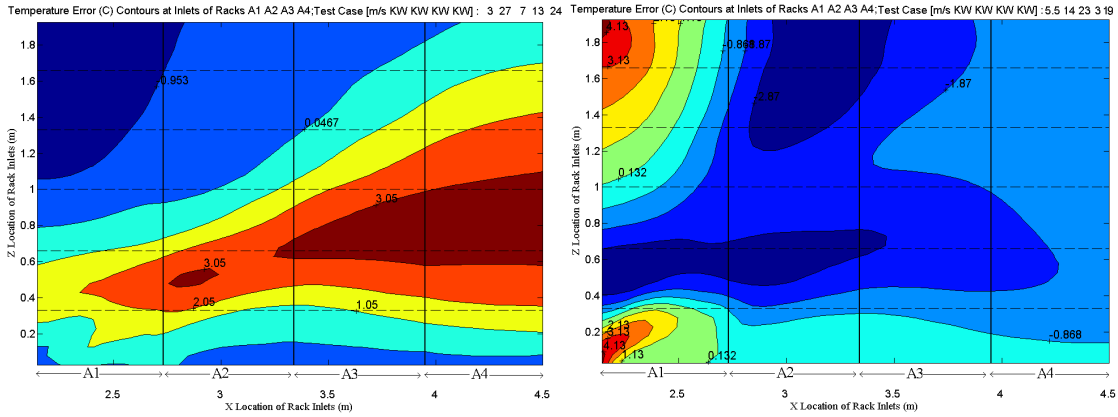

(c) Scenario 3; thermal information for 3 servers per rack, totally 26 equations and 20 modes

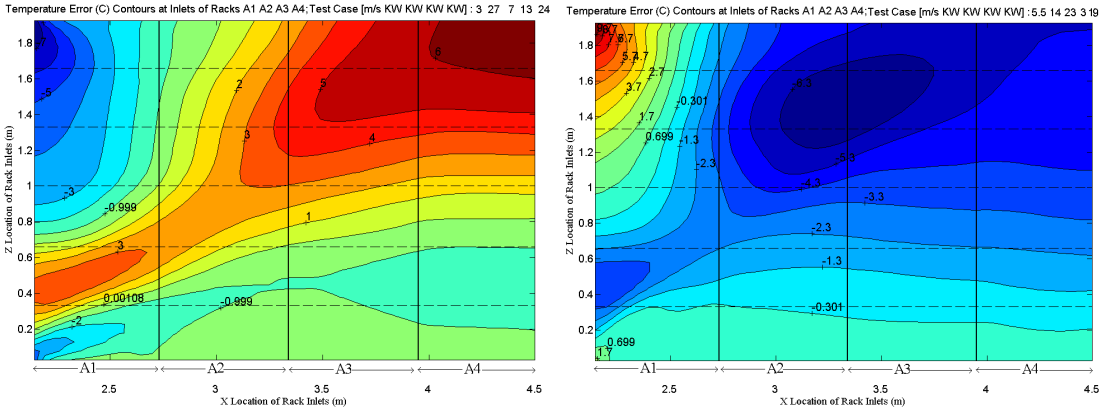

(d) Scenario 4; thermal information for 2 servers per rack, totally 18 equations and 18 modes

Figure 7.12. Continued.

As seen in Figure 7.11, the mean error in the POD solution for all scenarios reduces with the increase in the number of used POD modes until ~10 modes. As seen in Figure 7.5, the first 10 modes capture 89.4% of the energy of the system. The last modes, as seen in Figure 7.6c and Figure 7.6d, include small scale structures with low energy contribution to the system and fluctuate sharply throughout the domain. Adding these

fluctuating fine modes to the first dominant modes in the POD reconstruction of Eq. (7.1) generally results in numerical error and solution divergence. When successive modes are added to the POD solution for the data center example after 10 modes, the contribution of the numerical error to the POD reconstruction starts to increase. However, there is a competition between the numerical error and the given thermal information at the boundaries. As seen in Figure 7.12 and Table 7.4 for Scenarios 1 and 2, when number of available equations to satisfy is much higher than the number of POD coefficients, the POD solution does not diverge by adding more modes. In these situations, the POD solution is enforced to satisfy the thermal information at many system interior boundaries and is not allowed to diverge. But, as the available information and number of equations decrease, approaching the number of used modes and unknown POD coefficients, the numerical error contribution, and as a result the solution divergence becomes larger. This can be seen by comparing the results for Scenario 3 with 26 equations and Scenarios 1 and 2 with 50 and 34 equations respectively in Figure 7.12. In Scenario 4, when the number of equations, 18, is equal to the number of used modes, the numerical error contribution becomes dominant and the solution diverges after ~10 modes.

As discussed above and seen in Figure 7.12, we can obtain a converged POD solution for all four scenarios with using only 10 modes. The temperature error contours of the POD solution, using only 10 modes, for all scenarios are shown at the rack inlets for the two test cases in Figure 7.13. It is seen that the error is less than 1 ^{o}C at most of the regions at the rack inlets for all scenarios. Also, the mean absolute and relative errors with the standard deviation are shown in Table 7.5 for the four scenarios and six test cases, when only 10 modes are used in the POD reconstruction. As seen in Table 7.5, the

average error for all test cases increases slightly from 1.28 ^{o}C (5.05%) to 1.33 ^{o}C (5.23%), 1.38 ^{o}C (5.4%), and 1.58 ^{o}C (6.22%) as the number of server information equations decreases from 6 to 4, 3, and 2 per rack, respectively. It shows that even with temperature differences specified for only two servers per rack, the POD method can predict the temperatures at all 431,120 points in the data center with an average error of 6.2% if we know the number of required POD modes to reach a converged solution. This required POD mode number can be obtained directly from the POD solution through graphs such as Figure 7.7 and Figure 7.8 without a need to run and compare with CFD/HT solution.

Table 7.4. POD temperature error for Scenarios 1, 2, 3, and 4 with different known thermal information about the servers. The results have been obtained for six test cases using all possible modes.

		Scenario#1; Using Temperature Difference of all 6 Servers Per Rack; 50 Eqs & 20 Modes		Scenario#2; Using Temperature Difference of only 4 Servers (#1,3,4,6); 34 Eqs & 20 Modes		Scenario#3; Using Temperature Difference of only 3 Servers (#1,4,6); 26 Eqs. & 20 Modes		Scenario#4; Using Temperature Difference of only 2 Servers (#1,6); 18 Eqs. & 18 Modes	
Case#	**[Vin (m/s), Q1 (kW), Q2 (kW), Q3 (kW), Q4 (kW)]**	**Mean Error (C)**	**Mean Relative Error (%)**	**Mean Error (C)**	**Mean Relative Error (%)**	**Mean Error (C)**	**Mean Relative Error (%)**	**Mean Error (C)**	**Mean Relative Error (%)**
1	[1.5, 2, 30, 1, 3]	2.13	8.35	2.98	11.76	6.25	25.13	5.42	22.43
2	[2.31, 5, 5, 20, 30]	1.14	3.59	1.51	4.88	2.97	9.86	4.97	16.19
3	[3, 27, 7, 13, 24]	0.63	2.39	0.89	3.53	1.06	4.22	2.53	9.51
4	[4, 30, 29, 9, 28]	1.31	4.77	1.24	4.55	2.44	9.56	1.64	6.47
5	[4.62, 30, 30, 30, 30]	0.80	3.05	0.69	2.53	0.69	2.53	1.86	7.19
6	[5.5, 14, 23, 3, 19]	1.41	7.23	1.39	7.00	1.74	8.77	3.44	17.71
Average		1.24	4.90	1.45	5.71	2.52	10.01	3.31	13.25

Table 7.5. POD temperature error for Scenarios 1, 2, 3, and 4 with different known thermal information about the servers. The results have been obtained for six test cases using only 10 modes.

		Scenario#1; Using Temperature Difference of all 6 Servers Per Rack; 50 Eqs & 10 Modes		Scenario#2; Using Temperature Difference of only 4 Servers (#1,3,4,6); 34 Eqs & 10 Modes		Scenario#3; Using Temperature Difference of only 3 Servers (#1,4,6); 26 Eqs. & 10 Modes		Scenario#4; Using Temperature Difference of only 2 Servers (#1,6); 18 Eqs. & 10 Modes	
Case#	**[Vin (m/s), Q1 (kW), Q2 (kW), Q3 (kW), Q4 (kW)]**	**Mean Error (C)**	**Mean Relative Error (%)**	**Mean Error (C)**	**Mean Relative Error (%)**	**Mean Error (C)**	**Mean Relative Error (%)**	**Mean Error (C)**	**Mean Relative Error (%)**
1	[1.5, 2, 30, 1, 3]	2.25	8.81	2.36	9.18	2.55	9.90	2.39	9.48
2	[2.31, 5, 5, 20, 30]	1.24	3.80	1.23	3.78	1.26	3.86	1.43	4.41
3	[3, 27, 7, 13, 24]	0.60	2.25	0.59	2.20	0.56	2.07	0.72	2.69
4	[4, 30, 29, 9, 28]	1.27	4.86	1.30	4.74	1.29	4.74	2.37	9.12
5	[4.62, 30, 30, 30, 30]	1.07	4.08	1.09	4.17	1.16	4.47	1.18	4.50
6	[5.5, 14, 23, 3, 19]	1.27	6.49	1.44	7.33	1.44	7.37	1.38	7.12
Average		1.28	5.05	1.33	5.23	1.38	5.40	1.58	6.22

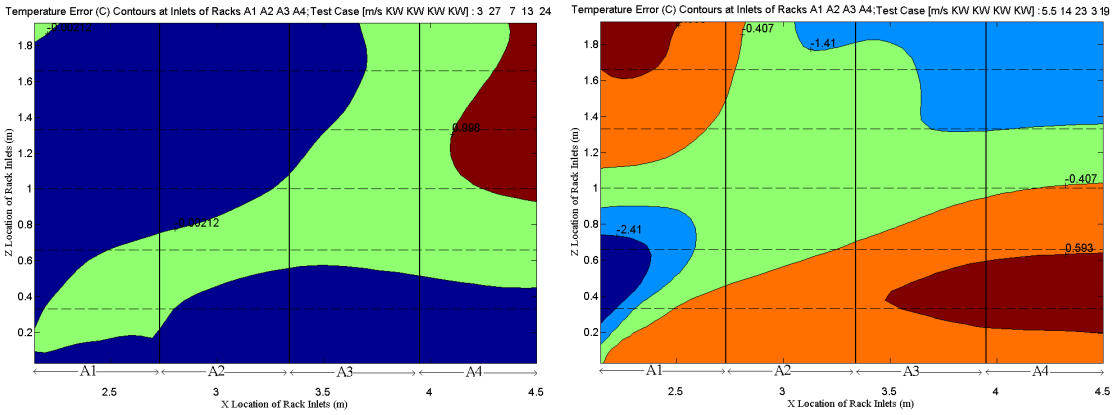

(a) Scenario 1; thermal information for 6 servers per rack, totally 50 equations and 10 modes

Figure 7.13. Contours of POD temperature error (^{o}C) at racks inlets for Scenarios 1, 2, 3, and 4 for two test cases. The results have been obtained using only 10 modes. Relevant test case is mentioned at the top of each contour plot.

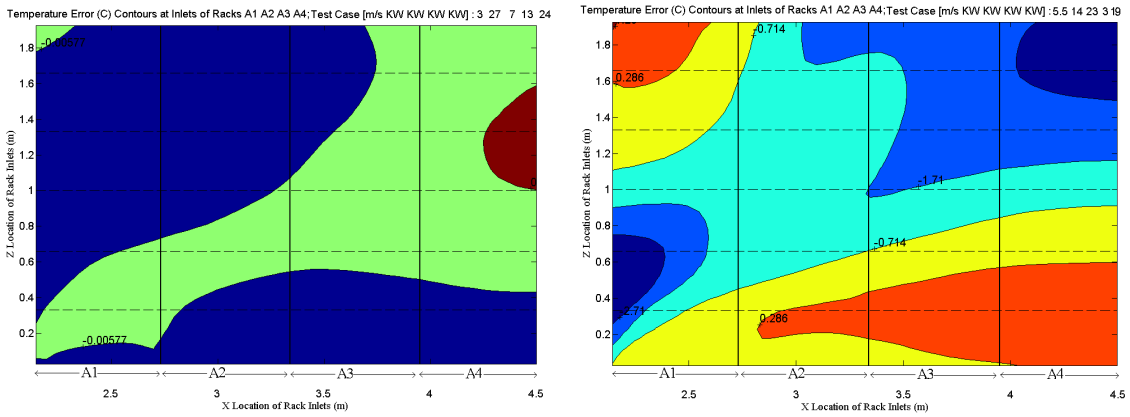

(b) Scenario 2; thermal information for 4 servers per rack, totally 34 equations and 10 modes

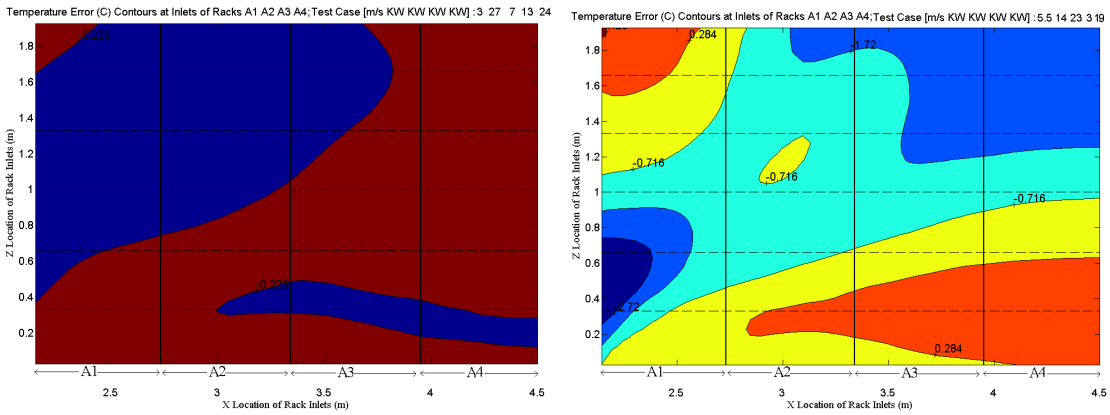

(c) Scenario 3; thermal information for 3 servers per rack, totally 26 equations and 10 modes

Figure 7.13. Continued.

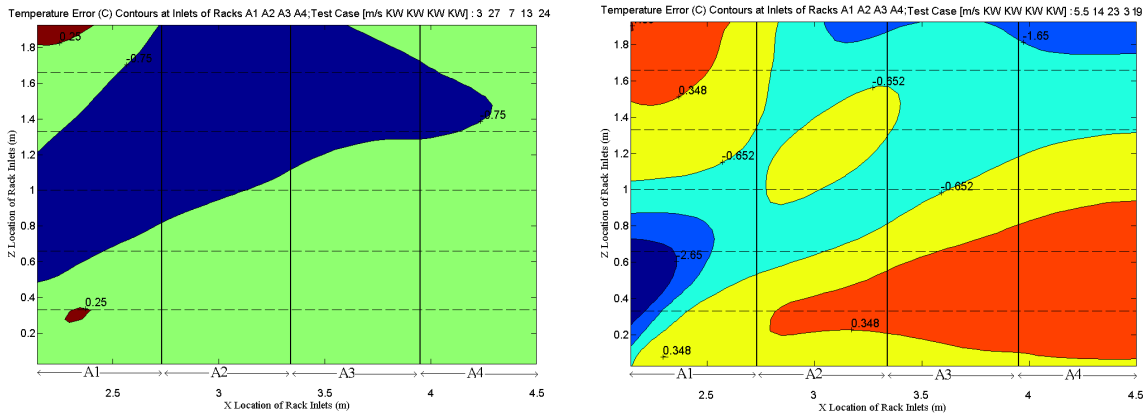

(d) Scenario 4; thermal information for 2 servers per rack, totally 18 equations and 10 modes

Figure 7.13. Continued.

7.2.4 Effect of the Number of System Components on the POD Results

As mentioned in Section 7.1, the maximum possible number of used POD modes is limited by the number of available algebraic equations in the presented method. This number is limited to the number of interior convective components or subsystems like the ones in Figure 7.2, for which we can use energy balance equations, heat flux matching, and/or surface temperature matching. In this section, the effect of the number of these components in the main system on the POD solution is studied considering four new scenarios in the data center example. These scenarios are listed in Table 7.3 and defined in the following:

Secenario 5: Each server in Figure 7.3b is considered as a component for which Eq. (7.3) is applied. This results in 6 components per rack and totally 50 equations to

solve for 20 mode coefficients. This scenario is the same as Scenario 1 in Section 7.2.3 and the results are as presented in Section 7.2.2.

Secnario 6: Two adjacent servers in each rack are assumed as one component. So, Eq. (7.3) is applied to only three components per rack. So, there are 26 equations in this scenario while the maximum possible number of used modes is 20.

Scenario 7: Each rack is assumed to have only two components. The combination of Server#1, 2, and 3 in Figure 7.3b makes one component as the combination of Server#4, 5, and 6 do. So, there are two equations per rack and totally 18 equations in the data center for this scenario. This reduces the possible number of used modes to only 18.

Scenario 8: All six servers in each rack are assumed as one component. So, there is 1 equation per rack and totally 10 equations in the data center in this scenario, while the possible number of used modes is only 10.

The effect of the number of used modes on the mean error for Scenarios 5 through 8 is shown in Figure 7.14 for four test cases. The trend of the results is very similar to the POD solution for Sceanrio 1 through 4 shown in Figure 7.11, when the available server thermal information drove the number of available equations. In Scenarios 5 through 8, the number of components drives the number of equations. Through comparing the results in Figure 7.14 with Figure 7.11, the following statements can be made about the presented method:

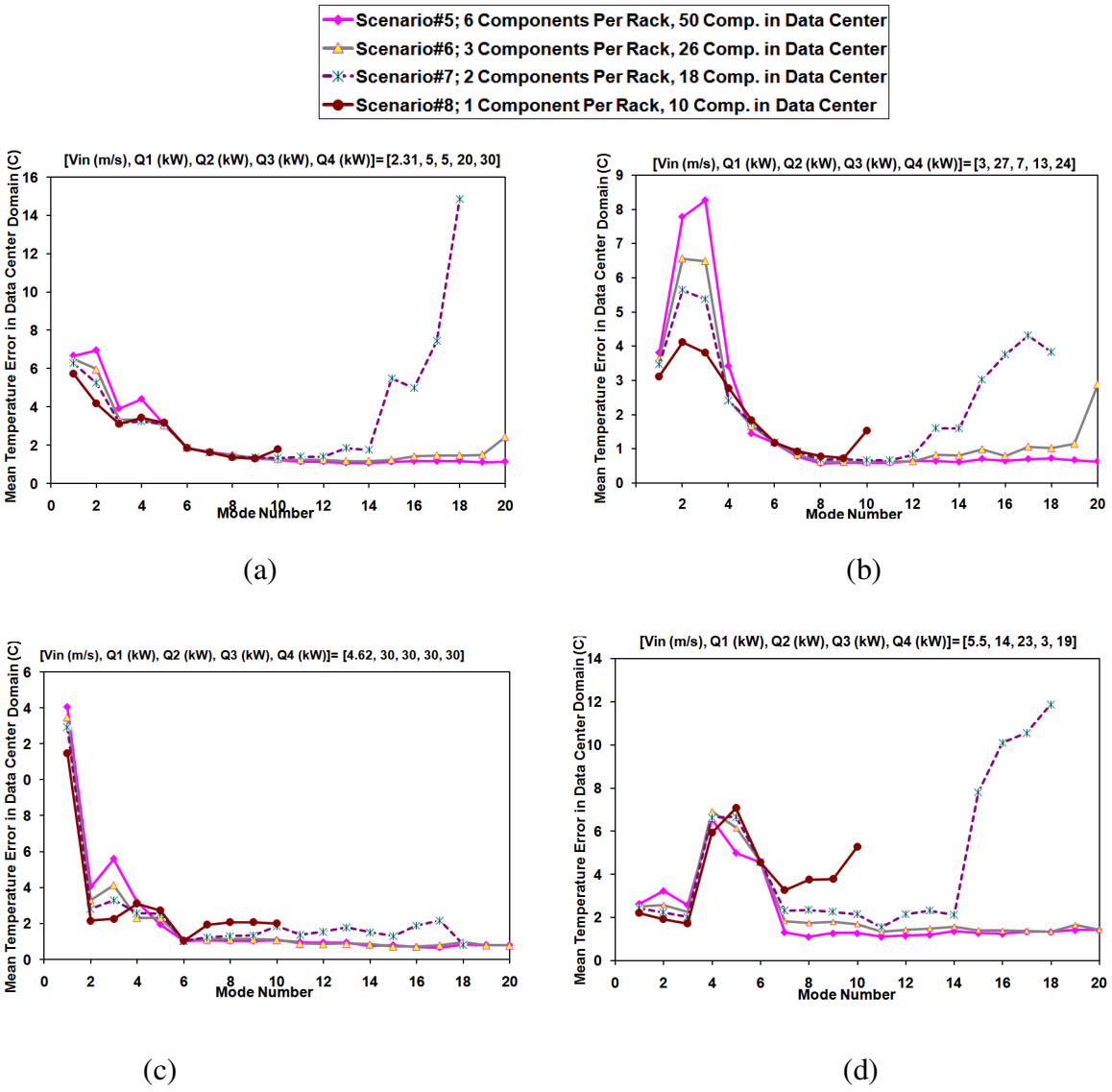

Figure 7.14. POD mean temperature error (^{o}C) versus used mode number for Scenarios 5, 6, 7, and 8 for four test cases. Relevant test case is mentioned at the top of each plot.

1) A converged and accurate temperature field in a complex system is generated only if the number of components and given thermal information is much higher than the number of available modes and the number of required dominant

modes to capture the main physics of the system. In this example as discussed before, ~10 modes is enough to capture the most important phenomena of the systems. For Scenarios 1, 2, and 5 in Figure 7.11 and Figure 7.14, the number of available equations is 50, 34, and 50 respectively, which is much higher than 20, the number of available modes. So, we have a converged and accurate solution for these scenarios.

2) The solution starts to diverge when the number of equations, which is equal to the number of components or given thermal information, decreases and becomes closer to the number of available POD modes. This trend is seen in Scenarios 3, 4, 6, 7, and 8 with 26, 18, 26, 18, and 10 available equations and 20, 18, 20, 18, and 10 available modes to use, respectively. There are two situations for these scenarios:

2a) if the number of available equations is still higher than the number of required modes to capture the main physics of the system, ~10 in this example, the method gives accurate results if only the required modes, and not all available modes, are used in the POD reconstruction. This is seen for Scenarios 3, 4, 6, and 7. As seen in Figure 7.11 and Figure 7.14, the POD solution using only 10 modes for these scenarios has not started diverging yet and is accurate.

2b) if the number of available equations is very close to, or less than, the number of required dominant modes for the system, the error changes nonlinearly with the number of used modes. In this situation, there is an optimal number of used modes to reach the minimum error in the solution. But, this optimal number changes on a case by case basis, and cannot be determined in advance. This happens for Scenario 8 in Figure

7.14, when the number of components and available equations is equal to the number of required modes, i.e., 10.

7.3 Comparison between two Presented POD Based Methods

In Chapter 4 and Chapter 7, two POD based reduced order modeling approaches have been presented to generate a reduced order thermal modeling in complex multi-scale thermal/fluid systems such as air-cooled data centers. As can be seen by comparing Figure 4.1 and Figure 7.1, the difference in the two algorithms is in obtaining the algebraic equations to be solved for POD coefficients. In the method developed in Chapter 4, POD is used with Galerkin projection for dominant components while energy balance, surface temperature or flux matching is used for other dominants. However, in the method presented in Chapter 7, energy balance, surface temperature or flux matching is used for all components of the systems regardless of being dominant or not.

Each of the two POD based methods has its own pros and cons. Unlike the POD based method in Chapter 4, the presented method in Chapter 7 does not need fluid flow modeling and is accurate throughout the entire domain. Also, the method in Chapter 7 is much simpler and its application is easier for reduced order thermal modeling of operational data centers, where the observation data are gathered experimentally and thermal sensors are deployed at the inlet/outlet of the servers.

As a deficiency, the number of available algebraic equations to be solved for the POD coefficients in the presented method in Chapter 7 is limited by the number of convective components and available thermal information for the components in the

system. This brings a limitation to the method whose effect on the results for the data center cell was studied in Section 7.2.3 and 7.2.4. It was concluded that the method can be used as a reliable and rapid predictor to obtain a new temperature field throughout the system, unless the number of components or available thermal information in the form of equations at the component boundaries is very close to or less than the number of dominant modes. This would not typically cause a problem in thermal model reduction of operational data centers with several housed servers if enough numbers of servers have thermal sensors at their inlet/outlet.

On the other hand, the POD technique based on Galerkin projection in Chapter 4 does not have any limitation regarding the number of components since using Galerkin projection to obtain the algebraic equations results in m distinct algebraic equations for each component, if m POD modes are used.

7.4 Chapter Closure

In this chapter, a POD based reduced order thermal modeling approach is presented to predict the temperature field in complex systems in terms of multiple design variables. This method, as explained in Section 7.3, is much simpler than the method developed in Chapter 4. Also, the application of this method is easier for reduced order thermal modeling of operational data centers, where the observation data are gathered experimentally and thermal sensors are deployed at the inlet/outlet of the servers. In this method, the algebraic equations to solve for the POD coefficients are obtained simply through energy balance equations, heat flux matching, and/or surface temperature matching for all convective components. The method was applied to a data center cell

with multiple turbulent convective components and five design variables. The method results in average error of 1.24 ^{o}C (4.9%) for different sets of design variables, while it is ~150 times faster than the CFD/HT simulation done by Fluent.

Also, the solution convergence and accuracy of the presented method were shown to depend on the number of components and given thermal information about the system. It was shown that the POD results remain accurate for the data center exampleeven if the given thermal information at the component boundaries decreases by 67%, if we use the required dominant POD modes to capture the most important phenomena of the system. In fact, the method could predict the air temperatures at all 431,120 points in the data center cell with an average error of 6.2% even with knowing the temperature differences for only two servers per rack, which makes the method very appropriate for operational data centers. It was discussed how to obtain this required number of dominant modes in advance, based on the changes in the POD coefficients and component boundary thermal errors. Generally, the presented method can be used as a reliable and rapid predictor to obtain a new temperature field throughout the complex system, unless the number of components or available thermal information in the form of equations at the component boundaries is very close to or less than the number of dominant modes.

The POD method modification to be used in operational data centers has been addressed in this chapter as one of the realization requirements of the open design method shown in Figure 1.8. The last requirement, the POD method experimental validation, is considered in the next chapter.

CHAPTER 8

EXPERIMENTAL VALIDATION OF POD BASED REDUCED ORDER THERMAL MODELING IN DATA CENTERS

In this chapter, the POD method validation for operational data centers is studied to address the realization part of the second research question. As explained in Section 1.2, this is one of the realization requirements of the open design method as shown in Figure 1.8. Although the experimental validation of the developed POD based methods in operational data centers was not possible due to the experimental limitations, a reduced order thermal modeling approach based on POD with interpolation among modal coefficients is experimentally validated, utilizing selected sets of observed thermal sensor data inside an operational data center. The method is used to predict the data center temperature field as a function of the air flow rates of CRAC units. In Section 8.1, the POD based method with interpolation among modal coefficients is explained. In Section 8.2, the specifications of the studied operational data center are explained. The studied data center is an IBM facility. The experimental data used in this Chapter have been obtained completely by the staff in IBM. A recently developed temperature mapping tool by IBM [119] is used to capture three dimensional temperature profiles of the facility with very fine spatial granularity. In Section 8.3, the POD based method is applied to the data center. The accuracy and efficiency of the POD generated temperature field for two CRAC air flow rates are examined through comparison with experimentally measured data. The chapter is summarized in Section 8.4. To the best knowledge of the author, this

work is the first attempt for POD thermal modeling of data centers via experimentally measured high spatial resolution temperature data.

8.1 POD with Interpolation among Modal Coefficients

The POD technique with modal coefficient interpolation is utilized here with experimentally measured data in a data center, for an efficient and effective prediction of new temperature fields as a function of CRAC air flow rates. The algorithm was explained in Section 3.4.2.2. The algorithm is briefly described here again:

a) *Observation generation*: Temperature fields in the entire data center domain for different combinations of CRAC air flow rates are obtained experimentally.

b) *POD modes,* ψ_i, *calculation*: Using the observation and solving the eigenvalue problem in Eq. (3.8), POD modes are calculated through Eq. (3.7).

c) *POD coefficients,* b_i *, calculation*: The POD coefficients b_i in Eq. (3.6) are needed to generate the temperature field for a new, not observed, test case corresponding to a new combination of CRAC flow rates. The coefficients used to reconstruct an observed field $T_{obs,k}$ can be found by projecting each of the POD modes onto the observation in turn:

$$b_{i,obs} = (T_{obs,k} - T_0) \bullet \psi_i \quad i = 1,...,m \tag{8.1}$$

This can be computed for all observations within the ensemble T_{obs}. The complete coefficient matrix $B \in \Re^{m \times n}$, in which each column is the coefficient vector to reconstruct

the corresponding observation from the ensemble T_{obs}, can be more efficiently computed as:

$$B = \psi^{+} \otimes (T_{obs} - T_0) \tag{8.2}$$

Where $(.)^{+}$ is the Moore-Penrose pseudo-inverse giving the least squares solution [90]. Once $b_{i,obs}$ has been found for all observations, each of which represents the solution under a specified combination of CRAC air flow rates, the POD coefficients b_i for a new combination of CRAC flow rates are calculated through the interpolation of the coefficients $b_{i,obs}$ between observations corresponding to the new CRAC air flow rates. In other words, rather than directly interpolating between observations, interpolation is performed in the POD mode space using the coefficients $b_{i,obs}$. For data centers with one CRAC unit, this interpolation can be done through linear or the slightly more accurate piecewise cubic spline interpolation between coefficients. This interpolation reconstruction approach can be extended to multiple CRAC parameter reconstructions using multi-dimensional interpolation approaches, such as krieging or multivariate adaptive regression splines (MARS) [21].

d) *POD temperature field generation*: With calculated T_0, ψ_i, and b_i for a new combination of CRAC flow rates, the corresponding temperature field for the test case can be generated inside the entire domain from Eq. (3.6) for different numbers of used POD modes, *m*.

In Section 8.2, an air cooled operational data center is introduced, while the method outlined above is applied to the data center in Section 8.3.

8.2 Specifications of the Data Center Facility

An operational data center of 102.2 m^2 (1,100 square feet) with a hot and cold aisle arrangement of racks cooled by a CRAC unit is studied in this paper. The floor of the facility, shown in Figure 8.1, is made up of a grid of 25 x 11 tiles. It contains 15 racks which are labeled as A1, …, A5, B1, …, B4, C1, ..., C3, D1, ..., D3. The total IT heat load of the center is 76 kW while ~25 kW of the heat loads of Racks A5 and C2 are removed by two attached water cooled rear door heat exchangers. In this study, CRAC#2 is kept off while the nominal capacity of CRAC#1 is 105.2 kW and 5.85 m^3/s (12,400 CFM).

A recently developed temperature mapping tool (MMT: Mobile Measurement Technology) [119] is used to capture three dimensional temperature profiles of the facility with very fine spatial granularity. As shown in Figure 8.2, an array of temperature sensors, 9 per tile area (0.37 m^2) in 8 different heights of 0.15, 0.46, 0.76, 1.07, 1.37, 1.68, 1.98, and 2.29 m (0.5, 1.5, 2.5, 3.5, 4.5, 5.5, 6.5, and 7.5 ft) are mounted to a measurement cart, which can be readily be moved through the data center, while temperature data are logged from all the sensors using multiplex electronics as a function of X, Y and Z coordinates. The cart itself is on wheels and by moving the cart from tile to tile (0.61 cm * 0.61 cm) within the data center, these measurements are repeated and recorded for every unoccupied tile to obtain a temperature field throughout the data center. For the facility shown in Figure 8.1, there will be 10,584 measurements.

In the next section, the presented POD based method is applied to the data center facility.

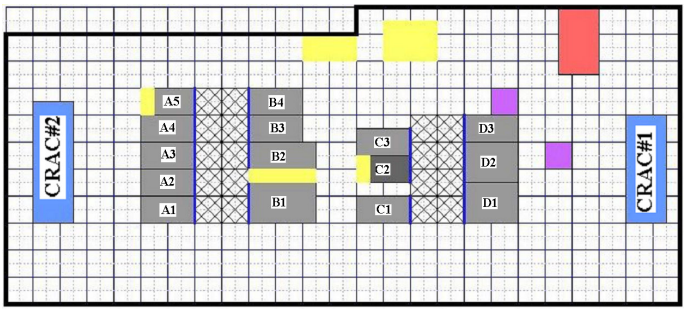

Figure 8.1. Layout of the data center facility (courtesy of Dr. Hendrik Hamann)

Figure 8.2. Mobile Measurement Technology (MMT): 3D temperature mapping tool (courtesy of Dr. Hendrik Hamann)

8.3 FacilityPOD Temperature Field Generation

The flow rate of CRAC#1 of the data center in Figure 8.1 as the input parameter is varied to generate observations required for the POD method. When the CRAC unit is operating at [96%, 92%, 88%, 80%, 76%, 72%, 65%] of the nominal capacity, the sensor

thermal data throughout the data center are collected by the temperature mapping tool shown in Figure 8.2 to obtain 7 observed temperature fields. The temperature contours for two observations at the height of 1.07 m (3.5 ft) are shown in Figure 8.3. Also, the average of all 7 observations, the reference field T_0 in Eq. (3.6), at the sensor locations at the inlet surface of Racks A1, …, A5 and C1, …, C3 are shown in Figure 8.4. Having obtained the observations, Eqs. (3.8) and (3.772) are used to obtain the POD modes. The energy percentage captured by each POD mode is plotted versus the mode number in Figure 8.5. As seen before for simulated data center cells in Chapter 4 and Chapter 7, the magnitude of the eigenvalue and the energy captured by each mode decreases sharply with the index of POD modes. Also, Figure 8.6 shows the first and last POD mode distribution at the sensors of racks A inlets. The modes with largest eigenvalues take the shape of large scale smooth structures, see Figure 8.6a. The modes with large index numbers include small scale structures, e.g. Figure 8.6b.

The observation POD coefficients $b_{i,obs}$ are calculated by Eq. (8.2) and shown in Table 8.1. A linear interpolation between the coefficients is used to generate two new temperature fields when the CRAC unit is operating at 84% and 68% of the nominal capacity. The POD generated temperature field, obtained in less than two seconds on a desktop computer with Xeon™ CPU, 2.8-GHz and 2.75 GB of RAM, is compared with measurements for these test cases to validate the accuracy of the presented method. For 84% operation of the CRAC unit, the mean error in the domain, 10,584 points, is 0.60 ^{o}C or 2.92%, while for 68% operation the mean error is 0.75 ^{o}C or 3.48%. However, the maximum local error is larger and equal to 6.14 ^{o}C and 8.15 ^{o}C respectively for the test cases. The total number of points where the local error is larger than 1 ^{o}C, is only 6.5%

and 5.5% of the total domain points for the test cases. The measured temperature, POD generated temperature, and error distribution at the sensor locations for 84% operation of the CRAC unit at the inlets of racks A and C are shown in Figure 8.7 and Figure 8.8, respectively. The same trend for the POD generated and measured temperatures is observed. Also, the error at most of the points is almost zero but there are some points with large error. These distributions for other test case, 68% operation, are shown in Figure 8.9 and Figure 8.10.

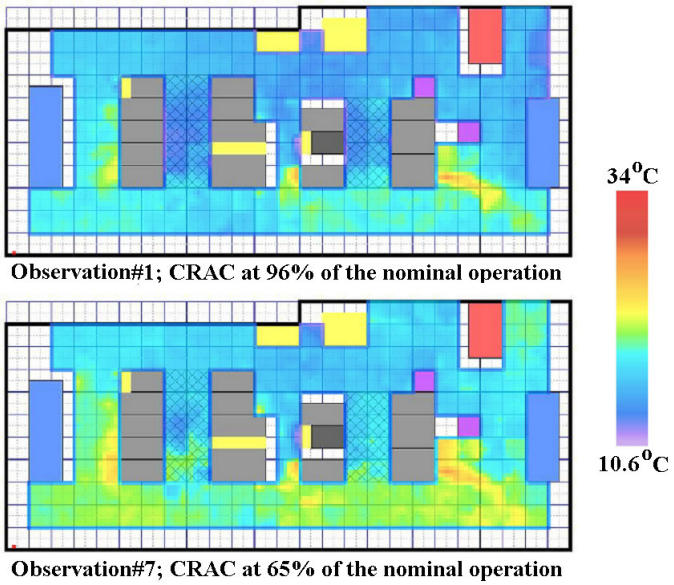

Figure 8.3. Temperature contours at the height of 1.07 m (3.5 ft) for two observations (courtesy of Dr. Hendrik Hamann)

Table 8.1. POD coefficients for observations

		Observation Number						
		1	2	3	4	5	6	7
Mode Number	1	-108.1	-95.9	-61.4	-0.2	24.2	71.9	169.5
	2	22.1	32.1	-18.5	-64.3	-25.1	43.1	10.7
	3	-29.8	-9.4	2.1	12.9	13.3	63.2	-52.3
	4	27.0	5.9	-64.5	36.7	-6.7	6.0	-4.4
	5	-2.8	8.8	-21.4	-24.5	60.9	-13.4	-7.6
	6	-39.5	47.8	-6.4	10.4	-8.1	-8.3	4.2
	7	0.0	0.0	0.0	0.0	0.0	0.0	0.0

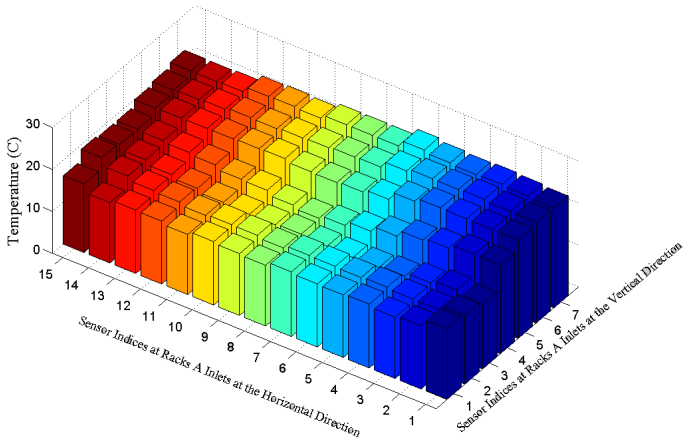

(a)

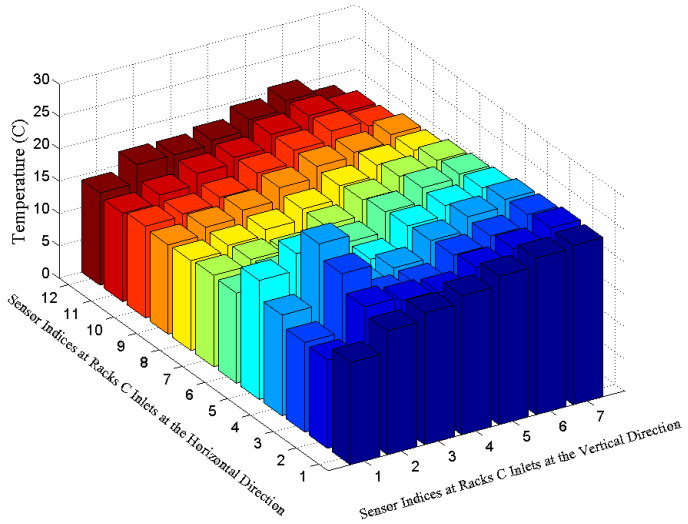

(b)

Figure 8.4. Air temperatures of the reference field at the sensor locations at inlets of a) Racks A and b) Racks C

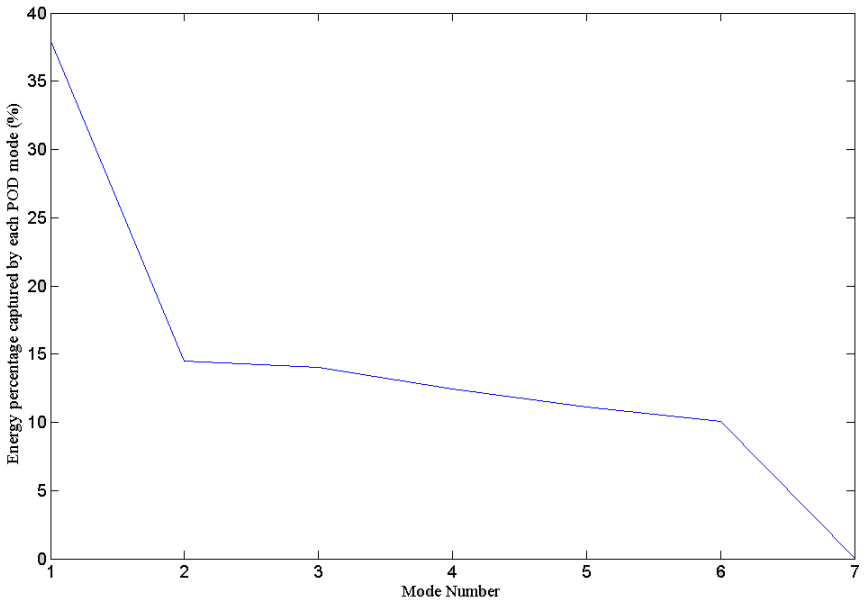

Figure 8.5. Energy percentage captured by each POD mode versus the mode number

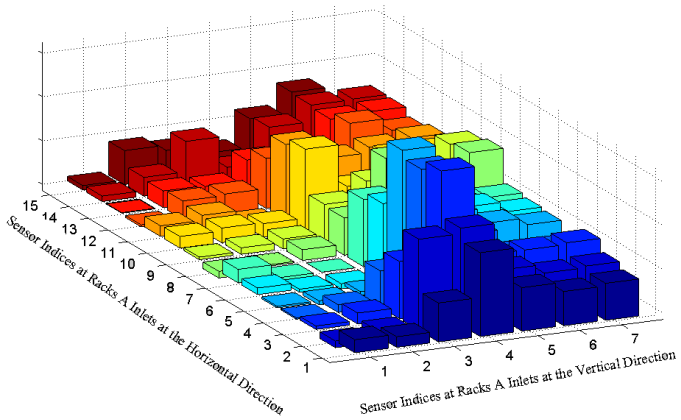

(a)

Figure 8.6. Normalized POD mode#1 (a) and #6 (b) at racks A inlet sensors

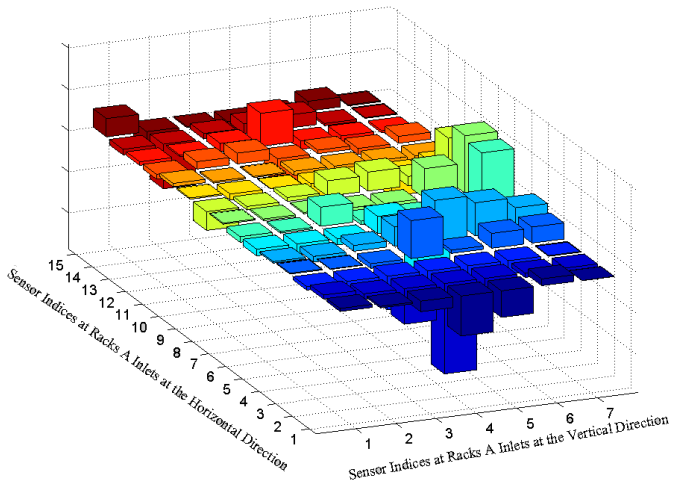

(b)

Figure 8.6. Continued.

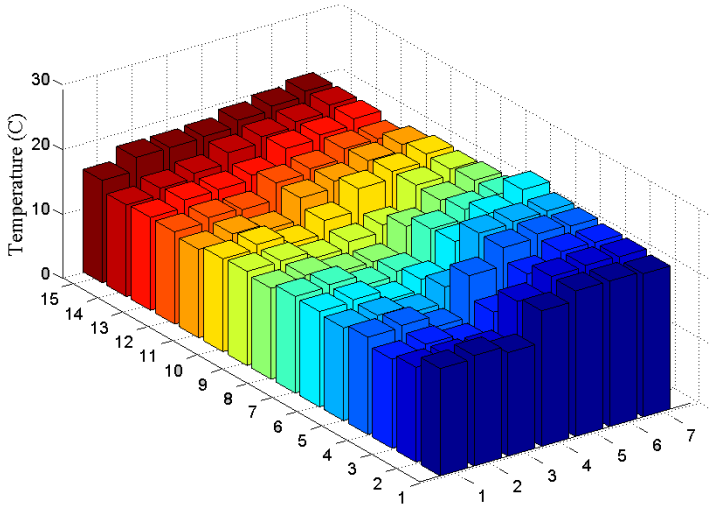

(a)

Figure 8.7. Measured temperatures (a), POD generated temperatures (b), and temperature errors (c) for 84% of CRAC operation at inlet sensors of Racks A

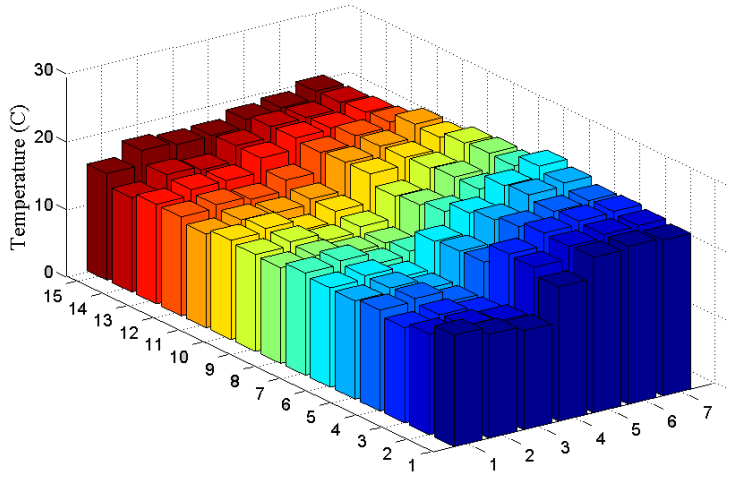

(b)

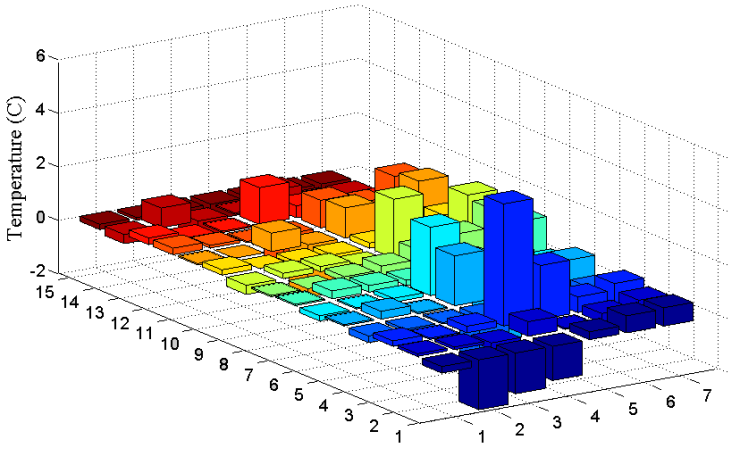

(c)

Figure 8.7. Continued

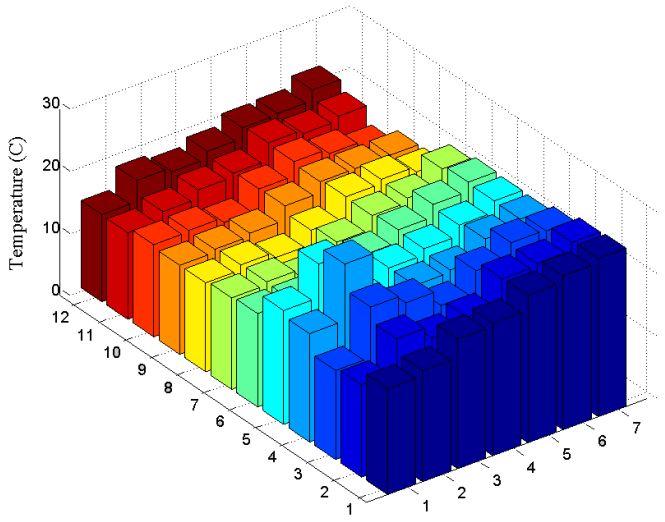

(a)

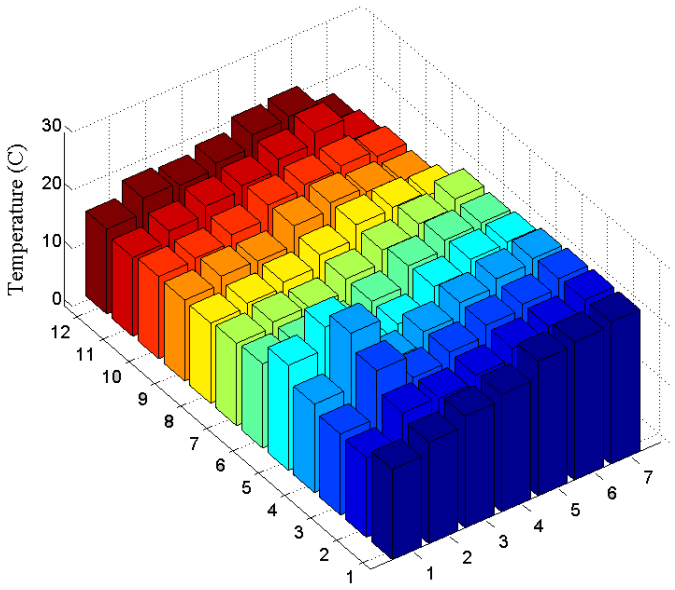

(b)

Figure 8.8. Measured temperatures (a), POD generated temperatures (b), and temperature errors (c) for 84% of CRAC operation at inlet sensors of Racks C

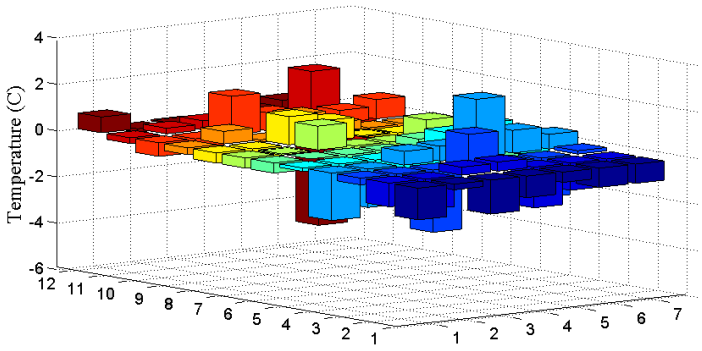

(c)

Figure 8.8. Continued

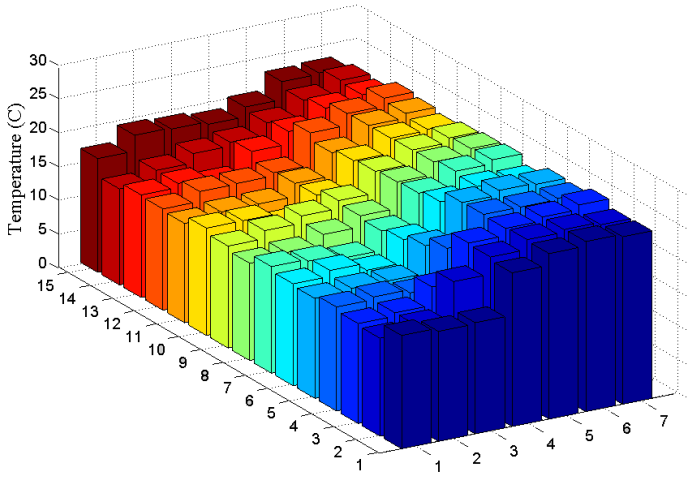

(a)

Figure 8.9. Measured temperatures (a), POD generated temperatures (b), and temperature errors (c) for 68% of CRAC operation at inlet sensors of Racks A

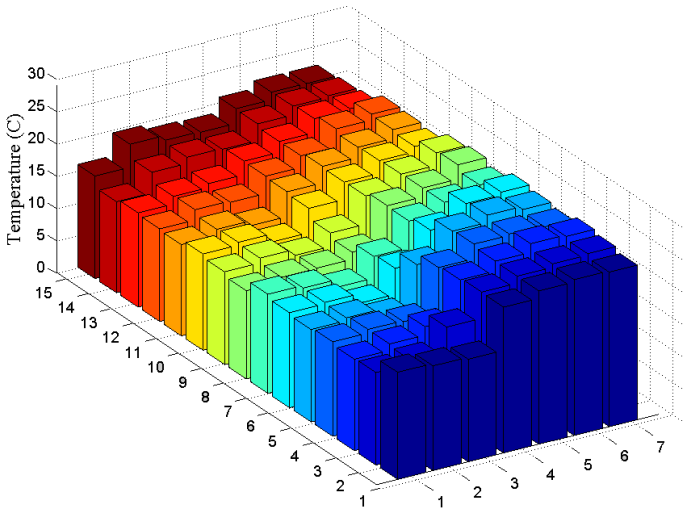

(b)

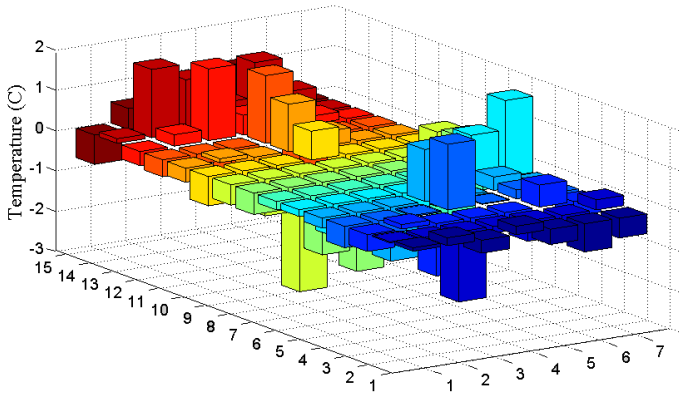

(c)

Figure 8.9. Continued.

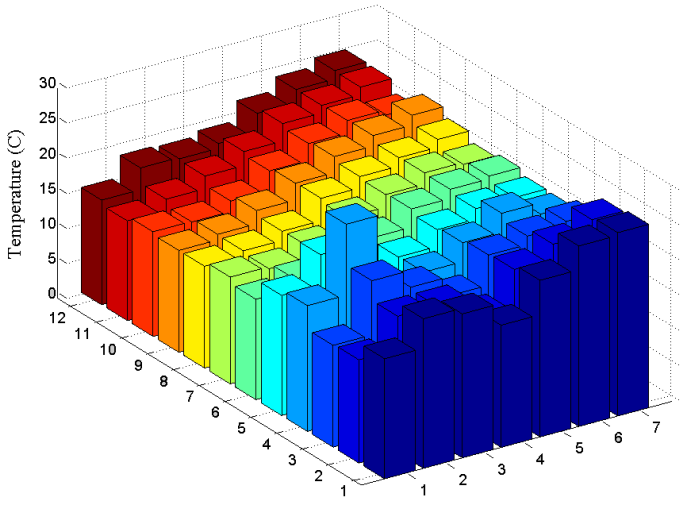

(a)

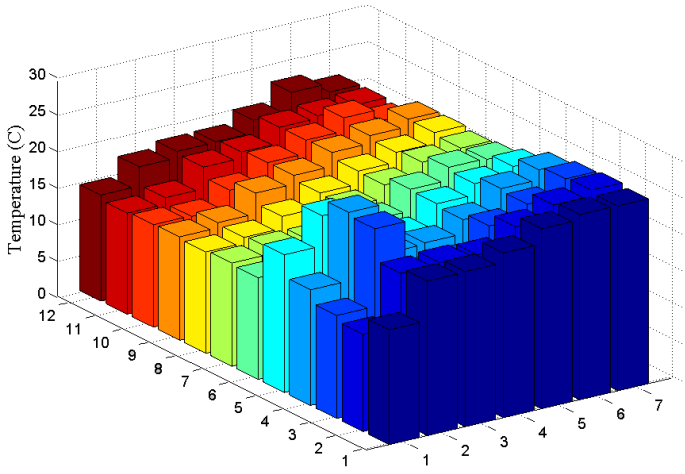

(b)

Figure 8.10. Measured temperatures (a), POD generated temperatures (b), and temperature errors (c) for 68% of CRAC operation at inlet sensors of Racks C

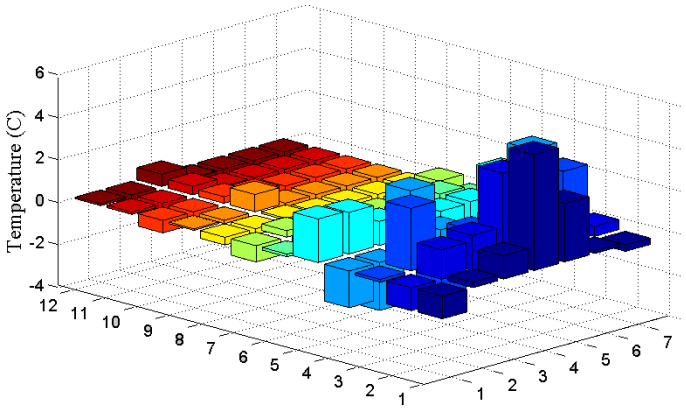

(c)

Figure 8.10. Continued.

8.4 Chapter Closure

An accurate CFD/HT model of an operational data center is very challenging, in addition to the difficulty in quantifying numerical uncertainties. The thermal data throughout the studied facility can be collected in about 30 minutes using the 3D temperature mapping tool shown in Figure 8.2. The reduced order modeling approach centered on proper orthogonal decomposition technique with modal coefficient interpolation can generate new temperature fields of the center as a function of the CRAC flow rate in less than 2 seconds on a high end desktop PC. It is found that the average error in POD re-construction is 0.68 ^{o}C or 3.2%, compared with the experimentally measured data for two different values of CRAC flow rates. However, there are some limited numbers of points with larger local error in the POD generated temperature field.

CHAPTER 9

CRITICAL REVIEW AND CONCLUDING REMARKS

9.1 Overall Effectiveness

As mentioned in Chapter 1, the principal goal of this dissertation is to:

Principal Research Objective: Identify and satisfy required design specifications of new energy efficient thermal management solutions for next generation data centers.

The identification of the required design specifications is aimed by answering the first research question:

First Research Question: What should the design specifications of new energy efficient thermal solutions be in the next generation data centers?

In Section 2.1, the requirements of an ideal thermal design for the next generation data centers are identified through examining existing state-of-the-art and classified into ten categories. Comparing these requirements with the specifications of the Open Engineering Systems paradigm in Section 2.2, it is concluded that new thermal solutions should be as close as possible to open engineering system specifications, which is the first research hypothesis. In summary, open systems are the systems that are readily adaptable and robust to their environment changes through continuous improvement of an existing technological base. In Section 2.3, a multi-scale thermal solution is introduced as a potential solution to achieve openness in data centers. The first research hypothesis is

validated through comparison of a typical air cooling system with a simple open multi-scale water cooling solution in a data center example with different scenarios in Section 2.4. The adaptability and possible improvement of the simple multi-scale water cooling system in addition to its theoretical advantages over a typical air cooling system demonstrate the effectiveness of an open thermal solution as a design requirement for future data center cooling systems. The general difficulties in design and realization of an open system for data centers are discussed in Section 2.5. With identification of the design framework for new thermal solution and its validation through Chapter 2, the first research question is answered completely.

Having identified the openness as the required design specifications for new thermal solution, satisfying these requirements in air-cooled data centers is aimed by answering the second research question:

Second Research Question: How can an energy efficient open air cooling system be designed and realized in data centers?

Both design and realization must be considered to answer the second research questions completely. The requirements, challenges, and tools to develop an open design process to achieve an open air cooling system are shown in Figure 1.7. Also, the requirements for realization of the open design process and air-cooling system in operational data centers are shown in Figure 1.8. To see if the second research question has been answered completely, each of the requirements listed in Figure 1.7 and Figure 1.8 must be satisfied in this dissertation.

Regarding the design part of the second research question, as shown in Figure 1.7 and explained in Section 3.1, without flexibility in both product and design method a system is not open. The flexibility and openness in the design method relies on three requirements: increasing design knowledge, maintaining design freedom, and increasing efficiency during design. The presented design method in this dissertation and shown in Figure 1.7 satisfies all these three requirements. The developed POD based methods in Chapters 4 and 7 which are the most important construct of the design method are computationally efficient. In Sections 4.2.3 and 7.2.2, it is shown that the developed POD methods can be up to 150 times faster than typical CFD/HT simulations in predicting the temperature filed inside data centers in terms of multiple parameters. The cDSP also is an adaptable and computationally efficient mathematic design framework. Using the POD method inside the cDSP makes the design approach very efficient. This increases the design knowledge and what-if questions can be answered quickly, as was demonstrated in the design method application in Section 5.2. Also, robust design consideration within the cDSP in the presented method increases the design freedom and maintains it before making the final decision. It was demonstrated in Section 5.2.4.2 that how a Pareto frontier between an optimal point and robust point for an open air-cooled data center gives designers a much great amount of information and freedom in configuring the data center for their desired goals.

As shown in Figure 1.7 and explained in Section 3.1, the openness in the product relies on two main requirements: adaptability and robustness. These requirements are shown to be satisfied through the application of the design method for a data center example in Chapter 5. It is demonstrated in Section 5.2.4 how the design method

application guarantees that the reliability and energy efficiency goals are fully satisfied during the next 10 years through adaptable changes in the cooling system in spite of the changes in the system and its environment. The designed open cooling system remains always adaptable and robust making the thermal solution very energy efficient. It is shown in Section 5.2.4 that 12-46% reduction in the energy consumption and 73.8% reduction in the variability of the thermal response are obtained for the data center example through application of the design method. So, the presented method satisfies all requirements in Figure 1.7 to achieve an open design process and open cooling system in data centers.

Having critically reviewed the design part of the second research question, the realization part needs to be considered. As shown in Figure 1.8, the realization of the open design method for operational data centers depends on three requirements: concurrency with IT management, POD method modification, and POD method validation in operational data centers.

Regarding the concurrency with IT management, the design method is modified in Chapter 6 to consider the design information from IT designers for a coordinated adaptable and energy efficient design. It is shown in Section 6.2.4 that the modified design method satisfies the concurrency requirements between IT and thermal designers in distributing the computing task among the servers in an adaptable and energy efficient way. The result shows a 12-70% reduction in the total IT and cooling energy consumption of the data center example. However, the modified method in Chapter 7 needs more investigation to be able to achieve an operational open data centers along

with IT management. First, it does not consider uncertainty management and robustness. So, the robustness application within cDSP construct for coordinated cooling and IT management should be considered for future work. Also, the utilization distribution among servers, which are considered in Chapter 7, should be replaced with Service Level Agreement (SLA)-based criteria in operational data centers. Finally, the deployment of management solutions based on such coordinated open design methods in operational data centers and its experimental validation are very interesting and need more work. These extensions are explained in more details in Section 9.3 as future work.

Regarding the POD method modification for operational data centers, a simple POD based design method is presented in Chapter 7 which is very efficient to be used in operational data centers. In Section 7.2.3, it is shown that the POD method results remain accurate even if the available thermal information at the server boundaries decreases by 67%. This shows the effectiveness and efficiency of the presented POD method in predicting the temperature filed in operational data centers.

Regarding the POD method validation, the developed POD methods in this dissertation are not experimentally validated due to the experimental limitations. However, a simpler POD method based on interpolation is validated for an operational data center in Chapter 8. It is shown in Section 8.3 that the method is very accurate and quick in predicting the new temperature filed for the studied data center facility. The validation of the presented POD methods in Chapters 4 and 7 need more investigation with controllable equipment.

In summary, the first research question has been answered completely in this dissertation. Also, the design part of the second research questions in achieving an open design method for open thermal solutions in air-cooled data centers has also been completely addressed. Although the realization part of the second research question has been addressed with enough details, realizing an open cooling system in operational data centers based on the presented design method in this dissertation needs more comprehensive work and research.

9.2 Unique Contributions

In this section a discussion of the research contributions is presented:

a) The concept of "openness" has been introduced in data centers and a systematic design method has been developed to achieve an adaptable, robust, and energy efficient complex multi-scale convective system such as an air-cooled data center.

While the typical designs of air-cooling systems are not energy efficient and will be soon inadequate for upcoming data centers, the design specifications of Open Engineering Systems are applied to maintain the IT reliability in current and future data centers. A simulation-based design approach is presented to bring adaptability and robustness in the multi-scale convective systems such as current air-cooled data centers. The presented approach is centered on the integration of three constructs: a) a new developed POD based multi-scale modeling, b) cDSP, and c) robust design. The method application for a data center example results shows a 12-46% reduction in the energy consumption of the center in addition to being adjustable to the newer IT equipment and

higher heat loads compared with a traditional design. Compared with an optimal solution, a robust solution can reduce the variability in the thermal response by 73.8% with only 7.8% increase in the center energy consumption.

b) Two deterministic approaches have been presented to develop multi-parameter reduced order thermal modeling of complex multi-scale convective systems such as air-cooled data centers.

Thermal modeling of complex multi-scale thermal-fluid systems such as data centers is currently done by CFD/HT models that are time-consuming and costly, especially for iterative optimization based design. As discussed in Section 3.4.3.2, there is a gap in the literature in developing a physics-based and rapid modeling approach for complex convective systems. In Chapters 4 and 7, two new methods based on POD are presented to develop reduced order models of the temperature field in these systems in terms of multiple design variables. In the method developed in Chapter 4, POD is used with Galerkin projection for dominant components while energy balance, surface temperature or flux matching is used for other dominants. However, in the method presented in Chapter 7, energy balance, surface temperature or flux matching is used for all components of the systems regardless of being dominant or not. The method were applied to a data center cell with five design parameters, one CRAC velocity and four racks heat loads. The methods result in average error norm of ~6% for different sets of design parameters, while they can be ~150 times faster than CFD/HT simulations.

c) A novel feature is the use of POD modes and Galerkin projection with special treatments of boundary conditions for solving the governing turbulent convection equation in a complex multi-scale system.

As discussed in Section 3.4.2.2, previous applications of Galerkin projection for POD based techniques are limited to simple flows and geometries due to difficulty in handling the non-homogonous boundary conditions. In Section 4.1, a special treatment of boundary conditions in terms of POD modes and coefficients is presented to solve the energy equation in complex convective systems. This special treatment can be extended and used to solve other governing partial differential equations in complex systems through Galerkin projection of the system POD modes onto the equations.

d) An explicit study has been conducted on the effects of the retained POD modes and available thermal information on the accuracy of the POD based thermal field.

As explained in Section 7.1, the effect of the retained POD modes and the quantity of the available thermal information has not been explicitly studied in the previous applications of the POD methods. In Sections 7.2.3 and 7.24, these effects are studied in details through application of the POD method for a data center example with different selected scenarios.

e) The POD based approach has been illustrated to predict the temperature field within an entire operational air-cooled data center in terms of the involved design variables, based on observed data from the minimum required thermal sensors.

As discussed in Section 3.4.3, the previous works on rapid thermal modeling of data centers are based on some heuristic approaches and can predict the air temperature only at some discrete points such as server inlets/outlets. It is demonstrated in Section 7.2.3 that the presented POD method is very effective and efficient considering the required number of server thermal information for accurate and rapid prediction of the air temperatures entire the data center. In fact, the method could predict the air temperatures at all 431,120 points in the data center cell with an average error of 6.2% even with knowing the temperature differences for only two servers per rack, which makes the method very appropriate for operational data centers.

f) The first POD thermal modeling of operational data centers via experimentally measured high spatial resolution temperature data has been developed and studied.

Although the experimental validation of the developed POD based methods was not possible due to the experimental limitations, a simpler reduced order modeling approach centered on POD technique with modal coefficient interpolation was validated against experimental measurements in an operational data center facility. The POD based reduced order modeling approach can generate new temperature fields of the data center as a function of the CRAC flow rate in less than 2 seconds on a high end desktop PC. The average error in POD re-construction is shown to be 0.68 ^{o}C or 3.2%, compared with the experimentally measured data for two different values of CRAC flow rates. To the best knowledge of the author, this is the first POD based reduced order thermal modeling of operational data centers.

9.3 Limitations of the Work and Recommended Future Work

In this section the limitations of the presented methods and validations are discussed along with some recommended future work:

a) *POD method limitations:* The presented POD methods are very effective and efficient in predicting the temperature filed in air-cooled data centers in terms of multiple parameters. However, there are some limitations to apply the methods for other complex systems. The approach developed in Chapter 4 is applicable for systems where the temperature field at selected scales drives the thermal design decision. So, it will be accurate only at these dominant scales. Regarding the method presented in Chapter 7, it should be noted that the method can be used as a reliable and rapid predictor to obtain a new temperature field throughout the system only if the number of components or available thermal information in the form of equations at the component boundaries is much higher than the number of dominant modes. More discussion is presented in Section 7.3.

Although they are not direct limitations of the presented methods, the POD itself has some limitations. First of all, the issue of determining appropriate required number of the observations and the values of the design variables at each observation are not solved yet. There is not any systematic method in the literature to determine these values for each domain accurately. One future study could focus on this issue for the data center domain. Considering dimensional analysis of the dominant variables in the data center domain can help in finding appropriate parameters and their values for each observation. Second unresolved issue is calculating the prediction error of the POD method in advance

before applying for a specific domain. This needs more research on the fundamentals of the POD to find the error bounds in the POD predictions for each domain. The third issue worthy of investigation is the effect of the data spatial granularity in the observations on the accuracy of the POD prediction. This investigation will help in reducing the cost of the experimental generation of the observations in operational data centers. Finally, although the presented POD based methods showed great reduction in computational time with good accuracy in modeling the complex multi-scale systems, there are some limited numbers of points with larger local error in the POD generated temperature field. This could be due to the inherent properties of POD. POD, like Fourier based techniques, cannot separate between coherent and incoherent structures throughout the domain. So, the average error can be reduced substantially through modifying the POD based technique while the local error does not necessarily decrease. As a solution, wavelet based techniques can be investigated to develop reduced order modeling approaches for complex convective systems.

b) *Uncertainty management:* The robust design used in this dissertation only considers the variability and uncertainty in the design parameters. Accordingly, the obtained design solution is robust against the changes in the design parameters. However, the thermal model obtained by the POD methods has some prediction error and uncertainty. These uncertainties were not considered in developing the design method in this research. More comprehensive robust design techniques are required to consider the uncertainty in the thermal model within the presented design approach. Modifying Type III robust design [120] along with calculation of the POD error bounds can be considered as one solution to manage the uncertainty in the thermal model.

c) *Multi-scale POD based modeling and design*: The presented reduced order thermal modeling and design approaches were focused on the rack and room level in an air-cooled data center. The details at the server level such as chip numbers, dimensions, and server power distribution can be modeled separately and connected to the already developed POD based modeling. Developing such a multi-scale reduced order modeling approach can enable designing an open air-cooled data center with more freedom in exploring several design parameters at different scales. Such an open multi-scale design can increase the energy efficiency in data centers substantially in addition to being able to model and design next generation multi-scale solutions integrating air, liquid, two phase, etc cooling systems for future high heat load data centers.

d) *POD experimental validation*: In this dissertation only a simple POD based method was validated against the experimental measurements in an operational data center. More comprehensive experimental validation of the developed POD based technique should be studied, using a facility with controllable rack heat loads. Also, in many facilities, there are several CRAC units with different combinations of airflow rates, making the thermal modeling more challenging. As the POD method has been used for simulation based reduced order modeling of data centers with multiple design parameters, its validation for real-world data centers with several rack and CRAC units needs more investigations to be utilized with experimentally measured data.

e) *Concurrency with IT management*: In this work, the effect of the rack inlet temperature on the server performance was not considered while the energy efficiency was the final objective. But the performance optimization can be simply considered as another

goal in the optimization-based design problem in the presented approach. Also, other design constraints from the IT and cooling perspectives can be added to the optimization problem. Having a computationally efficient thermal mapping throughout the data center obtained by the POD method gives the designer great freedom to apply his/her preferences and investigate the effects of the design parameters on the reliability and performance of the servers along with the data center power minimization. The general multi-objective constrained design problem can be solved through the compromise Decision Support Problem.

Also, the work done on the coordinated optimization of IT and cooling energy consumption is based on processor utilization usage. Utilization can be obtained through performance counters using existing platform counters or industrial products for rack-based monitoring. However, high utilization is not always the most appropriate metric to approximate higher-level application Service Level Agreements (SLAs). Also, additional energy savings can be attained by coordinated management of cooling and virtualization based on SLA violations [121]. In this regard, one interesting extension of the presented research would be modifying the POD method to be used along with virtualization management policies to develop coordinated SLA-based policies for online placement and migration of Virtual Machines (VMs) in operational data centers. Developing a flexible plug-and-play management solution based on the POD method and virtualization to be easily implemented for different servers in a practical data center needs more research from both thermal and IT sides.

f) *Open design realization*: Designing and realizing a controller for the real application of the open design framework in online adjustment of the design parameters of the CRAC and chiller units and also in online distribution of the computational work and VMs among different racks and servers using the virtualization technology in operational data centers is the final goal in realizing openness in data centers. Achieving such a goal is worthy of more research and investigation.

g) *Open design of other convective systems*: The developed POD based modeling and design methods should be applicable to other complex convective systems. One of the most interesting domains is modeling and designing open energy efficient HVAC systems in commercial and residential buildings. Similar to data centers, the application of the POD and open design methods for thermal management of the buildings can reduce the energy consumption of one of the most energy consumers in the US and make the world more green.

REFERENCES

1. C.D. Patel, R. Sharma, C. Bash, and M. Beitelmal, Thermal Considerations in Cooling of Large Scale High Compute Density Data Centers, Proc. ITHERM 2002- Eight Intersociety Conference on Thermal and Thermomechanical Phenomena in Electronic Systems, San Diego, California, pp. 767- 776, 2002.

2. J. Rambo and Y. Joshi, Multi-Scale Modeling of High Power Density Data Centers, Proc. ASME InterPACK03, Kauai, Hawaii, ASME, InterPack2003-35297, 2003.

3. J. Rambo and Y. Joshi, Physical Models in Data Center Airflow Simulations, Proc. IMECE-03 - ASME International Mechanical Engineering Congress and R&D Exposition, Washington D.C., IMECE03-41381, 2003.

4. S. Shrivastava, B. Sammakia, R. Schmidt, and M. Iyengar, Comparative Analysis of Different Data Center Airflow Management Configurations, Proc. ASME InterPACK05, San Francisco, California, USA, ASME, IPACK2005-73234, 2005.

5. M. Iyengar, R. Schmidt, A. Sharma, G. McVicker, S. Shrivastava, S. Sri-Jayantha, Y. Amemiya, H. Dang, T. Chainer, and B. Sammakia, Thermal Characterization of Non-Raised Floor Air Cooled Data Centers Using Numerical Modeling, Proc. ASME InterPACK05, San Francisco, California, USA, ASME, IPACK2005-73387, 2005.

6. R. Schmidt, K.C. Karki, and S.V. Patankar, Raised-Floor Data Center: Perforated Tile Flow Rates for Various Tile Layouts, Proc. ITHERM 2004 - Ninth Intersociety Conference on Thermal and Thermomechanical Phenomena in Electronic Systems, Las Vegas, NV, 2004.

7. J.W. VanGilder and R. Schmidt, Airflow Uniformity Through Perforated Tiles in a Raised-Floor Data Center, Proc. ASME InterPACK, San Francisco, California, USA, ASME, IPACK2005-73375, 2005.

8. *Report to Congress on Server and Data Center Energy Efficiency Public Law 109-431.* August 2, 2007, U.S. Environmental Protection Agency ENERGY STARProgram.

9. W. Chen, J.K. Allen, K. Tsui, and F. Mistree, A Procedure for Robust Design: Minimizing Variations Caused by Noise Factors and Control Factors, ASME Journal of Mechanical Design, vol. 118, pp. 478-485, 1996.

10. S. Greenberg, E. Mills, W. Tschudi, P. Rumsey, and B. Myatt, Best Practices for Data Centers: Lessons Learned from Benchmarking 22 Data Centers, Proc.

ACEEE Summer Study on Energy Efficiency in Buildings in Asilomar, CA, pp. 76-87, 2006.

11. Lawrence Berkeley National Laboratory and Rumsey Engineers, "Data Center Energy Benchmarking Case Study", http://datacenters.lbl.gov/. accessed on November 2005

12. F. Mistree, O.F. Hughes, and B. Bras, The Compromise Decision Support Problem and the Adaptive Linear Programming Algorithm, in M.P. Kamat (eds.), Structural Optimization: Status and Promise, pp. 247-286, AIAA, Washington, D.C, 1993.

13. E. Samadiani, Y. Joshi, and F. Mistree, The Thermal Design of a Next Generation Data Center: A Conceptual Exposition, Proc. Thermal Issues in Emerging Technologies, ThETA 1, Cairo, Egypt, pp. 93-102, 2007.

14. A. Shah, V. Carey, C. Bash, and C. Patel, Exergy-Based Optimization Strategies for Multi-Component Data Center Thermal Management: Part I, Analysis, Proc. ASME InterPACK05, San Francisco, California, USA, ASME, IPACK2005-73137, 2005.

15. A. Shah, V. Carey, C. Bash, and C. Patel, Exergy-Based Optimization Strategies for Multi-Component Data Center Thermal Management: Part II, Application and Validation, Proc. ASME InterPACK05, San Francisco, California, USA, ASME, IPACK2005-73138, 2005.

16. S. Bhopte, D. Agonafer, R. Schmidt, and B. Sammakia, Optimization of Data Center Room Layout to Minimize Rack Inlet Air Temperature, Proc. ASME InterPACK, San Francisco, California, USA, ASME, IPACK2005-73027, 2005.

17. R. Schmit and M. Iyengar, Effect of Data Center Layout on Rack Inlet Air Temperatures, Proc. ASME InterPACK 05, San Francisco, California, USA, ASME, IPACK2005-73385, 2005.

18. R.K. Sharma, C.E. Bash, and C.D. Patel, Dimensionless Parameters for the Evaluation of Thermal Design and Performance of Large-Scale Data Centers, Proc. the 8th AIAA/ASME Joint Thermophysics and Heat Transfer Conference, St. Louis, AIAA-2002-3091, 2002.

19. S. Kang, R. Schmidt, K.M. Kelkar, A. Radmehr, and S.V. Patankar, A Methodology for the Design of Perforated Tiles in a Raised Floor Data Center Using Computational Flow Analysis, IEEE Transactions on Components and Packaging Technologies, vol. 24(2), pp. 177-183, 2001.

20. T.D. Boucher, D.M. Auslander, C.E. Bash, C.C. Federspiel, and C.D. Patel, Viability of Dynamic Cooling Control in a Data Center Environment, Proc. Inter Society Conference on Thermal Phenomena, IEEE, pp. 593-600, 2004.

21. N. Rolander, An approach for the robust design of air cooled data center server cabinets. MS thesis, G.W. School of Mechanical Engineering, Georgia Institute of Technology, Atlanta, 2005.

22. J. Rambo and Y. Joshi, Thermal Modeling of Technology Infrastructure Facilities: A Case Study of Data Centers, in W.J. Minkowycz, E.M. Sparrow, and J.Y. Murthy (eds.), The Handbook of Numerical Heat Transfer, pp. 821-850, Taylor and Francis, New York, 2006.

23. ASHRAE, Datacom Equipment Power Trends and Cooling Applications, American Society of Heating, Refrigeration and Air-Conditioning Engineers Atlanta, Atlanta, 2005.

24. S. Greenberg, E. Mills, W. Tschudi, P. Rumsey, and B. Myatt, Best Practices for Data Centers: Lessons Learned from Benchmarking 22 Data Centers, Proc. Proceedings of the ACEEE Summer Study on Energy Efficiency in Buildings in Asilomar, CA, ACEEE, pp. 76-87, 2006.

25. M.J. Crippen, R.K. Alo, D. Champion, R.M. Clemo, C.M. Grosser, N.J. Gruendler, M.S. Mansuria, J.A. Matteson, M.S. Miller, and B.A. Trumbo, BladeCenter Packaging, Power, and Cooling, IBM J. Res. & Dev., vol. 49(6), pp. 887-904, 2005.

26. IBM, http://ibm.com/eserver/xseries/storage/rack.html/, accessed on November 2005

27. A. Shehabi, W. Tschudi, and A. Gadgil, *Data Center Economizer Contamination and Humidity Study*. 2007, Lawrence Berkeley National Laboratory.

28. Liebert Corporation, http://www.liebert.com/dynamic/displayproduct.asp?id=1077&cycles=60hz/, accessed on November 2005

29. APC (American Power Conversion) Corporation, http://www.apc.com/, accessed on November 2005

30. Thermacore International, Inc., http://www.thermacore.com/default.asp/, accessed on November 2005

31. V. Kamath, *Rear Door Heat Exchanger: A method for DataCenter Thermal Management*. Sep 16, 2005, Rreport by Power and Thermal Engineering in IBM Systems and Technology Group.

32. A. Heydari and P. Sabounchi, Refrigeration Assisted Spot Cooling of a High Heat Density Data Center, Proc. Inter Society Conference of Thermal Phenomena, IEEE, pp. 601-607, 2004.

33. P. Jeffery and T. Sharp, A New Thermal Management Solution for Data Centers, Server Farm Installations, Co-Location Enterprises and Web Hosting Facilities, accessed on Februray 2002.

34. R. Schmidt, R. Chu, M. Ellsworth, M. Iyengar, D. Porter, V. Kamath, and B. Lehman, Maintaining Datacom Rack Inlet Temperatures with Water Cooled Heat Exchanger, Proc. ASME InterPACK, San Fransisco, California, USA, ASME, IPACK2005-73468, 2005.

35. D. Wang, A Passive Solution to a Difficult Data Center Environmental Problem, Proc. Inter Society Conference on Thermal Phenomena, IEEE, pp. 586-593, 2004.

36. R.R. Schmidt, E.E. Cruz, and M.K. Lyengear, Challenges of Data Center Thermal Management, IBM J. Res. & Dev., vol. 49(4), pp. 709-723, July/September 2005.

37. D. Beaty and R.R. Schmidt, Back to the Future: Liquid Cooling Data Center Consideration, ASHRAE Journal, vol. 46(12), pp. 42-47, December 2004.

38. T.W. Simpson, U. Lautenschlager, and F. Mistree, Towards Mass Customization in the Age of Information: The Case for Open Engineering Systems, in W. Read and A. Porter (eds.), The Information Revolution: Present and Future, pp. 49-71, Ablex Publications, CT, 1998.

39. Z.J. Zuo, L.R. Hoover, and A.L. Phillips, An integrated thermal architecture for thermal management of high power electronics in Y. Joshi and S. Garimella (eds.), Thermal Challenges in Next Generation Electronic Systems, pp. 317-336, Millpress, Rotterdam, 2002.

40. S. Gurram, S. Suman, Y. Joshi, and A. Fedorov, Thermal Issues in Next Generation Integrated Circuits, IEEE Transactions on Device and Materials Reliability, vol. 4(4), pp. 709-714, 2004.

41. Y. Joshi and X. Wei, Micro and Meso Scale Compact Heat Exchangers in Electronics Thermal Management-A Review, Proc. Fifth International Conference on Enhanced, Compact and Ultra-Compact Heat Exchangers: Science, Engineering and Technology, Hoboken, NJ, pp. 162-179, 2005.

42. C.H. Amon, S.-C. Yao, C.-F. Wu, and C.-C. Hsieh, Microelectromechanical System-Based Evaporative Thermal Management of High Heat Flux Electronics, Journal of Heat Transfer, vol. 127, pp. 66-75, January 2005.

43. Z.A. Williams and J.A. Roux, Graphite foam thermal management of a high packing density array of power amplifiers, Proc. 9th AIAA/ASME Joint Thermophysics and Heat Transfer Conference, San francisco, California, AIAA 2006-3609, 2006.

44. C. Coggins, D. Gerlach, Y. Joshi, and A. Federov, Compact Low Temperature Refrigeration of Microprocessors, Proc. the International Refrigeration and Air Conditioning Conference at Purdue University, West Lafayette, IN, R064, 2006.

45. K.C. Karki, S.V. Patankar, and A. Radmehr, Techniques for controlling airflow distribution in raised-floor data centers, Proc. IPACK03 - The Pacific Rim/ASME International Electronic Packaging Technical Conference and Exhibition, Maui, HI, InterPack2003-35282, pp. 621-628, 2003.

46. E. Fried and I.E. Idelchik, Flow Resistance: A Design Guide for Engineers, Hemisphere Publishing, New York, 1989.

47. F. Incorporated, *FLUENT v. 6.1 Users Manual.* 2001: Lebanon, New Hampshir: Fluent Incorporated

48. *Workshop Report, Simulation Based Engineering Science*. 2004: National Science Foundation: Arlington, VA. p. 1-18.

49. J.H. Panchal, A framework for simulation-based integrated design of multiscale products and design processes. PhD Dissertation G.W. Woodruff School of Mechanical Engineering, Georgia Institute of Technology, Atlanta, GA, 2005.

50. W. Chen, D. Rosen, J.K. Allen, and F. Mistree, Modularity and the Independence of Functional Requirements in Designing Complex Systems, Concurrent Product Design, vol. 74, pp. 31-38, 1994.

51. G. Li, M. Li, S. Azarm, J. Rambo, and Y. Joshi, Optimizing thermal design of data center cabinets with a new multi-objective genetic algorithm, Distrib Parallel Databases, vol. 21, pp. 167-192, 2007.

52. N. Rolander, J. Rambo, Y. Joshi, F. Mistree, and J.K. Allen, Robust design of turbulent convective systems using the proper orthogonal decomposition, ASME Journal of Mechanical Design: Special Issue Robust and Risk Based Design, vol. 128, pp. 844-855, 2006.

53. J.D. Rambo, Reduced-order Modeling of Multiscale Turbulent Convection: Application to Data Center Thermal Management, PhD thesis, Mechanical Engineering, Georgia Institute of Technology, Atlanta, 2006.

54. C. Patel, C. Bash, C. Belady, L. Stahl, and D. Sullivan, Computational Fluid Dynamics Modeling of High Compute Density Data Centers to Assure System

Inlet Air Specifications, Proc. ASME IPACK'01, Kauai, Hawaii, ASME, IPACK2001-15622, 2001.

55. R. Schmidt, K.C. Karki, K.M. Kelkar, A. Radmehr, and S.V. Patankar, Measurements and Predictions of the Flow Distribution Through Perforated Tiles in Raised Floor Data Centers, Proc. ASME InterPACK01, Kauai, Hawaii, IPACK2001-15728, 2001.

56. A. Radmehr, R. Schmidt, K.C. Karki, and S.V. Patankar, Distributed Leakage Flow in Raised-Floor Data Centers, Proc. ASME InterPACK, San Francisco, California, USA, ASME, IPACK2005-73273, 2005.

57. K.C. Karki, A. Radmehr, and S.V. Patankar, Use of computational fluid dynamics for calculating flow rates through perforated tiles in raised-floor data centers, HVAC and R Research, vol. 9(2), pp. 153-166, 2003.

58. E. Samadiani, J. Rambo, and Y. Joshi, Numerical Modeling Of Perforated Tile Flow Distribution In A Raised-Floor Data Center, Proc. ASME InterPACK '07, Vancouver, British Columbia, Canada, IPACK2007-33428, 2007.

59. R. Schmidt and E. Cruz, Cluster of High Powered Racks within a Raised Floor Computer Data Center: Effects of Perforated Tiles Flow Distribution on Rack Inlet Air Temperature, Journal of Electronic Packaging, vol. 126(4), p. 510 (9 pages), 2004.

60. J. Rambo and Y. Joshi, Modeling of data center airflow and heat transfer: State of the art and future trends, Distributed and Parallel Databases, vol. 21, pp. 193-225, 2007.

61. T. Simpson, J. Peplinski, P. Koch, and J. Allen, Metamodels for Computer-based Engineering Design: Survey and Recommendations, Engineering With Computers, vol. 17, pp. 129-150, 2001.

62. J. Sacks, W.J. Welch, T.J. Mitchell, and H.P. Wynn, Design and Analysis of Computer Experiments, Stat. Sci., vol. 4, pp. 409-423, 1989.

63. T.J. Santner, B.J. Williams, and W.I. Notz, The Design and Analysis of Computer Experiments, Springer, New York, 2003.

64. R. Jin, W. Chen, and T. Simpson, Comparative Studies of Metamodeling Techniques Under Multiple Modeling Criteria, Struct. Multidiscip. Optim., vol. 23, pp. 1-13, 2001.

65. J.E. Pacheco, C.H. Amon, and S. Finger, Bayesian Surrogates Applied to Conceptual Stages of the Engineering Design Process, ASME J. Mech. Des., vol. 125, pp. 664-672, 2003.

66. D.J. Cappelleri, M.I. Frecker, T.W. Simpson, and A. Snyder, Design of a PZT Bimorph Actuator Using a Metamodel-Based Approach, ASME J. Mech. Des., vol. 124, pp. 354-357, 2002.

67. A.A. Giunta, Aircraft Multidisciplinary Design Optimization Using Design of Experiments Theory and Response Surface Modeling, PhD thesis, Department of Aerospace and Ocean Engineering, Virginia Polytechnic and State University, Blacksburg, VA, 1997.

68. V.R. Joseph, Y. Hung, and A. Sudjianto, Blind Kriging: A New Method for Developing Metamodels, Journal of Mechanical Design, vol. 130, p. 031102 (8 pages), 2008.

69. Z. Qian, C.C. Seepersad, V.R. Joseph, J.K. Allen, and C.F.J. Wu, Building Surrogate Models Based on Detailed and Approximate Simulations, ASME Journal of Mechanical Design, vol. 128, pp. 668-677, 2006.

70. P.Z.G. Qian and C.F.J. Wu, Bayesian Hierarchical Modeling for Integrating Low-Accuracy and High-Accuracy Experiments, Technometrics, vol. 50(2), pp. 192-204, 2008.

71. B. Shapiro, Creating Reduced-Order Models for Electronic Systems: An Overview and Suggested Use of Existing Model Reduction and Experimental System Identification Tools, in Y. Joshi and S.V. Garimella (eds.), Thermal Challenges in Next Generation Electronics Systems, pp. 299-306, Millpress, Rotterdam, Netherlands, 2002.

72. P. Holmes, J.L. Lumley, and G. Berkooz, Turbulence, Coherent Structures, Dynamical Systems and Symmetry, Cambridge University Press., Great Britain, 1996.

73. M. Farge, N. Kevlahan, V. Perrier, and E. Goirand, Wavelets and Turbulence, Proceedings of the IEEE, vol. 84(4), pp. 639-669, 1996.

74. J.C.R. Hunt, A.A. Wray, and P. Moin, Eddies, stream, and convergence zones in turbulent flows Center for Turbulence Research Rep. CTR-S88, 1988.

75. J. Zhou, R.J. Adrian, S. Balachandar, and T.M. Kendall, Mechanisms for generating coherent packets of hairpin vortices in channel flow, J. Fluid Mech., vol. 387, pp. 353–396, 1999.

76. G. Haller, An Objective Definition of a Vortex, J. Fluid Mech., vol. 525, pp. 1–26, 2005.

77. G. Haller, Lagrangian Coherent Structures from Approximate Velocity Data, Physics of Fluids, vol. 14(6), pp. 1851-1861, 2002.

78. M.A. Green, C.W. Rowley, and G. Haller, Detection of Lagrangian Coherent Structures in Three-dimensional Turbulence, J. Fluid Mech., vol. 572, pp. 111-120, 2007.

79. T. Kim, N. Thürey, D. James, and M. Gross, Wavelet Turbulence for Fluid Simulation, Proc. International Conference on Computer Graphics and Interactive Techniques archive (ACM SIGGRAPH), No. 50, 2008.

80. J. Rambo and Y. Joshi, Reduced-order modeling of turbulent forced convection with parametric conditions, International Journal of Heat and Mass Transfer, vol. 50(3-4), pp. 539-551, 2007.

81. S.S. Ravindran, Adaptive Reduced-Order Controllers for a Thermal Flow Using Proper Orthogonal Decomposition, SIAM Journal of Scientific Computing, vol. 23(6), pp. 1924-1942, 2002.

82. H.M. Park and D.H. Cho, The Use of the Karhunen-Loeve Decomposition for the Modeling of Distributed Parameter Systems, Chemical Engineering Science, vol. 51(1), pp. 81-98, 1996.

83. H.M. Park and D.H. Cho, Low Dimensional Modeling of Flow Reactors, International Journal of Heat and Mass Transfer, vol. 39(16), pp. 3311-3323, 1996.

84. L. Sirovich and H.M. Park, Turbulent Thermal Convection in a Finite Domain: Part I. Theory, Physics of Fluids, vol. 2(9), pp. 1649-1657, 1990.

85. L. Sirovich and H.M. Park, Turbulent Thermal Convection in a Finite Domain: Part II. Numerical Results, Physics of Fluids, vol. 2(9), pp. 1649-1657, 1990.

86. I.H. Tarman and L. Sirovich, Extensions of Karhunen-Loeve Based Approximations of Complicated Phenomena, Computer Methods in Applied Mechanics and Engineering, vol. 155, pp. 359-368, 1998.

87. H.M. Park and W.J. Li, Boundary Optimal Control of Natural Convection by Means of Mode Reduction, Journal of Dynamic Systems Measurement and Control, vol. 124, pp. 47-54, 2002.

88. P. Ding, X.-H. Wu, Y.-L. He, and W.-Q. Tao, A fast and efficient method for predicting fluid flow and heat transfer problems, ASME Journal of Heat Transfer, vol. 130(3), p. 032502, 2008.

89. H.V. Ly and H.T. Tran, Modeling and Control of Physical Processes Using Proper Orthogonal Decomposition, Mathematical and Computer Modeling, vol. 33, pp. 223-236, 2001.

90. G. Strang, Linear Algebra and its Applications, Thomson Learning, 1988.

91. Q. Nie and Y. Joshi, Multiscale Thermal Modeling Methodology for Thermoelectrically Cooled Electronic Cabinets, Numerical Heat Transfer, Part A: Applications, vol. 53(3), pp. 225 - 248, 2008.

92. Q. Nie and Y. Joshi, Reduced order modeling and experimental validation of steady turbulent convection in connected domains, International Journal of Heat and Mass Transfer, vol. 51(25-26), pp. 6063-6076, 2008.

93. J. Moore, J. Chase, P. Ranganathan, and R. Sharma, Making Scheduling Cool: Temperature-Aware Workload Placement in Data Centers, Proc. Usenix Technical Conference, 2005.

94. M. Karlsson, C. Karamanolis, and X. Zhu, Triage: Performance Isolation and Differentiation for Storage Systems, Proc. The Twelfth International Workshop on Quality of Service, pp. 67-74, 2004.

95. R.K. Sharma, C. Bash, C.D. Patel, R.J. Friedrich, and J.S. Chase, *Balance of Power: Dynamic Thermal Management for Internet Data Centers*. 2003, Whitepaper issued by Hewlet Packard Laboratories;Technical Report: HPL-2003-5.

96. J. Moore, J. Chase, K. Farkas, and P. Ranganathan, Data Center Workload Monitoring, Analysis, and Emulation, Proc. Eighth Workshop on Computer Architecture Evaluation using Commercial Workloads, 2005.

97. Q. Tang, T. Mukherjee, S.K.S. Gupta, and P. Cayton, Sensor-based Fast Thermal Evaluation Model for Energy-efficient High-performance Datacenters, Proc. Fourth International Conference on Intelligent Sensing and Information Processing (ICISIP), pp. 203-208, 2006.

98. R. Nathuji, A. Somani, K. Schwan, and Y. Joshi, CoolIT: Coordinating Facility and IT Management for Efficient Datacenters, Proc. HotPower '08; Workshop on Power Aware Computing and Systems, San Diego, CA, 2008.

99. A. Somani and Y. Joshi, *Ambient intelligence based load management, USPTO Provisional Patent, GTRC ID No. 4524*. 2008.

100. Z. Qian, Computer Experiments: Design, Modeling, and Integration, PhD thesis, School of Industrial and Systems Engineering, Georgia Institute of Technology, Atlanta, 2006.

101. E. Samadiani, Y. Joshi, and F. Mistree, The Thermal Design of A Next Generation DataCenter: A Conceptual Exposition, Journal of Electronic Packaging, vol. 130(4), pp. 041104 (8 pages), 2008.

102. ASHRAE, Thermal Guidelines for Data Processing Environments, American Society of Heating, Refrigeration, and Air-Conditioning Engineers, 2004.

103. J. Moore, J. Chase, P. Ranganathan, and R. Sharma, Making Scheduling Cool: Temperature-Aware Workload Placement in Data Centers, Proc. USENIX 2005 Annual Technical Conference, pp. 61-75, 2005.

104. E. Samadiani and Y. Joshi, Reduced Order Thermal Modeling of Data Centers via Proper Orthogonal Decomposition-A Review, Proc. First International Conference on Computational Methods for Thermal Problems, Naples, Italy, 2009.

105. R.M. Lewis and V. Torczon, Pattern Search Methods for Linearly Constrained Minimization, SIAM Journal on Optimization, vol. 10(3), pp. 917-941, 2000.

106. R.E. Steuer, Multiple Criteria Optimization, Theory Computations and Applications, New York: John Wiley & Sons, Inc., 1986.

107. C. Isci, G. Contreras, and M. Martonosi, Live, runtime phase monitoring and prediction on real systems with application to dynamic power management, Proc. the 39th International Symposium on Microarchitecture (MICRO-39), pp. 359-370, 2006.

108. Q. Zhu, Z. Chen, L. Tan, Y. Zhou, K. Keeton, and J. Wilkes, Hibernator: Helping disk arrays sleep through the winter, Operating Systems Review, vol. 39(5), pp. 177-190, 2005.

109. R. Kumar, D. Tullsen, P. Ranganathan, N. Jouppi, and K. Farkas, Single-isa heterogeneous multi-core architectures for multithreaded workload performance, ACM SIGARCH Computer Architecture News, vol. 32(2), p. 64, 2004.

110. R. Nathuji, C. Isci, and E. Gorbatov, Exploiting platform heterogeneity for power efficient data centers, Proc. the IEEE International Conference on Autonomic Computing (ICAC), pp. 5-5, 2007.

111. J. Chase, D. Anderson, P. Thakar, A. Vahdat, and R. Doyle, Managing energy and server resources in hosting centers, ACM SIGOPS Operating Systems Review, vol. 35(5), pp. 103-116, 2001.

112. J. Moore, J. Chase, and P. Ranganathan, Weatherman: Automated, online, and predictive thermal mapping and management for data centers, Proc. IEEE International Conference on Autonomic Computing (ICAC), pp. 155-164, 2006.

113. Q. Tang, S. Gupta, and G. Varsamopoulos, Energy-efficient thermal-aware task scheduling for homogeneous high-performance computing data centers: A cyber-physical approach, IEEE Transactions on Parallel and Distributed Systems, vol. 19(11), pp. 1458-1472, 2008.

114. T. Heath, A.P. Centeno, P. George, L. Ramos, Y. Jaluria, and R. Bianchini, Mercury and freon: Temperature emulation and management in server systems, Proc. the International Conference on Architectural Support for Programming Languages and Operating Systems (ASPLOS), pp. 106-116, 2006.

115. R. Raghavendra, P. Ranganathan, V. Talwar, Z. Wang, and X. Zhu, No power struggles: A unified multi-level power management architecture for the data center, ACM SIGARCH Computer Architecture News, vol. 36(1), pp. 48-59, 2008.

116. S. Kumar, V. Talwar, P. Ranganathan, R. Nathuji, and K. Schwan, Mchannels and m-brokers: Coordinated management in virtualized systems, Proc. the Workshop onManaged Many-Core Systems (MMCS) 2008.

117. R. Nathuji and K. Schwan, Virtualpower: Coordinated power management in virtualized enterprise systems, Proc. the 21st ACM Symposium on Operating Systems Principles (SOSP), pp. 265-278, 2007.

118. R. Nathuji and K. Schwan, Vpm tokens: Virtual machine-aware power budgeting in datacenters, Proc. the ACM/IEEE International Symposium on High Performance Distributed Computing (HPDC), pp. 119-128, 2008.

119. H. Hamann, J. Lacey, M. O'Boyle, R.R. Schmidt, and M. Iyengar, Rapid Three Dimensional Thermal Characterization of Large Scale Computing Facilities, IEEE Transactions of Components and Packaging Technologies, vol. 31(2), 2008.

120. H.-J. Choi, A Robust Design Method for Model and Propagated Uncertainty, G.W. Woodruff School of Mechanical Engineering, PhD Dissertation, Georgia Institute of Technology, Atlanta, GA, 2005.

121. S. Kumar, V. Talwar, V. Kumar, P. Ranganathan, and K. Schwan, vManage: Loosely Coupled Platform and Virtualization Management in Data Centers, Proc. the International Conference on Autonomic Computing (ICAC), pp. 127-136, 2009.